RIGA TECHNICAL UNIVERSITY
Faculty of Power and Electrical Engineering
Institute of Industrial Electronics and Electrical Engineering

Olegs TETERVENOKS
Doctoral Student of Programme "Computerised Control of Electrical Technologies"

DIRECT CURRENT CONTROL AND COMPENSATION OF NON-LINEARITY FOR THE IMPROVEMENT OF QUALITY PARAMETERS OF THE LED LAMP

Doctoral Thesis

Scientific supervisor
Dr. sc. ing., professor
Ilya GALKIN

Riga 2015

The present research been supported by the European Social Fund within the project “Support for the Implementation of Doctoral Studies at Riga Technical University”.

EIROPAS SOCIĀLAIS FONDS

EIROPAS SAVIENĪBA

ABSTRACT

The present Doctoral Thesis is devoted to the study and development of energy efficient drivers of LED lamps for smart lighting systems.

LEDs have already proved themselves as highly efficient light source with many benefits for use in modern high quality lighting systems. However, LEDs also have significant drawbacks. One of the main drawbacks is high initial costs when moving to a new LED based lighting system. High initial costs must be compensated by lower system maintenance costs (lower electrical power consumption, longer service life) in order to motivate consumer to implement LED based lighting system. At the same time, the service life of such lighting system depends on many factors, but there are two main problematic elements to highlight. LED by itself, which is temperature sensitive element (faster degradation under high temperature conditions) and LED driver, the service life of which usually is limited by presence of electrolytic capacitors. The issue of high temperature can be solved relatively easily: applying known procedure for thermal design calculations and appropriate heatsink in accordance with these calculations. The issues related to LED driver are more complicated. Thus, the main attention in this research is focused on the problems related to LED driver and proper application of LED.

A brief summary of the conventional lighting technologies is given in the introductory section of the Doctoral Thesis, as well as their main benefits and drawbacks are discussed. The main tasks and hypotheses of the research have been defined.

The second section of this Doctoral Thesis is devoted to general issues related to LEDs. The main benefits of LEDs are high efficiency, long service time and dimming (light regulation) possibility in a wide regulation range. However, the quality of the light can be affected by the dimming: the change in the light color temperature or the light fluctuations and related undesirable optical effects may appear. Therefore, the main light quantities have been also briefly considered in this section, as well as the issues related to photometry and colorimetry: light quality quantities. There are several dimming techniques, which have been described in this section in detail. Selected dimming approach in a large extent affects not only the light quality parameters, but also the structure of LED driver. From the point of view of efficiency and light quality parameters, the most appropriate dimming technique for general purpose lighting is fluent or amplitude mode light regulation technique. Slight color shift can be observed using this dimming technique, at the same time light fluctuations are minimal. Therefore, in the next two sections have been considered topologies and operation modes of the converters, which allow

simplifying implementation of amplitude mode dimming technique in microcontroller based systems.

The compensation of nonlinearity of LED curves by nonlinear transfer function of the converter has been considered in the following section of this research. For this purpose the family of tapped-inductor converters has been studied, as well as operation of the converter in a discontinuous conduction mode. During these studies it was found and confirmed (by analytical calculations and experiments) that both nonlinearity compensation approaches in case of amplitude mode dimming approach allows obtaining controllability curves with better parameters (lower nonlinearity and higher dimming resolution) in comparison with traditional converter topologies.

Direct current control and current fed converters have been considered in the fourth section of this Doctoral Thesis. These converters have been previously considered in other works as well. The main drawback has been specified there: the constant current source is necessary at the input of current fed converter for its proper operation, but the prevalent electrical power sources by their nature are voltage sources. The solution of the described problem has been proposed in this section: non-inverting buck-boost converter has been considered as combination of constant current source and current fed converter. Thus, special control algorithm allows obtaining properties of the converter with the direct current control using non-inverting buck boost converter. This allows improving the parameters of controllability curves (lower nonlinearity and higher dimming resolution) in comparison with the traditional converter topologies.

Conclusions summarize the results of this research and their accordance with the hypotheses.

The Doctoral thesis has been written in English. It consists of 5 chapters including introduction and conclusions, bibliography with 139 reference sources and 17 appendices. The volume of the present Doctoral Thesis is 135 pages. It has been illustrated by 85 figures and 11 tables.

ANOTĀCIJA

Šis darbs ir saistīts ar energoefektīvo viedo apgaismošanas sistēmu LED gaismekļu balastu izpēti un izstrādi.

Gaismas diodes jau ir pierādījušas savu efektivitāti augstās kvalitātes gaismekļu izstrādē un priekšrocības salīdzinājumā ar citiem tradicionālajiem gaismas avotiem. Tomēr, arī gaismas diodēm ir savi trūkumi. Augsta cena (lielās sākotnējas izmaksas), pārejot uz LED apgaismojumu, ir viens no galvenajiem trūkumiem. Lai pircējs/pasūtītājs būtu ieinteresēts jaunās apgaismojuma sistēmas ieviešanā, lielām sākotnējam izmaksām ir jābūt kompensētām ar samazinātām turpmākām sistēmas apkalpošanas/uzturēšanas izmaksām — mazāku elektroenerģijas patēriņu un ilgāku kalpošanas laiku. Savukārt LED apgaismojuma sistēmas kalpošanas laiks ir atkarīgs no daudziem faktoriem, tomēr īpaši var izdalīt divus problemātiskus elementus. Pašas diodes, kas ir jutīgas pret paaugstinātām temperatūrām (paātrināti degradē), un LED draiveris, kura kalpošanas mūžu parasti ierobežo elektrolītiskie kondensatori. Paaugstinātās temperatūras problēma ir atrisināmā salīdzinoši vienkārši: pēc zināmas metodikas tiek aprēķināta un uzprojektēta LED nepieciešamā dzesēšanas (siltuma novades) sistēma. Problēmas, kas saistītas ar LED draiveri, ir sarežģītāk risināmas, tām ir komplekss raksturs. Tieši tāpēc uzmanība šajā darbā ir pievērsta tām problēmām, kas saistītas ar LED draiveriem un pareizu LED darbināšanu.

Darba ievadā ir dots īss esošo apgaismošanas tehnoloģiju apkopojums, apskatītas galvenās priekšrocības un trūkumi. Ir definētas galvenās hipotēzes un galvenie darba uzdevumi.

Nākamajā nodaļā ir apskatīti vispārīgie jautājumi, kas saistīti ar gaismas diodēm. Pie galvenajām LED priekšrocībām ir pieskaitāmas augsta lietderība, ilgs kalpošanas laiks un apgaismojuma līmeņa regulēšanas iespēja plašā diapazonā. Tomēr apgaismojuma līmeņa regulēšana gaismas diodēm var ietekmēt apgaismojuma kvalitāti: var pamainīties gaismas krāsas temperatūra, vai parādīties gaismas pulsācijas un ar tām saistītas nevēlamās optiskās parādības. Tieši tāpēc ievadā īsi tiek apskatīti daži gaismas lielumi, jautājumi, kas saistīti ar fotometriju un kolorimetriju: ar gaismas kvalitāti saistītie lielumi. Pastāv vairākas apgaismojuma līmeņa regulēšanas metodes, kuras sīkāk ir apskatītas šī darba ievadā. Izvēlētā apgaismojuma līmeņa regulēšanas metode lielā mērā ietekmē ne tikai gaismas kvalitātes rādītājus, bet arī LED draivera uzbūvi. No lietderības un gaismas kvalitātes rādītāju viedokļa plašā pielietojuma apgaismojuma iekārtās un sistēmās izdevīgāka ir plūstošā jeb amplitūdas apgaismojuma līmeņa regulēšanas metode, kurai apgaismojuma līmeņa regulēšanas laikā ir vērojamas nelielas gaismas krāsas izmaiņas, toties gaismas pulsācijas ir minimālas. Līdz ar to divās turpmākajās darba nodaļās ir apskatītas pārveidotāju topoloģijas un darbināšanas paņēmieni, kas ļauj vienkāršāk realizēt plūstošo apgaismojuma līmeņa regulēšanu, kā arī izstrādāt vienkāršāku LED draivera vadības sistēmu uz mikrokontrollera pamata.

Trešajā nodaļā tiek pētīta nelineārās LED voltampēru raksturlīknes kompensēšana ar nelineāro pārveidotāja ieejas-izejas sprieguma pārvades funkciju. Šīm nolūkam tiek apskatīti pārveidotāji ar sadalīto droseli, kā arī tiek pētīta pārveidotāju darbība pārtrauktas strāvas režīmā. Pētījumu gaitā konstatēts un apstiprināts (gan analītisko aprēķinu ceļā, gan eksperimentu gaitā), ka abi LED nelinearitātes kompensēšanas paņēmieni plūstošās apgaismojuma līmeņa regulēšanas gadījumā ļauj iegūt regulēšanas raksturlīkni ar labākiem parametriem (mazāku nelinearitāti, lielāku regulēšanas izšķirtspēju), nekā tradicionālo sprieguma pārveidotāju gadījumā.

Ceturtajā nodaļā ir apskatīti pārveidotāji ar strāvas tiešo regulēšanu. Šāda tipa pārveidotāji iepriekš bija apskatīti arī citos darbos. Bija definēts arī to galvenais trūkums — pārveidotāja ieejā ir nepieciešamas strāvas avots. Elektroenerģijas avoti pēc savas dabas pārsvarā ir sprieguma avoti, tādējādi pārveidotāju ar strāvas tiešo regulēšanu praktiskā izmantošana ir apgrūtināma. Šajā nodaļā ir piedāvāts augstāk aprakstītās problēmas risinājums: neinvertējošais pazeminoši-paaugstinošs pārveidotājs ir apskatīts kā konstantas strāvas avota un pārveidotāja ar strāvas tiešo regulēšanu kombinācija. Tādējādi ar speciālo neinvertējošā pazeminoši-paaugstinoša pārveidotāja vadības algoritmu (paņēmienu), kas ir definēts un sīki aprakstīts šajā nodaļā, tiek panāktas pārveidotāja ar strāvas tiešo regulēšanu īpašības. Tas arī ļauj iegūt regulēšanas raksturlīkni ar labākiem parametriem (mazāku nelinearitāti un lielāku regulēšanas izšķirtspēju), nekā tradicionāliem sprieguma pārveidotājiem.

Secinājumos ir apkopotā informācija par pētījumu rezultātu atbilstību izvirzītajām hipotēzēm.

Promocijas darbs ir uzrakstīts angļu valodā uz 136 lpp, un tajā ir 5 nodaļas, ieskaitot ievadu un secinājumus un 17 pielikumus. Darbā iekļauti 85 attēli, 11 tabulas un 139 atsauces.

CONTENTS

1 INTRODUCTION

1.1. Conventional Lighting Technologies and LEDs

A comparison of different lighting technologies gives a good insight in the growing popularity and prevalence of LEDs. The summary of different lighting technologies is given in Table 1.1.

The overall luminous efficacy of incandescent lamp is rather low: greater part of the emission of blackbody (tungsten filament is regarded as blackbody) is in the infrared rather than visible range of electromagnetic waves. Depending on the operation temperature efficacy varies from 8 lm/W to 23 lm/W for 120V incandescent filament lamps. It also depends on the voltage they are designed for: 220–240 V lamps are approximately 20 % less efficient in comparison with 120 V lamps, but they also have a longer service life. The most common failure is evaporation of tungsten from the filament [1].

The tungsten evaporation rates can be reduced, but the efficacy can be increased by addition of the halogen to the gas filling. Halogens participate in chemical transport cycle, when halides are formed during tungsten diffusion process and are concentrated at the filament allowing higher

Table 1.1

Comparison of Different Lighting Technologies [1]

Type	Power (W)	Efficacy (lm/W)	Color Rendering Index	Service life (hours)
Incandescent (120V)	10…1,500	8...23	100	≈1,000
Tungsten halogen (120V)	5…2,000	10…35	100	1,700…2,500
Fluorescent (low-power units)	4…5	35…50	50…95	5,000…15,000
Fluorescent (higher-power linear)	70…125	75…100	50…95	5,000…15,000
Fluorescent (electronically ballasted)	10…60	75…100	50…95	7,000…30,000
LPS	18…180	100…200	-44	14,000…18,000
HPMV	45…1,000	20…50	16	8,000…10,000
HPS	50…1,000	60…130	20…25	24,000
MH	20…1,8000	70…110	60…95	2,000…30,000
Induction lamp	23…85	47…71	80	100,000
Sulfur lamp	1,425	95	79	20,000
High power LED (white)	0.1…100*	70…200**	60…97	25,000…150,000

* For single casing. ** For commercial high power LEDs. Over 300 lm/W efficacy can be achieved in the lab [4].

operation temperatures (3450 K). However, tungsten halogen lamps cannot be dimmed, since reduced temperature breaks the halogen cycle [1]. Furthermore, the sale of incandescent filament lamps is banned and the halogen lamps will be phased out in the nearer future [2], [3].

Also, light can be obtained during the discharge process in a gas. Low-pressure and high-pressure discharges are possible. Low-pressure discharge is used in fluorescent lamps (where the effective discharge emitter is mercury vapors) and low-pressure sodium lamps. In fluorescent lamps the main part of emission is ultraviolet (UV), but the visible light is produced by photoluminescence in tube wall coating phosphor. Thus, there are two energy conversions to obtain visible light in fluorescent lamps. Also, the light output of the fluorescent lamp is highly affected by the ambient temperature, making them less appropriate for outdoor lighting applications.

Low-pressure sodium (LPS) lamps are very efficient, but they have significant drawbacks: extremely poor color rendering and long warm-up time.

Color rendering of high-pressure discharge (high-intensity discharge — HID) lamps is better in comparison with LPS, but they are less efficient.

Lifetime of discharge lamp can be improved by elimination of electrodes. Induction and sulfur lamps are electrodeless discharge lamps. The lifetime of an induction lamp is approximately 3 to 5 times longer in comparison with other discharge lamps.

LEDs have the efficiency comparable to LPS (and it is still growing), lifetime comparable to induction lamps, and color rendering comparable with fluorescent and metal halide (MH) lamps. Thus, at the moment the LED technology is most efficient and most promising among other considered artificial light sources.

1.2. Topicality

Increasing energy consumption may have a strong impact on climate change due to greenhouse gases. At the same time, the shortage of primary energy sources is predicted in the near future, as well as the increase in the cost of electric energy due to implementation of new power plants on renewables [5]. This encourages researchers for new studies in the field of efficiency improvement for all kinds of electric devices, and the lighting systems are not an exception.

To date, LED lighting is gaining popularity and is becoming more and more common in lighting fixtures and lighting systems for different applications due to the many advantages in comparison with other lighting technologies [6], [7]. Also, in accordance with government directives and acts of many countries [2], [3], the production and sale of conventional incandescent bulbs used for general purpose lighting is banned (with some exceptions), but the halogen lamps will be phased out in the near future (in several years).

The main advantages of LEDs are high efficacy, high reliability and long life, convenient dimming possibilities for the smart lighting systems, as well as solid casing, which improve mechanical robustness. However, the proper supply as well as thermal and optical design is crucial to gain all the benefits of solid-state lighting SSL. All these aspects are more or less considered in the framework of the present Doctoral Thesis as they are closely related, but the main attention is paid to the part of LED lamp, which ensures proper supply of LED and the control of luminous flux — LED driver.

The ballast is also the weakest node of the luminaire. Thus, the ballast determines the reliability of whole luminaire to a great extent. It also determines the quality of the light, which depends on a dimming method to a great extent.

According to [8]-[12], LED is a powerful instrument for use in smart lighting systems to improve the efficiency and quality of lighting.

1.3. Main Hypotheses and Objectives

Hypotheses

1. The accuracy of fluent light regulation can be improved by the compensation of nonlinearities of LED (volt-ampere, lumen-ampere curves) with nonlinearity of driver.
2. Direct LED current regulation can be implemented on the basis of non-inverting buck-boost converter.

Objectives

1. To find the appropriate converter topology and/or operation mode of the converter for the compensation of nonlinearity of the LED load.
2. To evaluate controllability parameters and efficiency of the proposed converters.
3. To synthesize a practical solution of direct current control converter.
4. To develop hardware part of the direct current control converter.
5. To develop control system for the direct current control converter.

Means and methods of research

In order to simplify the process of theoretical calculations and graphically represent the obtained results, the Mathcad and MS Excel programs have been used. Additionally PSIM and LTspice have been used for simulation of electrical circuits.

The experimental verification of obtained results has been performed on the test bench in a laboratory (Appendix C). The configuration of the test bench depends on the test carried out, but the main elements are laboratory DC power supply with the constant current function, function generator capable of providing a control signal at different frequencies and duty cycles, precision power analyzer, one or several oscilloscopes, thermographic camera, luxmeter and configurable LED load (usually consisting of 7 high-power LEDs connected in series). Linear or polynomial interpolation has been used for graphical representation of the results of experiments.

IAR Embedded Workbench software has been used for the programming and debugging of MSP430 series microcontrollers. Printed circuit board designs have been developed using OrCAD software.

Scientific Novelties

1. Tapped-inductor buck converter has been used for the first time to compensate nonlinearities of LED, thus improving controllability parameters of the driver.
2. Discontinuous conduction mode of DC-DC converter has been used for the first time utilized to compensate nonlinearities of LED, thus improving controllability parameters of the driver.
3. Non-inverting buck-boost converter with double closed loop control has been used for the first time to operate in a direct current regulation mode, thus increasing dimming resolution of the driver.
4. A new control algorithm has been developed for non-inverting buck-boost converter. It allows obtaining the direct current control.

Practical Novelties

1. The technique for calculation of optimal turns ratio of tapped-inductor fitter-buck converter for the compensation of nonlinearity (improvement of controllability) of LED load has been proposed. A version of design for such a converter has been developed.
2. The energy efficient current measurement approach for the tapped-inductor converter has been implemented.
3. Parameters of switching frequency, duty cycle, and inductance for the compensation of nonlinearities of LED have been formulated using the converter in a discontinuous conduction mode.
4. Microcontroller based control system for non-inverting buck-boost has been implemented to obtain the properties of the converter with the direct current control.

Practical application of research results

The presented prototypes of tapped-inductor fitter-buck based LED dimmer and non-inverting buck-boost converter with direct current control can be easily re-designed (equipped with an appropriate communication module) for market-ready solutions. Additional standard conversion blocks (rectifier with input filter, power factor corrector, DC/DC converter) are necessary for the ballast sourced from the AC power grid. The typical application could be high and middle power LED lamps, such as street and park lighting lamps. The considered converters can be used in a direct way with the low voltage DC grid (nanogrids for households of the future [13]).

1.4. Dissemination of Research Results

There are 34 author's publications and 1 patent, in total. The following 11 publications, including 1 patent, are presented in the Doctoral Thesis:

1. **O. Tetervenoks**, «Reduction of Power Losses in Measurement Subsystem for Tapped-Inductor Based LED Driver, » in *Proceedings of the 15th European Conference on Power Electronics and Applications (EPE 2013)*, 2013, pp. 1-9.
2. I. Galkin and **O. Tetervenoks**, «Tapped-Inductor Converter for Dimmable Light-Emitting Diode Driver,» in *Proceedings of 4th International Conference on Power Engineering, Energy and Electrical Drives (POWERENG 2013)*, 2013, pp. 1307-1311.
3. **O. Tetervenoks**, «Choice of Power and Control Coupling Elements for Dimmable LED Driver for Smart Lighting Networks,» in *Proceedings of the 39th Annual Conference of the IEEE Industrial Electronics Society (IECON 2013)*, 2013, pp. 940-5944.
4. I. Galkin and **O. Tetervenoks**, «Validation of direct current control in LED lamp with non-inverting buck-boost converter,» in *39th Annual Conference of the IEEE Industrial Electronics Society (IECON 2013)*, 2013, pp. 6021-6026.
5. **O. Tetervenoks** and I. Milashevski, «Dimmable LED Drivers Operating in Discontinuous Conduction Mode,» *Electr. Control Commun. Eng.*, vol. 2, no. 1, pp. 27-33, 2013.
6. **O. Tetervenoks** and I. Galkin, «Assessment of Switch Mode Current Sources for Current Fed LED Drivers,» in *Technological Innovation for Collective Awareness System: 5th IFIP WG 5.5/SOCOLNET Doctoral Conference on Computing Electrical and Industrial Systems*, L. M. Camarinha — Matos, N. S. Barrento, and R. M. (Editor), Eds. Berlin: Springer Berlin Heidelberg, 2014, p. 621.
7. **O. Tetervenoks** and I. Galkin, «Assessment of Light Fluctuations of LED Lamp at Different Pulse Mode Regulation Methods,» *Elektron. ir Elektrotechnika*, vol. 20, no. 6, pp. 42-45, 2014.
8. I. Galkin and **O. Tetervenoks**, «Efficiency considerations for non-inverting buck-boost converter operating with direct current control,» in *2014 16th European Conference on Power Electronics and Applications*, 2014, pp 1-8.

9. **O. Tetervenoks** and I. Galkin, «Considerations on Practical Implementation of Control System for Switch Mode Current Regulator,» in *Proceedings of 14th Biennial Baltic Electronics Conference (BEC2014)*, 2014, pp. 225-228.
10. **O. Tetervenoks** and I. Galkin, «Evaluation of Stability of Several LED Drivers in Smart Lighting Applications,» in *Proceedings of 55th International Scientific Conference on Power and Electrical Engineering of Riga Technical University (RTUCON2014)*, 2014, pp. 48-51.
11. I. Galkin, **O. Tetervenoks**. Adjustable electronic current source with doubled current stabilization. Latvian patent. Nr. LV14796. 2014.04.20

2 LED LIGHTING TECHNOLOGIES

2.1. Introduction

As mentioned previously, LEDs are the heart of modern lighting system. They are efficient and robust by themselves; however, they are not capable to operate directly from the power grid: some kind of the ballast (LED driver) is necessary for their proper operation. Thus, the overall efficiency as well as reliability is determined by the LED — driver combination. Besides, driving technique and dimming technique may to a great extent affect the efficiency of whole lighting system as well as some optical characteristics (light quality). This chapter starts with a very brief introduction of photometry and properties of the human vision in order to quantify these optical characteristics.

In the framework of this work a lot of time and effort was spent on the studies of LED properties, existing driving techniques, dimming techniques and the problems related with them.

Another point is the control gear of the LED lamp (including communication module), which usually is incorporated in driver or is closely related and interacts with it. It applies additional costs to the driver. Just a few years ago the price of LEDs was a major part of the lamp costs [14]. However, the price of LEDs gradually reduces [15], [16] and now for low power and middle power lamps the major part of price is driver costs (especially for smart lighting systems). Thus, particular attention should be paid on the simplification of control system and reduction of initial costs of the driver.

The chapter is devoted to the studies on topics discussed above and takes a significant part of the work. Although this chapter can be considered as literature review and is not directly related to the main hypotheses, in most cases it includes deeper analysis, as well as experiments, making a stable base for the main research topic.

2.2. Light Quality

Color Temperature

There are many different ways to represent color of the light source. CIE XYZ values give full color and luminance information, while x and y values of chromaticity diagram give full color information, eliminating luminance information (Appendix D). In general, white color lighting is used for illumination. Therefore, it is more convenient to use one simple parameter to describe color hue of white light. The temperature of blackbody radiator has become a standard for this purpose. The blackbody spectrum was first derived by Max Planck and is described by the following equation

$$I_{black}(\lambda,T) = \frac{2hc^2}{\lambda^5 \cdot \left[e^{(hc/\lambda kT)} - 1\right]} \tag{2.1}$$

with dimensions of power per solid angle per area per wavelength [W/(sr·m^2·m)], or

$$I_{black}(\lambda,T) = \frac{8\pi hc^2}{\lambda^5 \cdot \left[e^{(hc/\lambda kT)} - 1\right]} \tag{2.2}$$

with dimensions of power per area per wavelength [W/(m^2·m)], where c is the speed of light in vacuum ($c = 299792457$ [m/s]); h is the Planck's constant ($h = 6.62606896 \cdot 10^{-34}$ [J·s]); k is the Boltzmann's constant ($k = 1.3806504 \cdot 10^{-34}$ [J/K]); T is the temperature in Kelvin degrees [K] [17], [18], [20].

The example of blackbody spectral irradiance at different temperatures is given in Fig. 2.1. Depending on temperature, the peak (and dominant value) of irradiance moves over the whole range of visible wavelengths, changing the hue of the white light (as shown in Appendix D Fig. 6.5 (b)): red hue at peak on longer wavelengths (lower temperatures of blackbody) and blue hue at peak on shorter wavelengths (higher temperatures of blackbody). It can be represented as a curve on chromaticity diagram (Appendix D Fig. 6.5 Fig. 6.5 (b)). This curve is called Planckian locus or blackbody locus.

The place of the point on chromaticity diagram, which represents the color of the white light source, not always falls on the blackbody locus. Therefore the concept of *correlated color temperature* (CCT) was also defined. Correlated color temperature is temperature of blackbody radiator whose color is closest to the color of the white light source. Geometrically correctly it can be determined on CIE 1976 (u′, v′) chromaticity diagram. CIE 1931 (x, y) chromaticity diagram is inappropriate for determination of correlated color temperature [17], [21].

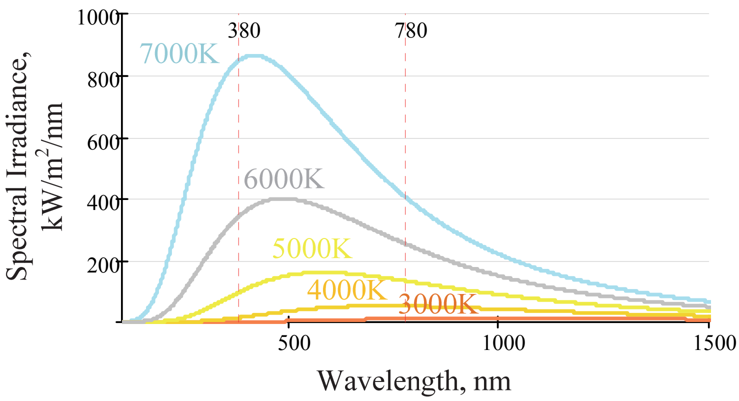

Fig. 2.1 Spectral irradiance of blackbody at different temperatures.

Color bins are defined as parallelograms in the 1931 CIE (x, y) color space. These parallelograms are sized and oriented to approximately enclose a MacAdam ellipse whose center is at a particular blackbody radiator locus. LED binning is defined by American National Standards Institute (ANSI) in the C78.377-2008 standard (7 parallelograms). In Fig. 2.2 four of seven ANSI C78.377-2008 parallelograms and subdivided color bins of a particular LED manufacturer are given [21], [22]. Mixing LEDs from different bins allows achieving light color between these bins.

Color rendering

In the International Lighting Vocabulary [23] the CIE defines the color rendering as "Effect of an illuminant on the color appearance of objects by conscious or subconscious comparison with their color appearance under a reference illuminant."

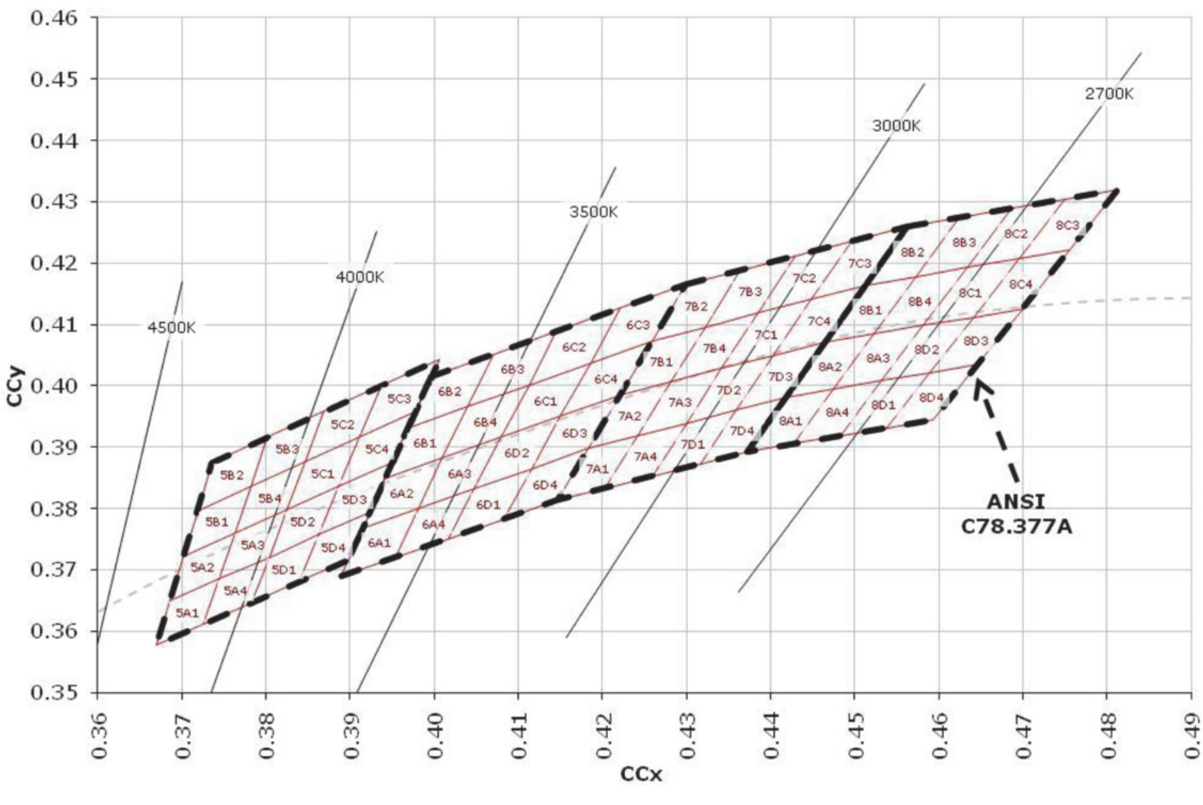

Fig. 2.2 Four ANSI C78.377-2008 parallelograms and subdivided color bins of a particular LED manufacturer (Cree Inc.) [21], [22].

Color rendering index (CRI) is defined as being the measure of the degree of color shift of an object when illuminated by a light source as compared to when illuminated by a reference source of comparable color temperature. Color rendering index mathematically compares how a light source shifts the location of eight specified pastel colors as defined by CIE compared to the same colors lit by a reference source of the same color temperature by subtraction of average differences from 100. It means the small differences in color appearance between the reference colors illuminated by the light source under test and reference illuminant leads to high color rendering values (close to 100) [24].

However, there are many problems and restrictions in CRI measurements. The first and the most difficult problem of this definition is that it requires "a reference illuminant," but leaves the selection of the reference light source open [18]. When comparing color temperatures ranging from 2000 K to 5000 K the reference source is a blackbody radiator. The reference source for color temperature above 5000 K is daylight [18], [24]. Therefore, CRI is not an ideal measure to evaluate color appearance under particular illumination.

CIE Technical Report 177:2007 [25] states, "The conclusion of the Technical Committee is that the CIE CRI is generally not applicable to predict the color rendering rank order of a set of light sources when white LED light sources are involved in this set" [26]. New metrics — *color quality scale* (CQS) — was developed at the National Institute of Standards and Technology (NIST) to define and better qualify LED lighting [27]. CQS involves several facets of color quality, including: color rendering, chromatic discrimination, and observer preferences. The main differences from CRI are the following: 1) it takes into account subjective color saturation perception; 2) it measures color fidelity with regard to color saturation preferences; 3) the moderate increase of saturation is often correlated with desired color perception [27], [28].

In 2010 Lighting Research Center (LRC) published a new volume in the ASSIST Recommends Series. It defines a two-metric approach for comparison of light sources for good quality illumination and color rendering [29]. The volume includes two issues: "Guide to light and color in retail merchandising" [30] and "Recommendations for specifying color properties of light sources for retail merchandising" [31]. ASSIST recommends using CRI along with a new metric called *gamut area index* (GAI) [29]. GAI is a good indicator of saturation, while CRI evaluates fidelity. Using CRI and GAI together can ensure good color rendering (properly evaluate such parameters as vividness, naturalness, and acceptability) [28]-[31].

Light Fluctuations

Flickering is the light fluctuations that can lead to unsteadiness of human vision. Visual perception of flicker can be characterized in two ways: a) direct perception of flickering at frequencies < 80 Hz; b) indirect perception of a stroboscopic effect [32]. According to the latest studies, direct perception of flickering can lead to a different kind of hallucinations depending on frequency of flickering [33]. The International Electrotechnical Commission (IEC) has defined the standard instrument for the measurements of light flicker (IEC flickermeter). Functional block diagram of this instrument is shown in Fig. 2.3 [34]. Detailed description of the blocks shown in Fig. 2.3 is described in [35].

The flickermeter provides the insight about the impact of flickering on the human brain. The output of this device is the Instantaneous Flicker Sensation (IFS) expressed in perceptibility units. The instrument makes assessment of flickering in indirect way by measuring the voltage fluctuations and then predicting the light flux pulsations of the standard 60W/230V incandescent lamp (block 2) and human eye-brain chain (blocks 3-5) which is not suitable for the new lighting technologies. Therefore, in [36] the new approach is described by measuring luminous flux fluctuations in direct way from light sensor (photodiode) which is suitable for all kinds of lamps.

Objects may appear to move discretely rather than continuously under flickering illumination; this is known as a *stroboscopic effect* (can be perceived by human eye indirectly). The magnitude of the effect depends on the rate and amplitude of the flicker, the rate of object motion, and the viewing conditions [32].

To quantify the stroboscopic effect first of all it is necessary to define photometric flicker quantities. According to [37], lighting experts have proposed and used two metrics for this purpose.

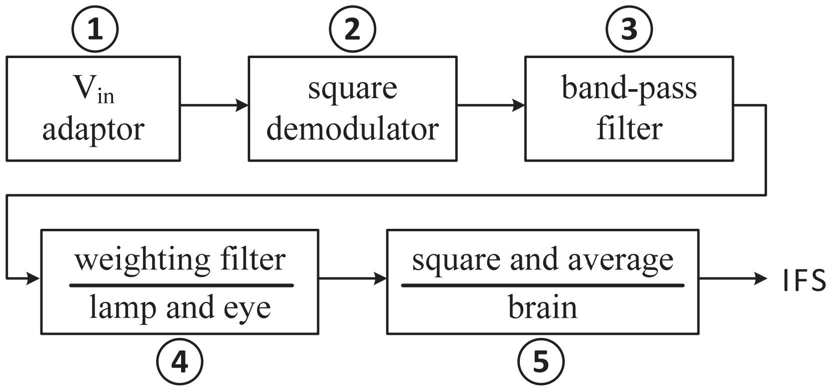

Fig. 2.3 Block diagram of IEC flickermeter.

First and the best known is percent flicker *P*. It describes peak-to-peak contrast and can be expressed by equation

$$P = \frac{A - B}{A + B} \cdot 100\% \tag{2.3}$$

where *A* is the maximum value of periodical waveform of light output (can be in relative units) of the lamp, but *B* is the maximum value of this waveform as shown in Fig. 2.4 [37].

The second is the flicker index I which is more reliable than percent flicker when comparing periodic waveforms with different shapes or duty cycles. The expression of flicker index is

$$I = \frac{Area1}{Area1 + Area2} \cdot 100\% \tag{2.4}$$

where *Area1* is the area enclosed by the average value line and the waveform above this average value, but the *Area2* is the area enclosed by the average value line and the waveform below this average value as shown in Fig. 2.4 [37].

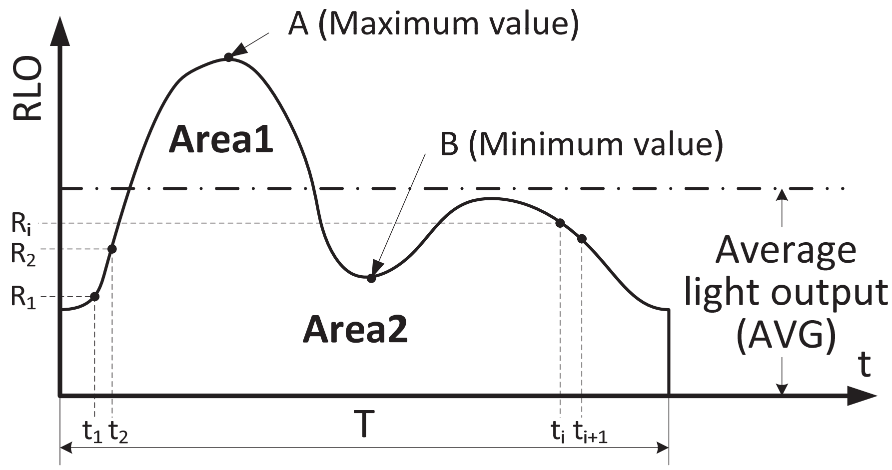

Fig. 2.4 Example of relative light output (RLO) variation from a lamp during one period and the explanation of method for calculation of percent flicker and flicker index.

Detection of the stroboscopic effect (percent likelihood of detection d, in percent) for rectangular waveforms operated so that the maximum light output is produced 50 % of the time and the minimum light output is produced 50 % of the time (50 % duty cycle), has been described in [32] by the equation

$$d = \frac{25P + 140}{f + 25P + 140} \cdot 100\% \tag{2.5}$$

where f is the frequency of analyzed waveform and P is the percent flicker of this form.

For the data sequence taken from the light sensor by measurement instrument, for example, by oscilloscope, the expression of the flicker index I can be expressed as:

$$I = \left(\sum_{n=0}^{N-1} \left| AVG - R_n \right| \right) \Bigg/ \left(2 \cdot \sum_{n=0}^{N-1} R_n \right) \tag{2.6}$$

where R_n is the sequence of samples from light sensor during period T, N is the number of samples in one period, but AVG is the average value of the waveform, which can be found from

$$AVG = \frac{1}{N}\sum_{n=0}^{N-1} R_n \quad (2.7)$$

It should be noted that (2.6) and (2.7) are true if the time interval between measured points of data sequence is constant ($\Delta t = t_n - t_{n+1} = const$).

Considered above light quality parameters can be affected by selected dimming approach.

2.3. White Light Producing Methods Used in LEDs

In general there are three ways how to generate white color light using LEDs: wavelength conversion, color mixing, and homoepitaxial ZnSe technology.

In case of **wavelength conversion** blue or UV emission of LED is used to excite phosphor(s) or quantum dots, coated on the upper part of LED. The emitted light of LED can be converted completely or partially depending on the used approach. Blue LEDs are usually covered with yellow or several color phosphors, and the original blue light is mixed with the light produced by these phosphor(s) resulting in white light. Also, UV LED can be used with red, green, and blue phosphors. The use of several phosphors improves light quality making a wavelength spectrum broader, but at the same time also increasing manufacturing costs in comparison with blue LED — yellow phosphor approach [38].

Another example of wavelength conversion is use of quantum dots in blue LED. Blue light emitted by LED excites the quantum dots, which are extremely small semiconductor crystals. The quantum dots represent a thin layer of nanocrystal particles that contain 33 or 34 pairs of cadmium or selenium and are coated on top of the LED. This results in generation of white light with the wavelength spectrum similar to the ultraviolet LED that uses RGB phosphors [38].

Color mixing approach utilizes mixing of emission of monochromatic LEDs. At least two different color LEDs are necessary to obtain white light. Color mixing mechanisms and schematic examples are shown in Fig. 2.5. CIE (International Commission on Illumination) 1931 (x, y) chromaticity diagrams are shown in this figure, and any color light source can be represented as a single point on these diagrams (the coordinates of white light are $x = 0.33$ and $y = 0.33$). The spectrum of different color light sources can be additively mixed. It means that any color lying on the straight line between two color points on chromaticity diagram (Fig. 2.5

(a)) or any color inside the figure formed by color many color points (Fig. 2.5 (b)) can be achieved. Blue and yellow or red, green and blue combinations are usually used in additive color mixing to obtain white light. However, the quality of white light can be improved by increasing the number of different color monochromatic LEDs. This approach has several advantages such as potentially high efficacy (no loss of energy during conversion process) and the possibility to adjust color temperature [38].

The main drawback is different forward voltage for different color LEDs, which means separate supply for each monochromatic LED group.

The third method is based on mixing of blue-green color emission from ZnCdSe quantum well and a yellow emission from ZnSe substrate (**homoepitaxial ZnSe)**. This type of LEDs is less suitable for general lighting. However, they are being used in a range of applications such as indicators and backlights, in thin film electroluminescent display (TFEL). The studies in this field show that there is a possibility to create color tunable (by applied voltage) LED [38], [39].

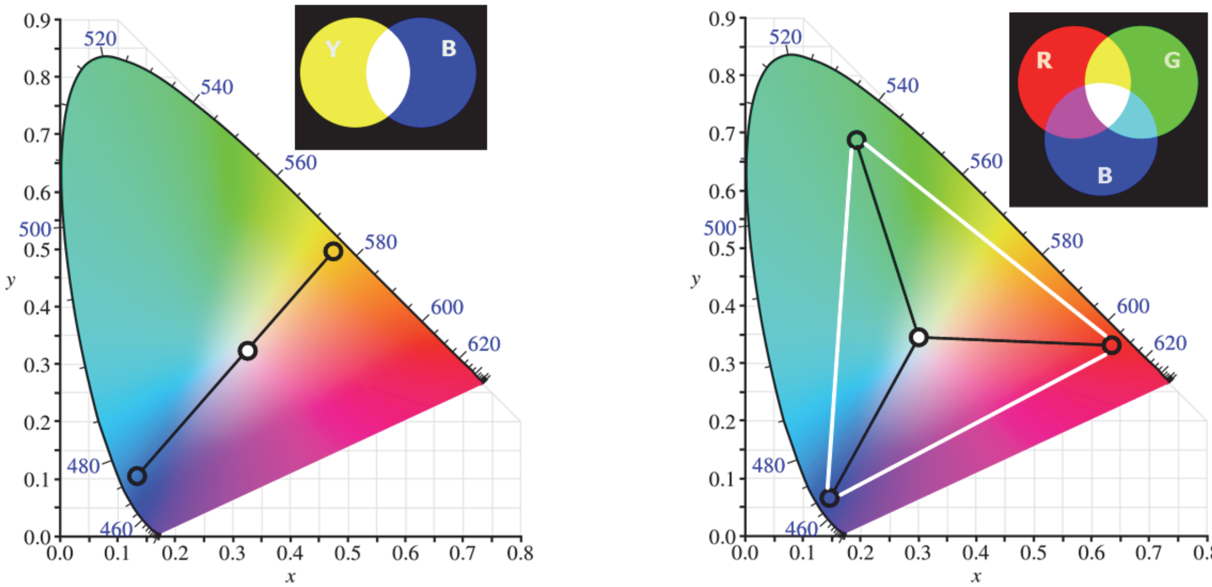

a) b)

Fig. 2.5 Color mixing to obtain white light: a) mixing two colors — blue and yellow; b) mixing three colors — red, green and blue.

The most common manufacturing technology of high power LED today is blue LED with yellow or several color phosphors. So, it is worth taking a closer look at the process of production of this type of LEDs.

2.4. Production and Binning of White LEDs

During the production of the most common white LEDs (blue LED with phosphor), a single round wafer is coated with various materials (the process is known as epitaxial growth) using metalorganic chemical vapor deposition (MOCVD) reactor to create the semiconductor, which is the base of blue LED. This is most expensive and time consuming process. Then this wafer is sliced into very small rectangles (dies). After that the die is encapsulated making the package of LED and adding electrical connections (wire bonds) between the case and die. Phosphors are added either as a coating or suspension.

Both processes (epitaxial growth and attachment of phosphors) have significant variations that impact the performance of LEDs (uncertainty in light output, color temperature, and forward voltage). Even making huge investments LED manufacturers are unable to create highly consistent products. Therefore, the LED manufacturers use especial approach — they sort their products into lumen, color and voltage bins, giving the opportunity for luminaire manufacturers to select and use the products with known characteristics. Also, it is worth keeping in mind the these variable electrical parameters during the development of LED driver.

Each bin is usually defined as a range of expected parameters. It is worth mentioning that all the binning is done at nominal current and junction temperature $T_j = 25°C$ [40], [41].

2.5. Electrical Properties and Mathematical Model of LED

Mathematical model of LED is necessary to define the properties of the load connected to the power supply. LED is semiconductor device, the electrical properties of which can be in the best way described by voltage-current (V-A) curve. A typical LED V-A curve is shown in Fig. 2.6 (a).

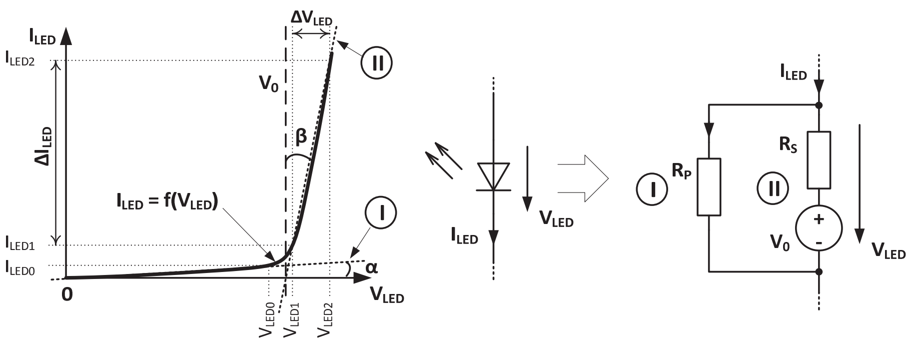

(a) (b)

Fig. 2.6 Definition of mathematical model of LED: a) typical LED voltage-current curve; b) the simplest equivalent circuit.

The simplest equivalent circuits for separate sections of LED V-A curve are shown in Fig. 2.6 (b), but the complete voltage-current relationship can be expressed by the following equation:

$$I_{LED} - \frac{(V_{LED} - I_{LED}R_s)}{R_P} = I_S \cdot e^{e(V_{LED} - I_{LED}R_S)/(n_d k T_j)}, \tag{2.8}$$

where I_{LED} - forward current of LED, I_S - reverse bias saturation current, V_{LED} - diode forward voltage, n_d - diode ideality factor (for ideal diodes it is equal to 1, for real diodes the value of this factor is between 1,1 to 1,5), k - Boltzmann's constant, T_j - temperature [17]. R_P is equivalent parallel resistance of LED (Fig. 2.6 (b)), which in fact is slope of V-A curve in range of $0 \ldots V_{LED0}$ that can be expressed as

$$R_p = ctg\alpha = \frac{\Delta V_{LED}}{\Delta I_{LED}} = \frac{V_{LED0}}{I_{LED0}} \tag{2.9}$$

but R_S is equivalent series resistance of LED. Resistance R_S is slope of V-A curve in range of $V_{LED1} \ldots V_{LED2}$ that can be written as follows:

$$R_S = tg\beta = \frac{\Delta V_{LED}}{\Delta I_{LED}} = \frac{V_{LED2} - V_{LED1}}{I_{LED2} - I_{LED1}}. \tag{2.10}$$

So, for simplified calculation parallel resistance R_P can be neglected then the relationship between the LED forward voltage and current can be expressed as:

$$V_{LED}(I_{LED}) = V_0 + R_S \cdot I_{LED} \tag{2.11}$$

For the analysis with experimentally measured points of V-A curve either linear interpolation or polynomial fitting function is used in this work. The expression for the linear interpolation is:

$$I_{LED}(V_{LED}) = I_{LED\,n} + \frac{V_{LED} - V_{LED\,n}}{V_{LED\,n+1} - V_{LED\,n}}\left(I_{LED\,n+1} - I_{LED\,n}\right), \tag{2.12}$$

where I_{LED} is the forward current of LED load at the corresponding forward voltage V_{LED} arbitrary selected between two known (measured) points $I_{LEDn}(V_{LEDn})$ and $I_{LEDn+1}(V_{LEDn+1})$.

The expression for the polynomial fitting function is:

$$I_{LED}(V_{LED}) = a_0 + a_1 \cdot (V_{LED} - V_0) + a_2 \cdot (V_{LED} - V_0)^2 + \ldots + a_n \cdot (V_{LED} - V_0)^n, \tag{2.13}$$

where a_0, a_1, a_2 and a_3 are the polynomial coefficients for the explored LED(s) selected for correct appearance of experimental data [8].

If V-A curve of one LED is expressed by the equation in form $I_{LED}=f(V_{LED})$, then the relationship for the matrix connection of these LEDs can be found from

$$I_{LED} = l \cdot f\left(\frac{V_{LED}}{k}\right) \tag{2.14}$$

where k is the number of LEDs connected in series, but l is the number of LEDs connected in parallel.

2.6. Thermal and Optical Properties

LEDs are stated as current consumers rather than voltage consumers. This means the dependence of relative light output (RLO) of LED from its forward current is more pronounced than from LED voltage. RLO is value in relative units or percent, which is normalized at nominal (test) point of LED. At the same time the parameters for the test point are usually well defined in datasheets, thus the lumen-ampere (Lm-A) dependency easily can be found. The typical relationship between LED forward current and produced light amount is given in Fig. 2.7. It is clearly seen from Fig. 2.7 that light amount produced by LED is not proportional to the forward current of LED. If the appropriate heat sink is applied, LED can operate at higher current. However, due to nonlinearity of Lm-A relationship (deviation of blue Lm-A curve from dashed linear function in Fig. 2.7) the efficacy as well as the lifespan of LED decreases when operating at higher currents. In most part this effect is caused by increased junction temperature of the LED (Fig. 2.7 (a) and Fig. 2.8).

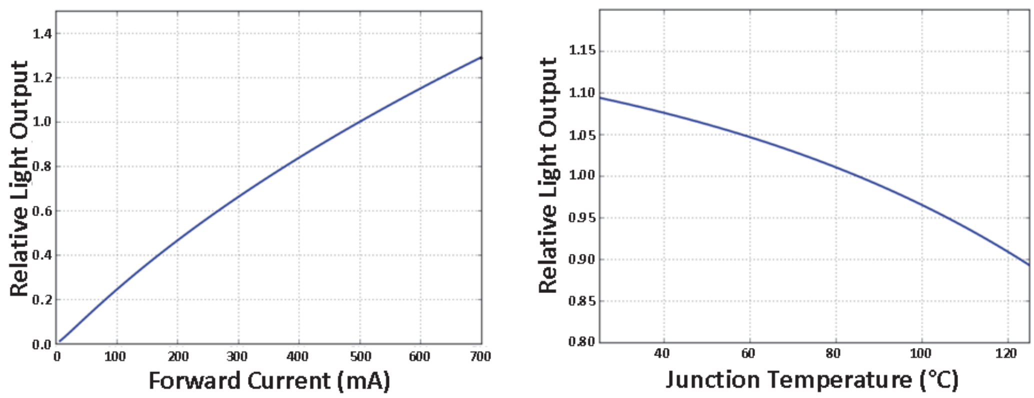

(a) (b)

Fig. 2.7 Typical curves of high power LED: a) lumen-ampere relationship; b) relationship between the relative light output and junction temperature [42].

Junction temperature of the LED depends on applied power (forward current) and the ability of the heat sink to transfer heat from junction to ambient. At the same time the temperature of LED junction has significant influence on LED performance (Fig. 2.7). On one hand, it is possible to use fewer LEDs at higher current decreasing initial costs in this way.

On the other hand, the temperature of LED junction increases, but the efficiency and the lifetime (Fig. 2.8) decreases at higher currents, thus increasing the maintenance costs.

The search of trade-off between initial and maintenance costs is not a trivial task for a lighting engineer. The reference point at the beginning of the design could be the foreseen lifetime of the LED lamp, and then the maximum allowable junction temperature can be determined from the relationships given in LED datasheet (Fig. 2.8).

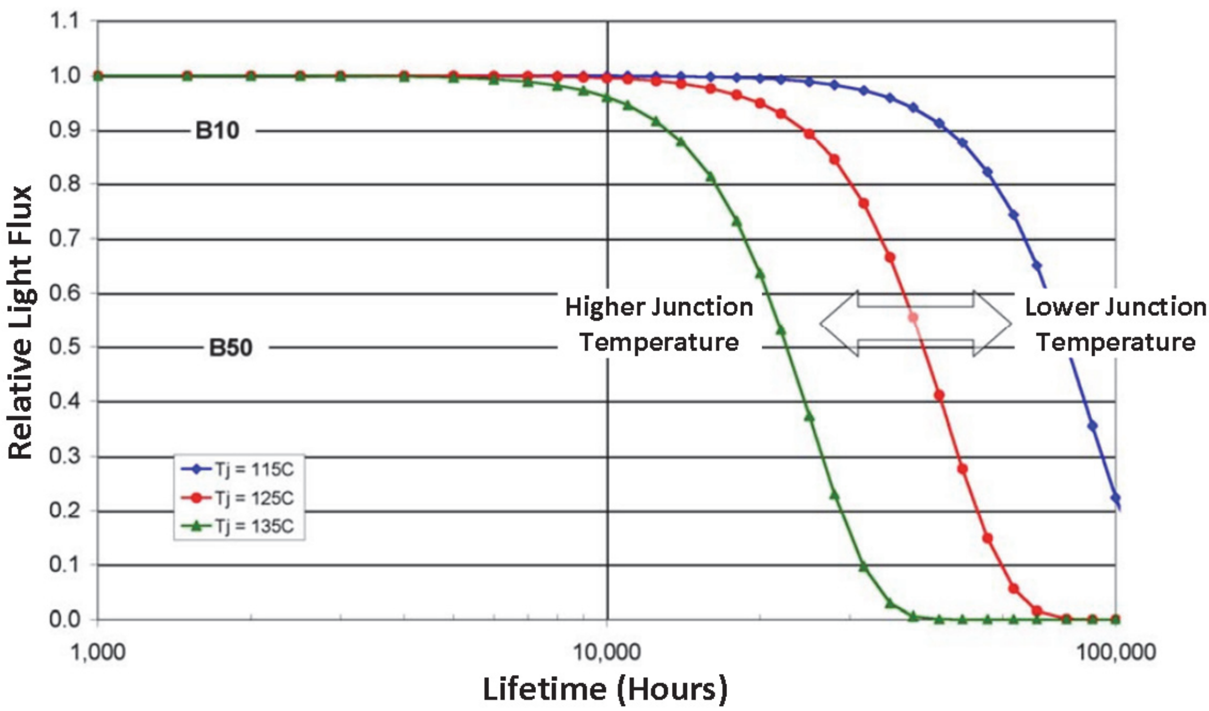

Fig. 2.8 Influence of the junction temperature on the lifetime of LED [43].

The allowable power applied to the LED can be determined knowing the desired LED junction temperature T_{jmax}, the properties of the LED lamp (Fig. 2.9) and the operation conditions (ambient temperature T_a, velocity of airflow etc.):

$$P_{LED} = kP_{heat} = k\frac{T_{j\max} - T_a}{R_{j-a}}, \tag{2.15}$$

where k is the coefficient that characterizes efficacy of LED ($k \approx 1.1 \ldots 1.2$), P_{heat} is the power released by LED in heat form, R_{j-a} is the thermal resistance of whole heat transfer system.

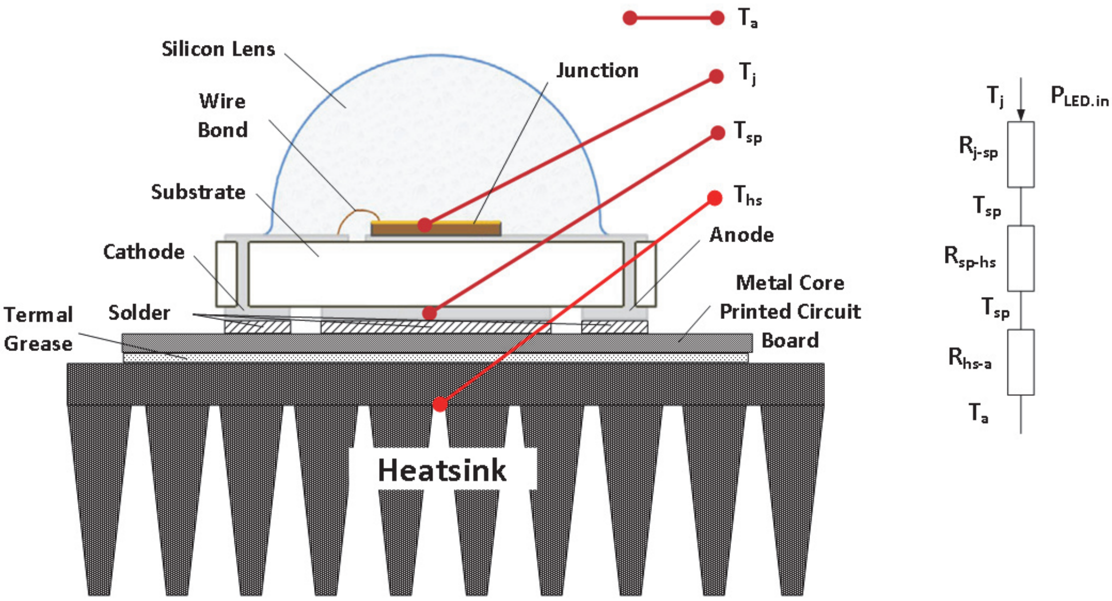

Fig. 2.9 Heat transfer way from LED junction to the ambient.

2.7. Configurations of the LED Light Sources

Usually one LED is not capable to deliver the necessary light amount for the particular application; therefore, one lighting fixture incorporates several LEDs. Three different connection types are possible: parallel connection, series connection, and matrix connection. This section provides information about the appropriate LED connection types for constant voltage and constant current sources.

Parallel connection (Fig. 2.10 (a)) is the least suitable for any type of LEDs. Theoretically, parallel connection of the LEDs may be used to increase allowable forward current of the light source combined of these LEDs (Fig. 2.10 (b)).

In practice there are a lot of restrictions for parallel connection. LED production is complicated industrial process and it is very difficult to achieve the same V-A characteristics for all the LEDs (Fig. 2.11 (a)). Different V-A curves lead to non-uniform distribution of current between parallel branches. One of the branches connected in parallel will always conduct more current. This, in turn, will increase the temperature of the LED junction, thus decreasing series resistance (forward voltage) of this LED even more (Fig. 2.11 b) and increasing forward current. The process described above can rapidly damage the LED. Depending on failure type the current may increase for all leftover LEDs (open circuit failure) and the process is repeated as long as all the LEDs will fail, or in case of short circuit failure all the current will flows through failed LED. In any case the failure of one LED in parallel connection will leads to the failure of whole light source.

The problems described above can be circumvented by several methods. As mentioned previously, manufacturers are sorting LEDs in bins by forward voltage drop, efficacy, and color temperature. LEDs in parallel connection should be selected from the same voltage bin. But even the same voltage bin does not give the insurance from un-uniform current distribution, if junction temperatures of LEDs are different (Fig. 2.11 (b)). Thus, pure parallel connection (Fig. 2.10 (a)) is usually used only for the connection of several LED dies in single enclosure (thus forming high power, high current and low voltage LED). In this case all dies are located closely to one another on the same base (substrate), thus insuring the same temperature for all the LED dies (Fig. 2.12).

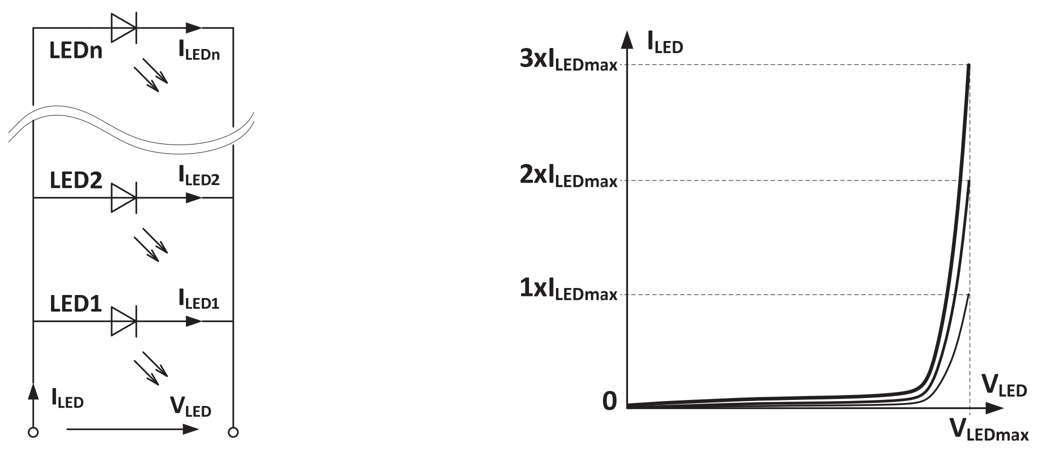

(a) (b)

Fig. 2.10 Parallel connection of LEDs: a) circuit; b) V-A curve for one, two and three LEDs in parallel connection.

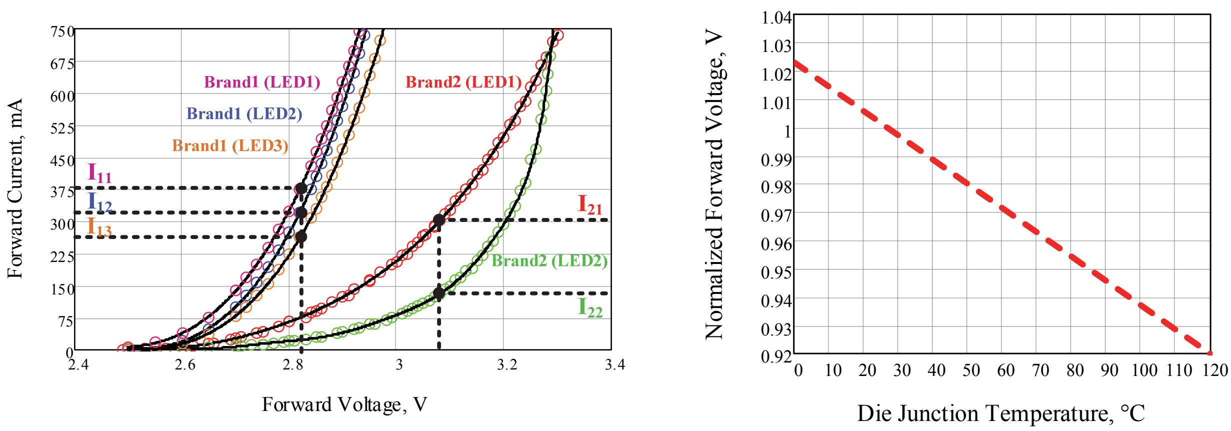

(a) (b)

Fig. 2.11 Variations of the operation current across the parallel connected LEDs: a) different V-A curves for several LEDs of the same brand (experimental data of some LED examples available in the laboratory); b) typical relationship between the forward voltage and LED die junction temperature [44].

The second approach is the additional resistance in series with LED in each parallel branch (Fig. 2.13 (a)). Additional resistance makes LED V-A curve less steep (Fig. 2.13 (b)), thus making forward current of LED "less sensitive" to the voltage changes. Despite this, it is almost impossible to achieve the same current for all the LEDs. In general case it is necessary to pick up resistance for each parallel branch which is unacceptable for industrial production. Additional resistance also leads to additional power losses.

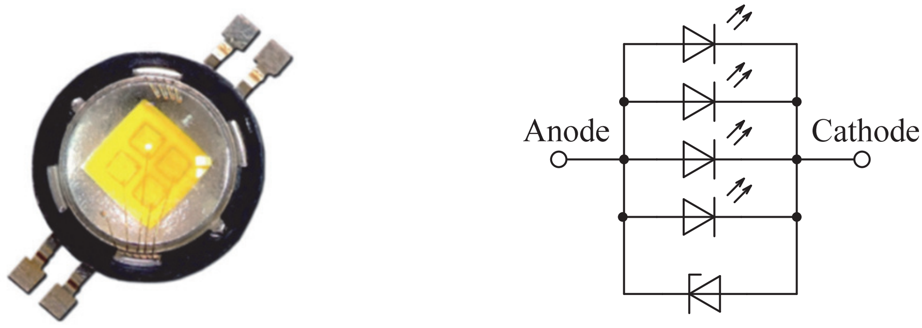

(a) (b)

Fig. 2.12 Seoul Semiconductor W724C0 P7 LED: a) high power LED enclosure; b) internal circuit — parallel connection of four LED chips and protective Zener diode.

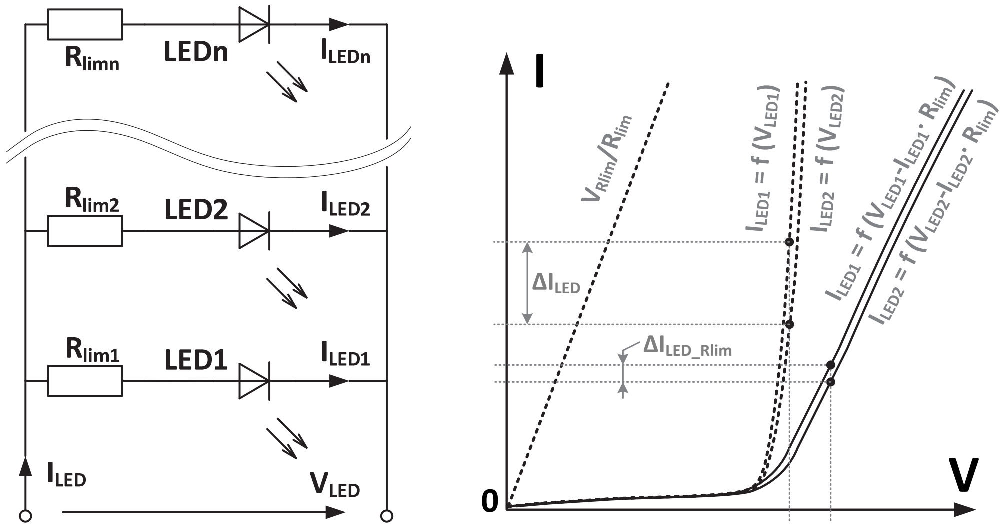

(a) (b)

Fig. 2.13 Additional resistance in series with LED in each parallel branch: a) circuit; b) resulting V-A curve for one parallel branch.

Series connection is most common and the most suitable for high power LEDs. The current is the same for all the LEDs connected in one string (Fig. 2.14) regardless of the voltage drop differences across individual LEDs. Series connection is common configuration in middle power

LED applications. In high power applications (street and park lighting) combined series parallel connection is usually used (Fig. 2.15).

For smaller power LED light sources the tradeoff between the good current distribution and the price could be combined series parallel connection with additional resistance in each parallel branch (Fig. 2.16).

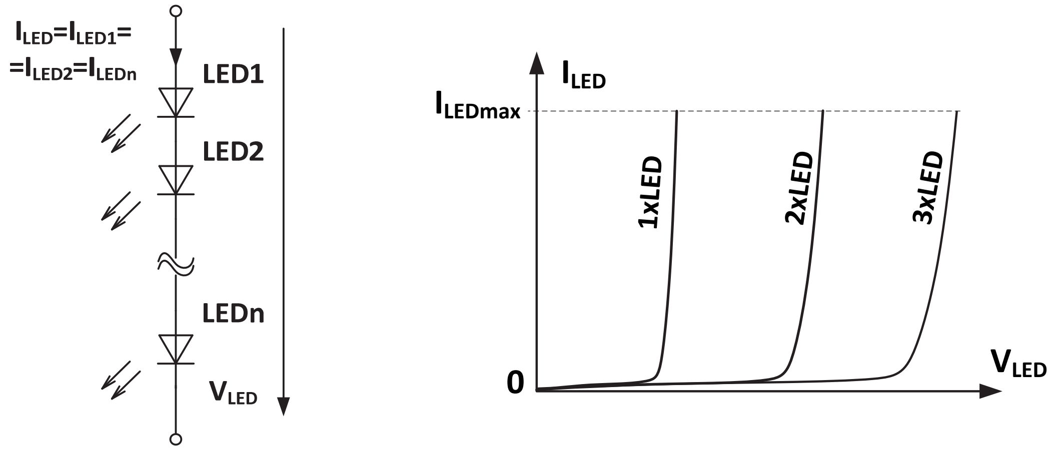

(a) (b)

Fig. 2.14 Series connection of LEDs: a) circuit; b) V-A curve for one two and three LEDs connected in series.

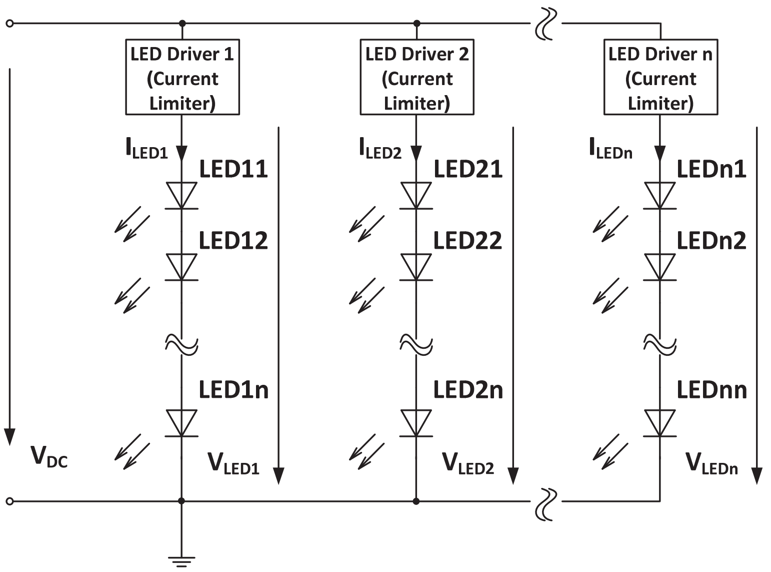

Fig. 2.15 Common configuration of high power (>30W) LED light sources.

Matrix connection is the combination of the two previously described connections. It is most suitable for small and middle power LED light sources. The failure of one LED does not have such a critical influence on the operation of the whole LED light source. In the worst case, failure of one LED will lead to failure of all the LEDs connected in parallel. However, some precautions must be taken when using this connection type. For the best performance, the LEDs connected in the matrix should be selected from the same voltage bin. Common configuration of LED light source combined of LEDs connected in matrix is shown in Fig. 2.17.

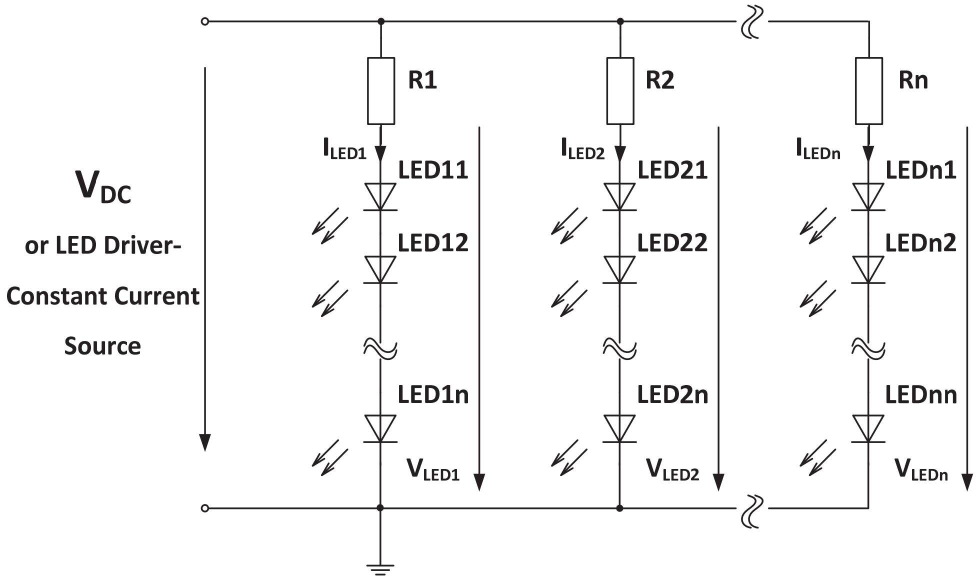

Fig. 2.16 Combined series parallel connection with additional resistance in each parallel branch.

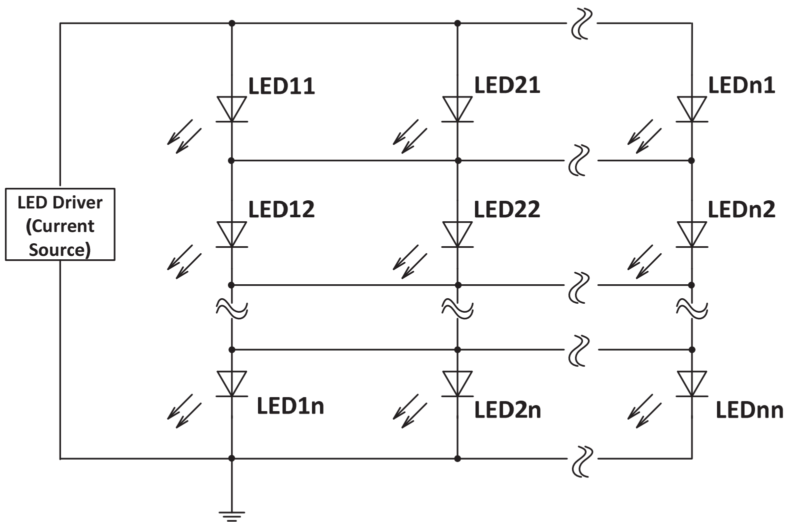

Fig. 2.17 Common configuration of LED light source with matrix connection of LEDs.

For constant voltage source the most appropriate are configurations with additional resistance in each parallel branch ((Fig. 2.13 (a) and Fig. 2.16) or current limiter in each parallel branch (Fig. 2.15). For single constant current source the most appropriate is the series connection of LEDs (Fig. 2.14) and the matrix connection of LEDs (Fig. 2.17).

2.8. Simple Current Limiting and Sharing in Parallel Branches

As mentioned previously, the series connection is most suitable for LEDs. However, the maximum voltage over the string limits the maximum power. To achieve higher power using small power devices, several strings can be connected in parallel (as shown in Fig. 2.15 and Fig. 2.16). In this case it is very important to ensure the same (or very close) current values in all the strings. Different current sharing approaches are discussed in literature. This section provides a brief overview of several the most common current limiting and sharing approaches in LED lighting applications.

Passive current limiting. The most popular passive current limiting approach for inexpensive LED applications is additional resistance in each parallel branch (description is given in the previous subsection, Fig. 2.16). This approach gives more or less acceptable results with constant voltage or current source connected to the input of this series-parallel circuit (with all the drawbacks described above). However, there is a plenty of applications, where the voltage is variable. For instance, in portable devices energy storage (voltage source) has voltage drop during discharge process. In this case the approach can't provide the same luminous flux during all the operation time: luminous flux decreases with the discharge of the battery.

Capacitor can also be used as a passive current limiting element. AC voltage is applied to the series-parallel circuit, where additional capacitor is placed in each branch. However, the anti-parallel connection of LEDs is required to achieve bi-directional current flow as shown in Fig. 2.18. The AC voltage source can be the output of the resonant converter transformer [45].

The expression, which allows finding necessary capacitor value C_n is given in [45]:

$$C_n = \frac{I_F}{2\sqrt{2} f \cdot \sqrt{V_{IN}^2 - V_{LED}^2}}, \tag{2.16}$$

where V_{IN} is the voltage of sinusoidal source (e.g. output of the resonant converter transformer), f is the frequency of this source, V_{LED} is the forward voltage drop on the LED string, I_F is the LED rated forward current.

The problem is that each string conducts only during one rectified half sine wave. Then the relationship between the average current I_{AVG} and peak current I_{PK} in each string can be expressed as:

$$I_{AVG} = \frac{I_{PK}}{\pi}, \tag{2.17}$$

where I_{AVG} acts also as a forward current of LED I_F and the rated current of LED is the limiting factor in this case [45]. Peak current exceeds the rated current, thus decreasing efficacy of LED [46], [47].

There are also other LED driver configurations, where capacitors are used for current sharing or current limiting [48], [49].

In [50] DCM operation of the converter and separate filtering inductors in each branch are used for current sharing. This approach has been presented for three fundamental converter topologies: buck, boost, and buck-boost Fig. 2.19. The operation principles are shown in the example of buck converter Fig. 2.20.

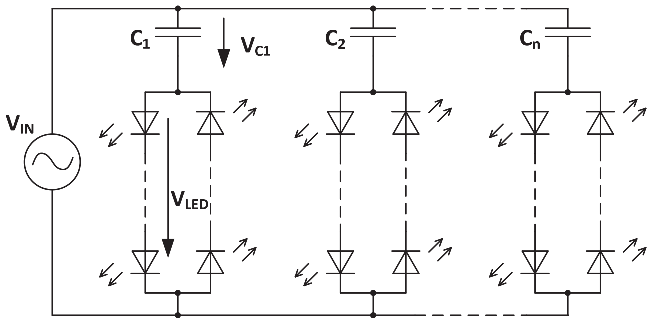

Fig. 2.18 Current sharing approach with capacitors in parallel branches

In Fig. 2.20 it is assumed that if there are no filtering capacitors, the inductor and LEDs of one string have the same current waveforms. It is shown in Fig. 2.20 that the different voltage drop over separate LED strings causes difference in current rising/falling slope and a peak current (it also means the average current). However, the current deviation due to different voltage drop over separate LED strings in DCM is much smaller than in CCM (in CCM converter output becomes pure voltage source, while in DCM it can be considered as current source) [50].

A plenty of studies on the current sharing approaches with different kind of magnetic elements (coupled inductors, transformers) can be found ([51]-[52] etc.).

Active Current Limiting

Passive current control approaches are good when the input voltage is stable. If the input voltage has a wide tolerance, the active current control is necessary to keep the same current of LEDs in the whole input voltage range.

Active current control node has several main elements and conditions to fulfill: it has regulating device (for instance adjustable linear voltage regulator), current sensor (resistor), and the feedback between both these elements, as shown in Fig. 2.21 (a) [54].

The simplest configuration for active current control is shown in Fig. 2.21 (b). In this case depletion MOSFET performs the function of a regulating device, but the current sensor is a low resistance resistor. The typical transfer characteristic of depletion mode MOSFET is shown in Fig. 2.21 (c). Depletion MOSFET is normally-on, and current flows through drain-source channel when the gate-source voltage is equal to zero $V_{GS} = 0$. The device turns off, when the gate voltage becomes negative with respect to the source as shown in Fig. 2.21 (c). The higher current value through the resistor (Fig. 2.21 (b)), the more negative becomes voltage on the gate with respect to the source, reaching MOSFET pinch-off voltage. It will appear at certain point, which can be adjusted by current sensing resistor R_{LIM}, as shown in Fig. 2.21 (c). The main drawback of this approach is the wide tolerance of the gate threshold voltage of depletion mode MOSFET (−1.5 V…−3.5 V). The advantage is the high drain-source voltage of depletion mode MOSFET, which can protect against short transients [54], [55].

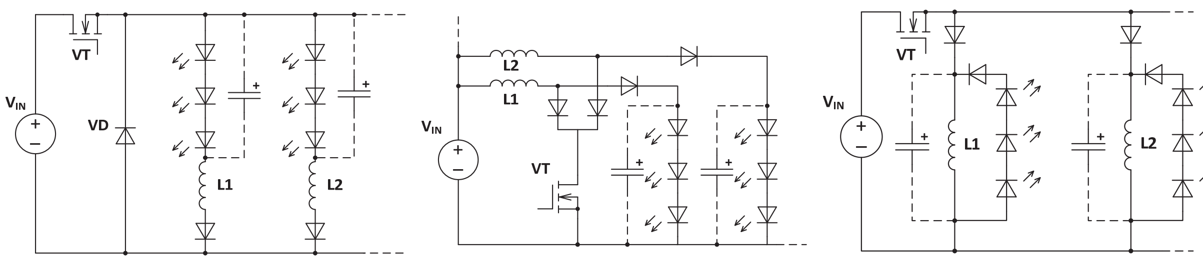

(a) (b) (c)

Fig. 2.19 Current sharing approach for fundamental converter topologies: a) electrical circuit for buck converter; b) for boost converter; c) for buck-boost converter [50].

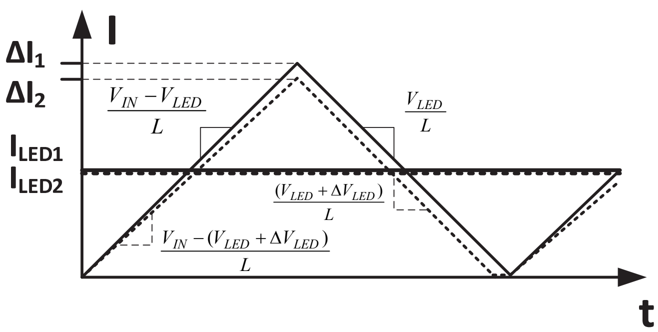

Fig. 2.20 Inductor current waveforms in two separate strings of the buck converter operating in CCM shown in Fig. 2.19 (a) [50].

Depletion mode MOSFET can be replaced by other regulating device such as adjustable linear voltage regulator, for instance LM317. The LM317 has three terminals: input “IN”, output “OUT” and feedback terminal “ADJ”. It also has an internal reference voltage source 1.25 V, which is compared with the voltage applied to “ADJ” terminal (with respect to the “OUT” terminal). If the voltage applied to the “ADJ” terminal exceeds 1.25 V, the current through LM317 reduces in this way performing current regulation [54], [56].

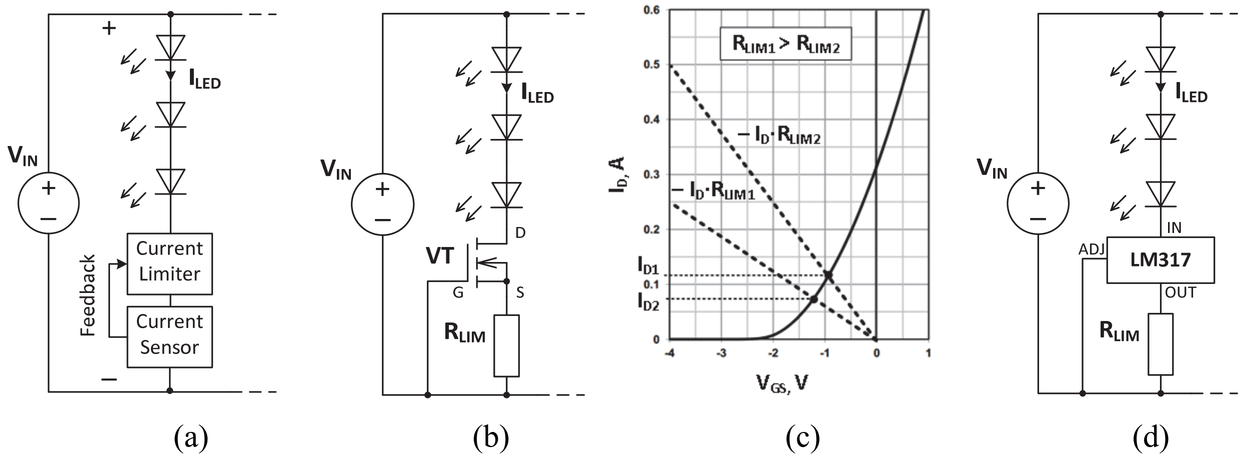

Fig. 2.21 Active current limiting: a) the main elements of active current control node; b) the simplest current limiting element — depletion MOSFET; c) typical transfer characteristic of depletion MOSFET and description of current regulation approach; d) current regulation with adjustable linear voltage regulator [54], [55].

Current mirror can be used for equal current distribution between strings, if the LED driving source performs as a current source, which provides more current than a single LED device can consume. The circuit of current mirror is shown in Fig. 2.22, where the first string determines the (equal) current of other strings.

The main drawback of all the resistive and active current limiters is power dissipation in these elements, resulting in reduction of the overall efficiency of LED lamp.

However, it is worth mentioning that all the problems with current sharing eliminates, if the configuration shown in Fig. 2.15 is used. Such a combination is economically proven only for high power LED lamps (for instance, in street lighting and for floodlights).

2.9. Common Configurations of LED Lamp Power Supply

Configuration of the power supply in a large extent depends on the energy source, the application, and the power range of the LED lamp. The main applications for the LED lamps are: 1) indoor lighting (office and residential); 2) street and park lighting; 3) architectural lighting; 4) horticultural lighting; 5) retrofit lighting; 6) automotive applications; 7) portable lighting etc.

Usually LED lamps are supplied from the standard AC power grid, except the LED lamps for automotive applications and portable lighting (or other specific lighting applications), where some kind of energy storage (battery) or DC on-board supply is used.

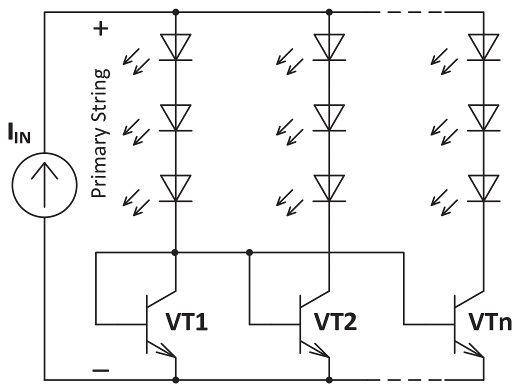

Fig. 2.22 Current sharing using current mirror [54].

By the power range LED lamps can be divided in low, middle, and high input power level as shown in Fig. 2.23 [57]. According to the IEC EN 61000-3-2 standard, power factor (PF) must be at least 0.85 for high and middle power supplies (input power above 25W) [58]. However, the market requirements can be as high as PF > 0.9 for LED lamps starting from 5W input power.

The common configuration of the high power range LED lamp power supply with power factor correction function is conventional (constant output voltage) power supply, equipped with additional output stage (additional converter) called LED driver (Fig. 2.24 (a) and (b)). Also, it can be said that this configurations is historical. The blocks of conventional power supply are standardized, well known, tested and developed. By applying additional LED driver block (which can also be well known, tested and developed solution, for instance, automotive LED driver), development costs are minimal. High technical parameters can be achieved: high power factor, low total harmonic distortion, tight LED current regulation, different dimming approaches are possible. The main drawbacks are comparatively small efficiency and high production costs due to many conversion stages, as well as comparatively short lifetime due to bulky electrolytic capacitors, which are necessary for stable output voltage of PFC and DC/DC converter blocks. The problems with efficiency become especially topical at low input power ranges.

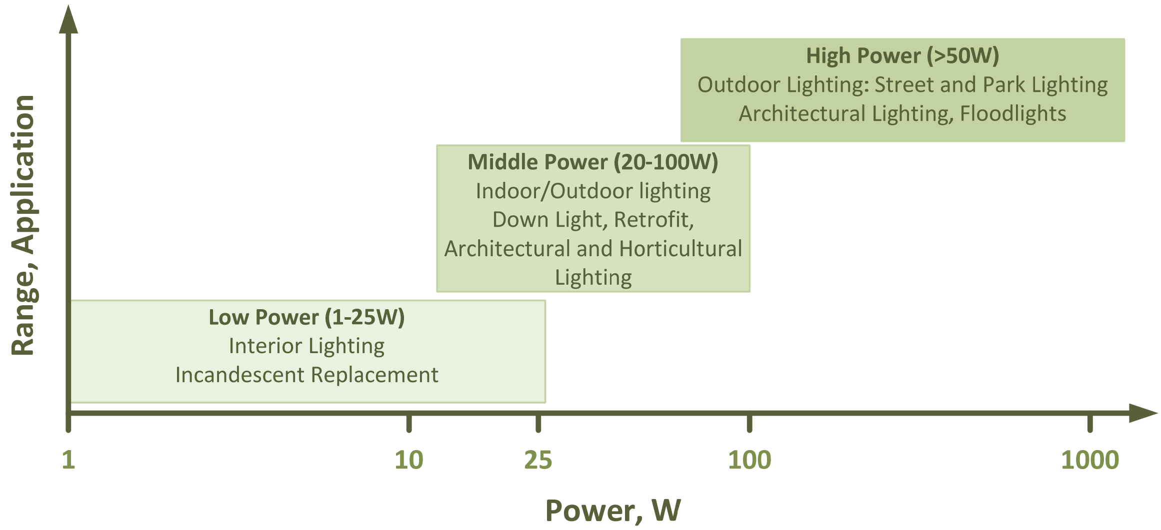

Fig. 2.23 Typical power ranges and applications of LED lamps [57].

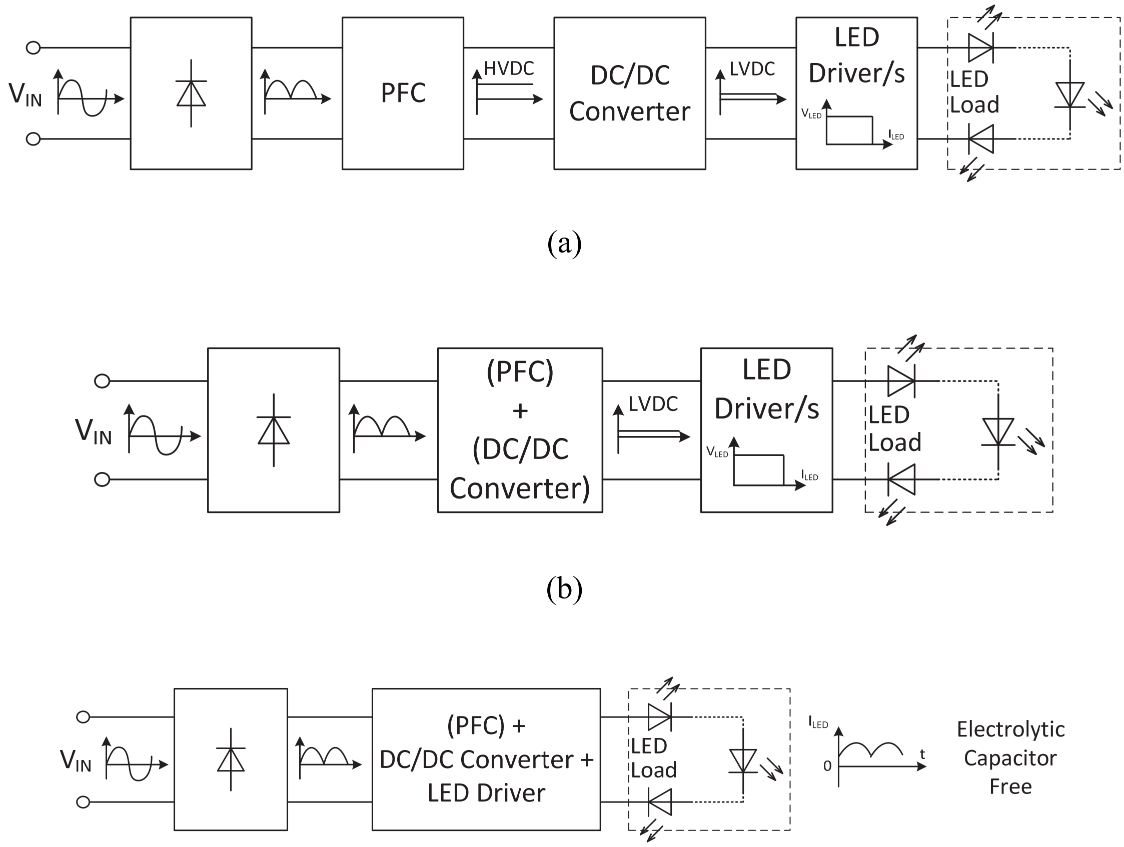

(a)

(b)

(c)

Fig. 2.24 Common configurations of LED lamp power supply: a) separate blocks for PFC, DC/DC converter and LED driver; b) with single block, which combines PFC and DC/DC converter functions; c) with single block, which combines PFC DC/DC converter, and LED driver function.

Theoretically, efficiency can be improved by combining several functions in one block or eliminating conversion stages (Fig. 2.24 (b) and (c)) [59]-[71], or eliminating converters at all [72], [73]. However, one or several technical parameters of the power supply usually suffer from such a combination [74]. Therefore, this approach is usually used only for low and middle power LED lamps, where high power factor or tight current regulation is not so critical. It is always a tradeoff between the efficiency, costs, and functionality.

High power LED lamp configurations given in Fig. 2.24 (a) and (b) are still topical. Also, the separate LED driver module is more convenient in smart lighting applications, as it provides flexible dimming and interconnection possibilities with communication modules. The similar situation is with horticultural and architectural multicolor lighting, where different color LEDs (with different forward voltage drop) are connected to the same converter output.

Switch mode power supply (SMPS), connected to the grid line, consumes non-sinusoidal current, which leads to higher consumed reactive power and higher losses in transmission lines. In fact, this problem is caused by the capacitor (capacitive load) connected after the bridge rectifier.

The popular power factor correction approach for small power devices is so called passive PFC (Fig. 2.25 (a)). Different kinds of passive LED power supply circuits as well as the improved circuits with passive power factor corrector (PFC) are discussed in [75].

The common circuit of active PFC (separate stage shown in Fig. 2.25 (b)) is a boost converter with bulky capacitor C_{PFC} at the output [76]-[78]. This capacitor is necessary to keep output voltage V_{OUT} high enough during the valleys in rectified input voltage V_{IN}.

There are two possible operation options for boost converter based active PFC: inductor L1 can operate ether in continuous conduction mode (CCM) or discontinuous conduction mode (DCM). In CCM operation input filter can be reduced, while the DCM usually allows achieving higher efficiency due to smaller switching losses [76]-[78].

There are also many approaches to implement PFC together with other functional blocks as shown in Fig. 2.24 b [59]-[61], [63] etc., or combining all the functions in single stage [67], [69]-[71]. In this case, the most popular is fly-back converter, which can be considered as buck-boost converter. Fly-back converter is briefly discussed in the section, which describes conventional topologies for amplitude mode light regulation approach.

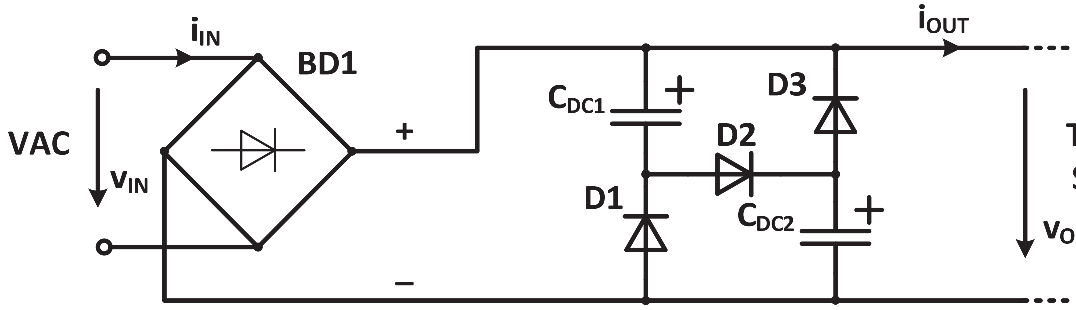

(a)

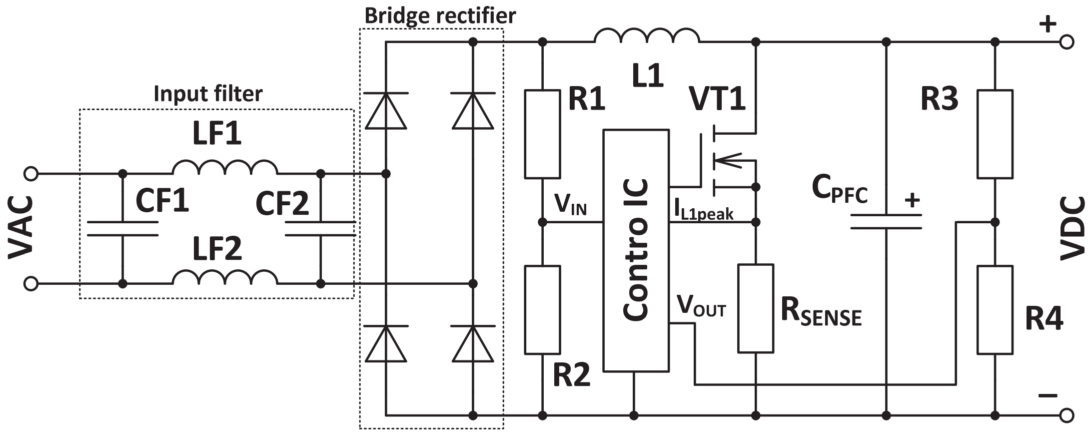

(b)

Fig. 2.25 Circuits for the most popular PFC correction approaches: a) passive PFC; b) active boost converter based PFC.

In [79] sensorless converter based on simple half-bridge controller with inherent PFC function has been proposed.

2.10. Dimming Techniques

Pulse mode light regulation method is the simplest way how to regulate the brightness of LED. The principal circuit for this technique depends on the source being in use (Fig. 2.26). Voltage source and limiting resistor (Fig. 2.26 (a)) is usually used for low power devices because of power losses in this resistor. The common configuration with the current source for high power devices is shown in Fig. 2.26 b. The main drawback of the configuration shown in Fig. 2.26 b is relatively low switching frequency due to specifics of the current source (LED driver).

The voltage (current) is applied to the LED periodically at a relatively high frequency (so that human eye cannot recognize the luminous flux pulsations of the produced light). The average amount of produced light Φ_{V_avg} is regulated by the duty cycle D — the ratio between time the voltage (current) has been applied t_{on} to the switching period T_{sw} (time of one cycle):

$$\Phi_{V\_avg} = \Phi_{V\_\max} \cdot D = \frac{\Phi_{V\_\max} \cdot t_{on}}{T_{sw}}, \tag{2.18}$$

where Φ_{V_max} is the maximum luminous flux corresponding to the maximum (operation point) current. The explanations are given in Fig. 2.27.

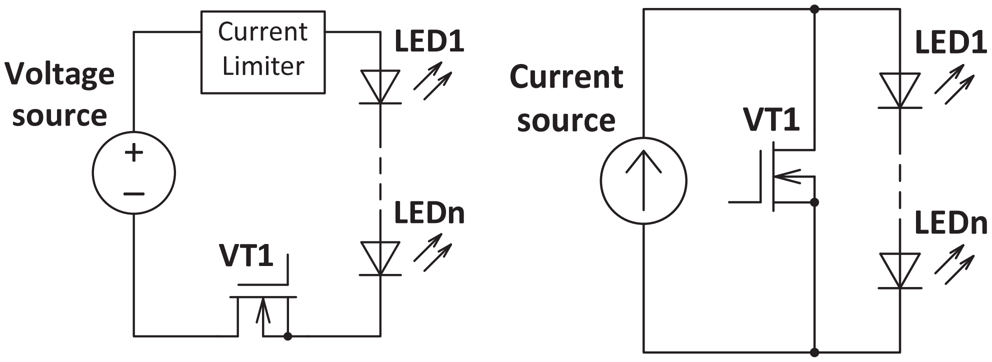

(a) (b)

Fig. 2.26 Two possible implementations of pulse mode light regulation depending on source: a) voltage source; b) current source.

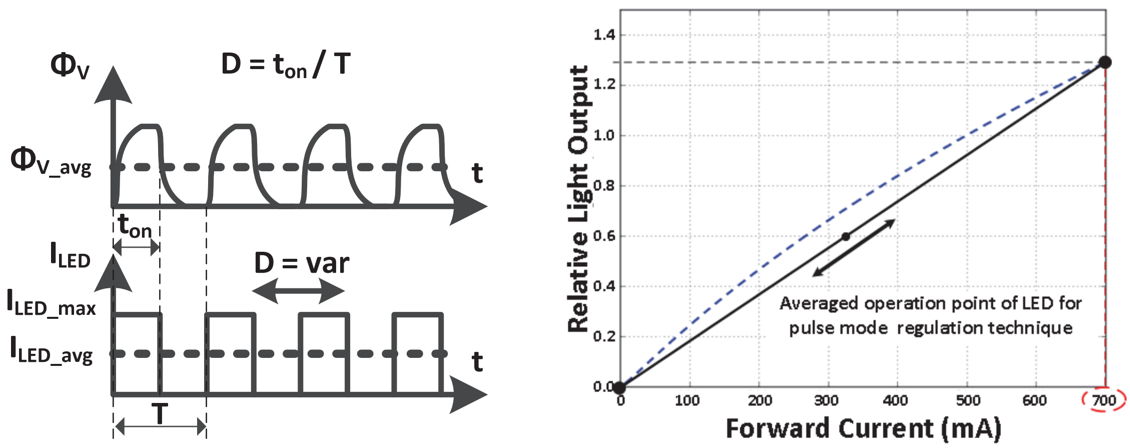

(a) (b)

Fig. 2.27 Pulse mode light regulation principles: a) typical luminous flux and current waveforms; b) operation point of LED — maximum current regardless of dimming rate

Either full power (current) or no power is applied to the LED during this process (Fig. 2.27 (a)). It means that LEDs work in the same operation point regardless of dimming level (Fig. 2.27 (b)). Therefore, the light color temperature is more stable (see Fig. 2.28 (a)). Due to this property pulse mode light regulation is widespread in high performance applications such as backlist of LCD panels and displays of portable electronics. However, color shift due to temperature changes still takes place (Fig. 2.28 (b)).

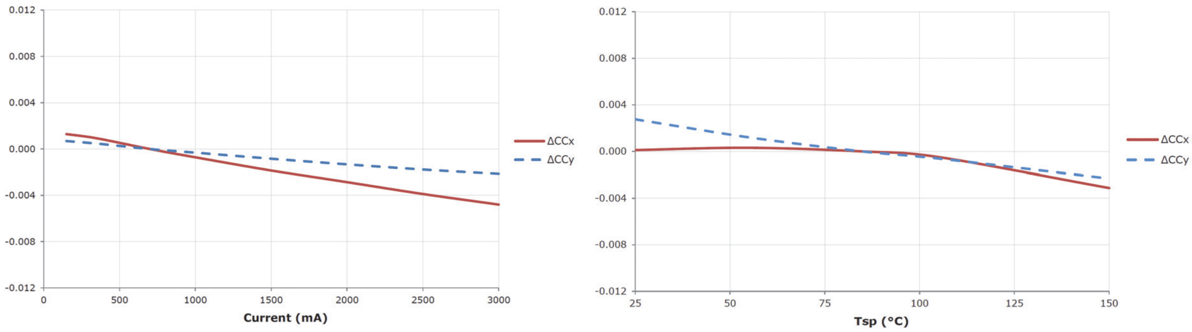

Fig. 2.28 Example of LED light color shift: a) color shift at changing current; b) color shift at changing junction temperature [80].

Luminous flux of LED follows the forward current at a very high speed. Therefore, undesirable effects (flickering, stroboscopic effect, "wagon-wheel effect") may appear using pulse mode light regulation technique. It is possible to reduce these effects increasing switching frequency or using special approaches (Appendix D).

Amplitude mode or fluent light regulation technique is based on the fact that the luminous flux of LED is almost proportional to the forward current flowing through LED. The operation principles are explained in Fig. 2.29. The main advantage of this regulation technique is higher possible efficacy of LED which also means higher overall efficiency of the lighting device operating in this mode. In Fig. 2.29 (b) the lumen-ampere curve of common high power LED is shown. It can be imagined that an operation point of LED moves along this curve in case of amplitude mode light regulation. Also, it is seen from Fig. 2.29 (b) that the same amount of average forward current of LED produces higher amount of light in case of amplitude mode (large point) in comparison with the pulse mode light regulation technique (small point).

The main problem of this light regulation technique is the nature of LED: it is rather current than voltage consumer, but the main topologies of the converters are voltage regulators, resulting in a necessity of special control approaches and more complicated control systems.

The explanations are given on the example of conventional switch mode converter (voltage regulator) with linear relationship between the duty cycle and output voltage (conventional buck, half bridge etc.) operating in continuous conduction mode. As the volt-ampere curve of the LED (load of the converter) and lumen-ampere curve are nonlinear, the resulting relationship between the duty cycle and luminous flux is also nonlinear (this topic will be discussed in more detail in the following section).

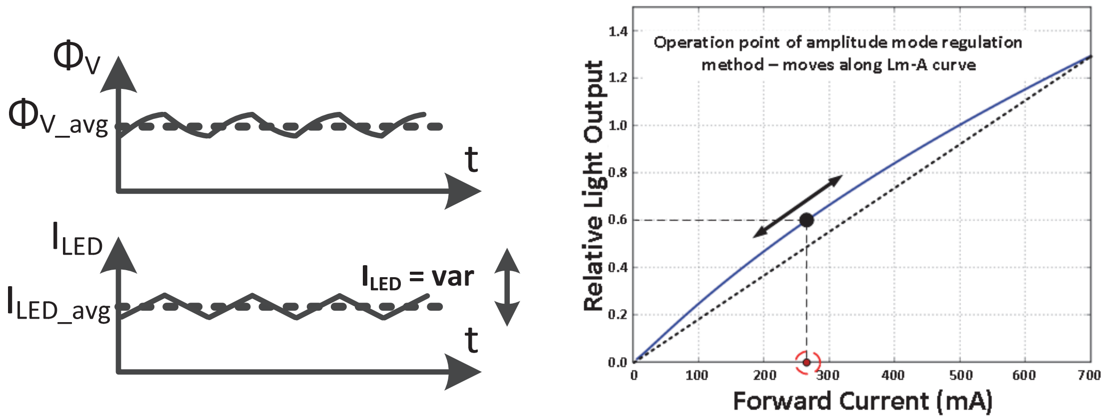

(a) (b)

Fig. 2.29 Amplitude mode or fluent light regulation principles: a) typical luminous flux and current waveforms; b) operation point of LED — variable, depends on dimming rate.

This causes certain problems for the investigation of control system with closed loop regulation.

There is also the color shift problem described previously in pulse mode light regulation section and shown in Fig. 2.28. However, the color shift problem caused by this light regulation technique is not significant for general purpose lighting.

The basic **converters** for amplitude mode light regulation are conventional switch mode voltage regulators and isolated converters shown in Fig. 2.30 [81] [82]. They can be used alone (automotive lighting, portable lighting) or as output stage of LED lamp power supply (high power range: street lighting, floodlights, etc.).

To achieve stable operation and accurate current regulation, special current control approaches are used with conventional voltage regulators (Fig. 2.30 (a), (b) and (c)). The most popular are peak and hysteretic current control [83], [84]. Peak current control requires additional compensation as the RMS output current decreases with increasing input voltage [84]. Hysteretic control shows better regulation results. This current control approach is discussed in more detail in direct current control section.

In many applications the galvanic isolation between the power grid and the load is required. In this case an isolated converter is used. The most popular topologies of isolated converters for LED applications are shown in Fig. 2.30 (c) and (d) [82]. Fly-back converter (Fig. 2.30 (c)) is a widespread topology for single stage off-line LED drivers in middle power applications. Resonant converter (Fig. 2.30 (d)) is suitable for high power LED applications. It acts as a voltage to current converter without employing a current sensor [82]. Dimming function is achieved by frequency regulation.

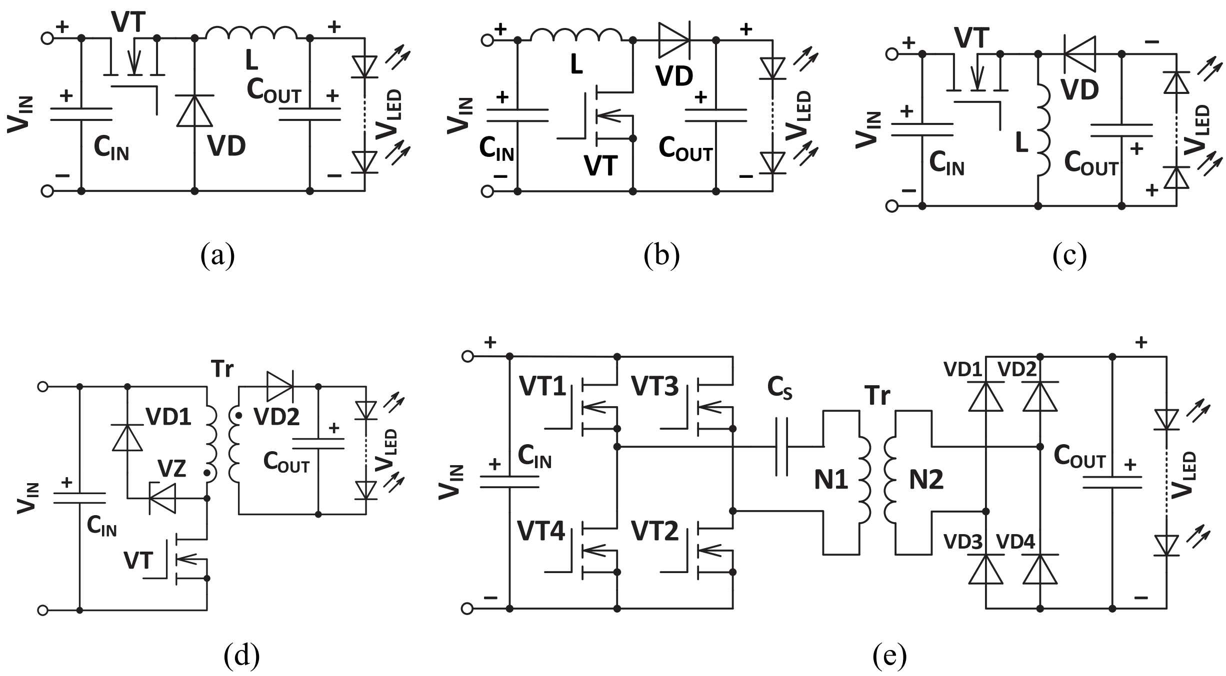

Fig. 2.30 Typical converter topologies for amplitude mode light regulation: a) buck converter; b) boost converter; c) buck-boost converter, d) fly-back converter; e) full-bridge resonant converter.

There are also other resonant converter topologies. For instance, half-bridge LLC converter based LED driver. Detailed description for this solution is given in [85].

Converters for **step regulation approach** are in fact arrays of electronic switches for commutation of LED groups. Regulation of the overall luminous flux is done through separate powering of each group by switches driven by the control system. The source can be either the voltage or current source. The circuits for both configurations are shown in Fig. 2.31 (a) and (b). The main drawback of this circuit is the large number of electronic switches.

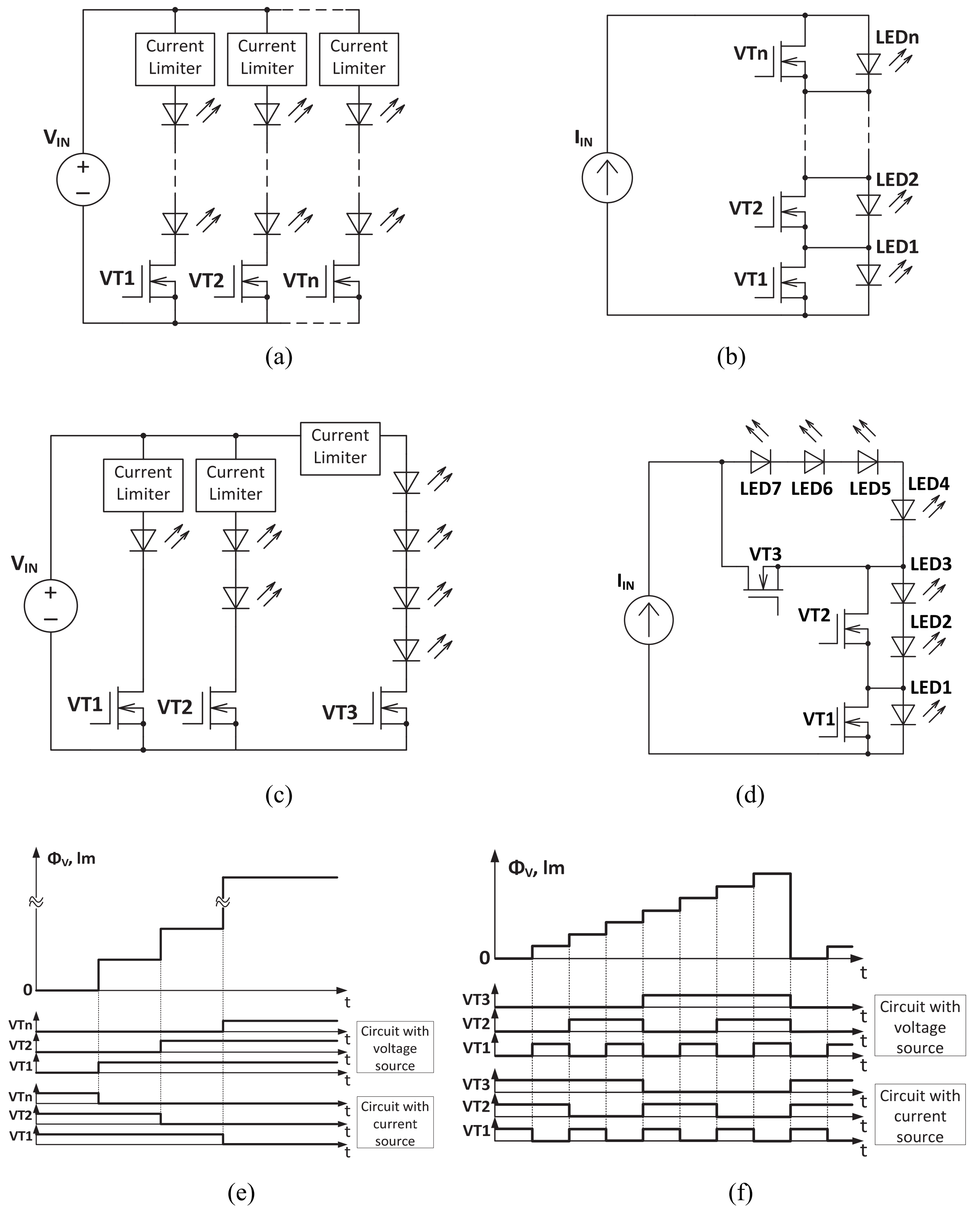

Fig. 2.31 Step mode luminous flux regulation — basic principles: a) circuit for the voltage source based regulation system; b) circuit for the current source based regulation system; e) control signals of electronic switches and resulting luminous flux curve. Use of binary weighted number of LEDs for each electronic switch: c) circuit for the voltage source based regulation system; d) circuit for the current source based regulation system; f) control signals of electronic switches and resulting luminous flux curve.

The number of electronic switches can be reduced by using binary weighted number of LEDs for each electronic switch, as shown in Fig. 2.31 (c) and (d). Then the maximum number of regulation steps n is equal to the number of LEDs while the step of regulation is equal to power (or produced light amount) of sole LED. The relationship between the number of regulation steps n and number of electronic switches is described by

$$n = 2^k \,, \tag{2.19}$$

where k is the number of electronic switches.

Also, in this case LED groups can be supplied from either voltage or current sources. The configuration of switch arrays is different for these two occasions Fig. 2.31 (c) and (d).

The main drawbacks of this luminous flux regulation technique are less efficient dimming (LEDs always operates at rated current value, which is not the most efficient operation point) and discrete luminous flux regulation steps.

The additional drawback of the circuit shown in Fig. 2.31 (d) is problems with drivers of upper transistors (VT2 and VT3 in Fig. 2.31 (d)).

2.11. Criteria for Comparison of the Control Performance

The controllability of LED drivers is understood as a set of parameters of these drivers that reflects their capability to control lighting parameters. The parameters of controllability are important in the context of a closed loop system that consists of a regulator and an LED lamp. The last one, in turn, includes an LED driver and LED matrix.

The parameters for evaluation of control performance have been discussed in: ([8]). In this research the following parameters have been used as criteria of evaluation:

1) maximum gain of the lamp (G_{LEDmax}),
2) ratio of its maximum and minimum (G_{LED}),
3) nonlinearity of regulation (NL),
4) span of the practically usable values of duty cycle (G_a).

The first parameter is the rate of changes of relative output (RO) with the corresponding changes of duty cycle D, where RO is defined as a ratio of regulated parameter (luminous flux, illuminance, current etc.) to its maximum value expressed in percent. In generalized form the gain can be found as a derivative of RO with respect to D and is also a function of D:

$$G_{LED} = f(D) = \frac{dRO}{dD} \approx \frac{\Delta RO_k}{\Delta D_k}, \tag{2.20}$$

where ΔRO and ΔD are the finite changes of RO and D in the k-th point. The ratio of maximum and minimum values of the gain forms the dynamic range:

$$RG_{LED} = \frac{G_{LED\max}}{G_{LED\min}}, \tag{2.21}$$

which express also gain changes of the regulation system. In (2.21):

$$G_{LED\max} = \Delta RO_{@\max} / \Delta D_{@\max} \text{ and} \tag{2.22}$$

$$G_{LED\min} = \Delta RO_{@\min} / \Delta D_{@\min}, \tag{2.23}$$

where $\Delta RO_{@\max}$ and $\Delta RO_{@\min}$ are changes of the relative output achieved at the corresponding values of the duty cycle $\Delta D_{@\max}$ and $\Delta D_{@\min}$ that produces the maximum and minimum.

The nonlinearity NL is a root-mean declination ΔS of regulation curve $RO(D)$ from the equivalent linear one $RO_L(D)$ related to the root-mean value of the curve S:

$$NL = \frac{\Delta S}{S} \cdot 100\%, \tag{2.24}$$

where ΔS is defined as:

$$\Delta S = \sqrt{\frac{1}{D_{\max} - D_{\min}} \int_{D_{\min}}^{D_{\max}} \left[RO(D) - RO_L(D)\right]^2 dD}, \tag{2.25}$$

but S - as:

$$S = \sqrt{\frac{1}{D_{\max} - D_{\min}} \int_{D_{\min}}^{D_{\max}} RO^2(D) dD}. \tag{2.26}$$

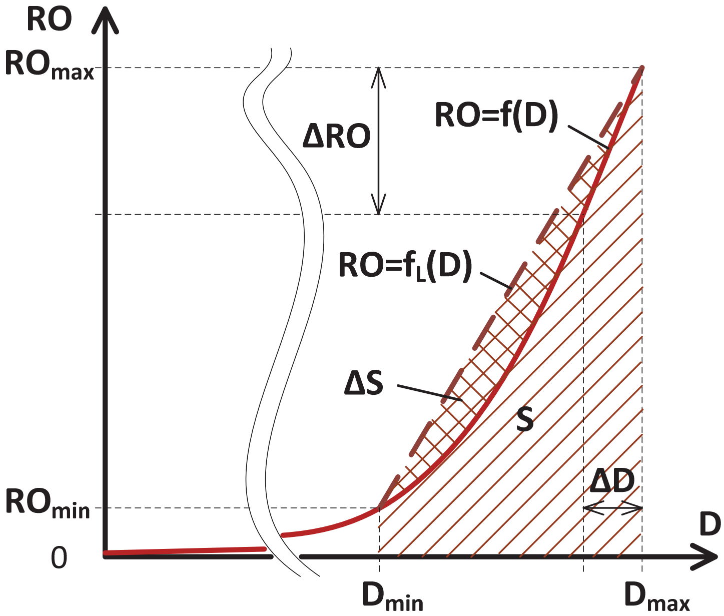

Fig. 2.32 Clarifications to the calculation of the parameters of control performance.

The last estimated parameter is a ratio of achievable span of relative output vs. span of usable values of duty cycle (average gain) showing how complete is the utilization of control hardware. It is found as the following ratio:

$$G_a = \frac{RO_{\max} - RO_{\min}}{D_{\max} - D_{\min}} , \tag{2.27}$$

where $D_{\min}$ and $D_{\max}$ are the values of duty cycle that provides the maximum $RO_{\max}$ and minimum $RO_{\min}$ values of RO (when it is assumed that he curve has no extremes).

2.12.Summary

The solid state lighting is becoming one of the most popular technologies in the lighting industry due to many advantages. However, the LEDs must be used in proper way to achieve all the benefits of SSL technology. During the development of LED lamp power supply it is important to ensure that LED driver is capable to perform required functions (dimming, current control, protection functions), at the same time providing a good quality of produced light. So, the impact of the LED driver on the quality parameters of produced light should be evaluated. Dimming method can influence these parameters to a great extent.

The manufacturing process of LED is very complicated resulting in slight differences in V-A curve even for LEDs made from the same wafer. The differences in V-A curve creates restrictions in the choice of connection type for LEDs. Series connection is most appropriate for

LEDs to overcome this problem. Light output of all LEDs connected in series is almost proportional to the forward current flowing through them. Change of current amplitude in LEDs is the main dimming approach. There are also several other convenient dimming options, which are discussed in the next sections. Therefore, LEDs are also the most convenient for distributed lighting and smart lighting systems, where the dimming function is vital [86], [87].

There are different configurations for the ballasts of the dimmable LED lamps. Conventional configuration of the ballast powered from the grid consists of several typical stages: rectifier from the side of the power grid, filter, power factor corrector, DC/DC converter, and LED driver. Every stage has its own efficiency; therefore, the overall efficiency of the ballast decreases with increasing number of conversion stages. The standard approach to improve the efficiency is the combination of the functions of several typical stages in one, but the dimming function usually suffers in this case (TRIAC dimmer, or pulse mode dimming). Such complicated configuration (in case of multistage converter) or functionality (in case of a single stage converter) is dictated by the requirements for the existing power grid.

Single stage converters usually are used in small-to-middle power range applications. For high power applications multistage configuration is still relevant. There are also specific applications, where multistage converters are more convenient. They are multicolor LED lamps for architectural and stage lighting, horticultural lighting applications etc.

Besides, the idea of smart grids is becoming more and more relevant. In accordance with this concept, some researchers and scientists propose the use of low voltage DC grid for domestic electrical systems [13] and smart LED lighting systems [87]. Thus, the studies in the field of conventional DC LED drivers with a dimming function are still relevant. Some researchers suggest the transformation of domestic customers from static customers into active participants of the production of electrical power. To achieve this it is necessary to develop new appliances with controllable load, microgeneration, and domestic energy storage [88]. Usually the parameters of domestic generation sources (photovoltaic panels, small wind turbines, fuel cells) do not correspond to the parameters of the grid. It means that all of these sources should be equipped with some kind of controllable converters [89]. In the same way the load (consumers of electrical power) should be compatible with the concept of smart grid, so they also should be equipped with some kind of regulating converter [9].

Lighting systems are no exception. Smart lighting systems are capable of reducing electrical power consumption significantly by the regulation of the illumination level in accordance with the proper light regulation strategy. The main element of such a system is a lighting fixture with dimming possibilities. As the ballast of lighting fixture affects the overall efficacy of the device, it is important to evaluate ballast at all operation points (in the whole regulation range). Also, the approach of the illumination level control should be taken into account.

This work considers controllable ballasts (dimmable LED drivers) from point of view of parameters, which are important for the implementation of microcontroller based closed loop regulation system. However, a great variety of application specific integrated circuits (ASIC) of dimmable LED drivers is available on the market today. ASICs increase the total costs of smart lighting system LED luminaire in case if a microprocessor must be utilized for the communication between luminaries in any case.

Generally there are three main light regulation techniques to drive LED's: 1) pulse mode, 2) amplitude (or fluent), and 3) step mode light regulation technique [90], [91]. LED light regulation techniques have been studied in [8]. In this work light regulation techniques are also highlighted and briefly described, since the quality of the light produced by LED as well as the efficacy depends heavily on dimming method.

The considered light regulation techniques are summarized in Fig. 2.33. Their benefits and drawbacks are listed in Table 2.1. Pulse mode flux regulation is most appropriate for high performance devices where stable light color temperature is critical (backlit of LCD panels, displays) [92], [93]. This method might suffer from the stroboscopic effect (because the luminous flux of LED follows the forward current at a very high speed [47]), which is unwanted phenomenon in general lighting. The stroboscopic effect is especially dangerous for industrial lighting, where spinning mechanisms under certain conditions may seem motionless. Therefore, step mode and amplitude (fluent) luminous flux regulation methods are the most appropriate in general lighting applications; however, a fluent mode regulation technique allows utilizing LED in a more efficient way (approximately by 7 % in case of dimming at 50 %) [47].

In Fig. 2.27 (b) and Fig. 2.29 (b), the ampere-lumen (A-Lm) curve of the common high power LED is shown. In case of pulse mode or step mode luminous flux regulation the LED operates at a fixed point, usually maximum allowable or nominal (test) current. This maximum or nominal current is applied to LED periodically at a high frequency, but the luminous flux is proportional to the duty cycle D (ratio of the time when the current is applied to the time of the whole period). It can be imagined that a change in duty cycle moves the averaged operation point of LED in a straight line, which is connected between a crossing point of the axes and the previously mentioned fixed point (thick dashed line in Fig. 2.27 (b)).

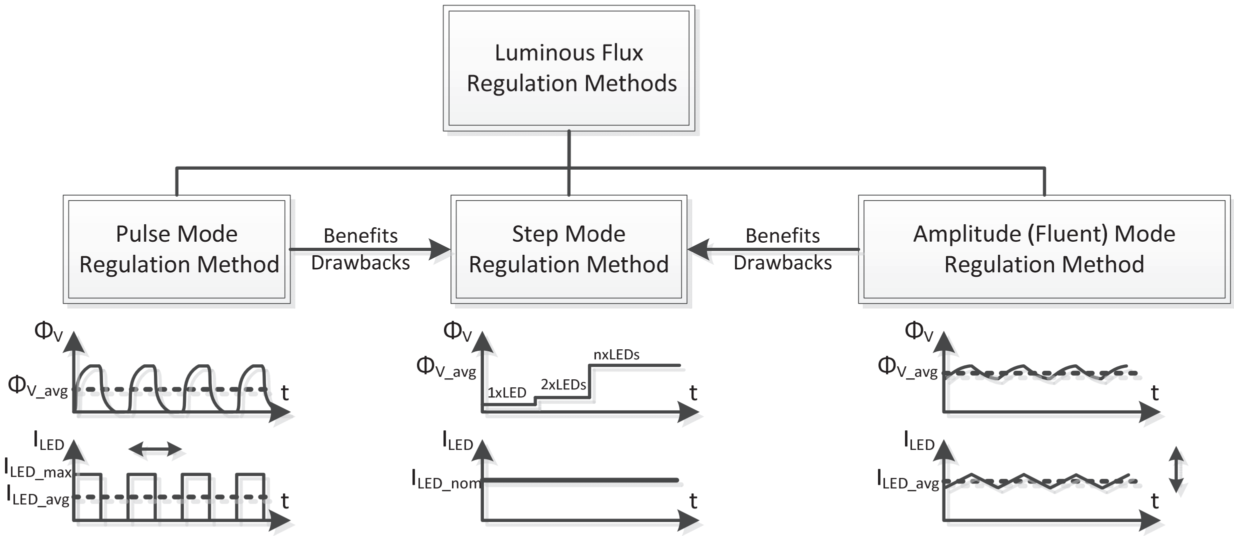

Fig. 2.33 Luminous flux regulation methods for LED lamps as well as typical waveforms of LED forward current and luminous flux.

Table 2.1

Benefits and Drawbacks of Luminous Flux Regulation Methods

Pulse Mode	Step Mode	Amplitude (Fluent) Mode
+ high accuracy and resolution	+ no stroboscopic effect	+ higher efficiency of LEDs
+ stable color temperature	+ stable color temperature	+ no stroboscopic effect
+ simple control system	+ simple control system	+ longer life span
- undesirable stroboscopic effect	- shorter life span	- relatively complex control system
- shorter life span	- low resolution (small number of regulation steps)	- unstable color temperature
- worse efficiency of LEDs	- worse efficiency of LEDs	- accuracy and resolution depends on complexity of control system

In case of fluent luminous flux regulation the operation point of LED moves along A-Lm curve, thus achieving higher efficacy, especially at a smaller input current (power) as it shown in Fig. 2.29 (b). Therefore, amplitude mode regulation is most suitable for general lighting applications.

As the goal of these studies is LED lamp control system based on highly integrated MCU with reduced complexity and costs, the following sections concentrate on the search of converters (capable of providing amplitude mode dimming) with the properties, which allows achieving more or less linear relationship between the input and output signals of the plant (combination converter — LED load).

3 COMPENSATION OF NONLINEARITIES OF LED

3.1. Introduction

One of the ways how to simplify the control system of the LED luminaire is to try to overcome the problems with nonlinear relationships in control chain (Fig. 3.1 (d)). LED is nonlinear part of this control chain. Thus, one of the options is to try to compensate this nonlinearity by the nonlinearity of the other part, for example, by the relationship of the voltage regulator (converter) as shown in Fig. 3.1 (a) and (b).

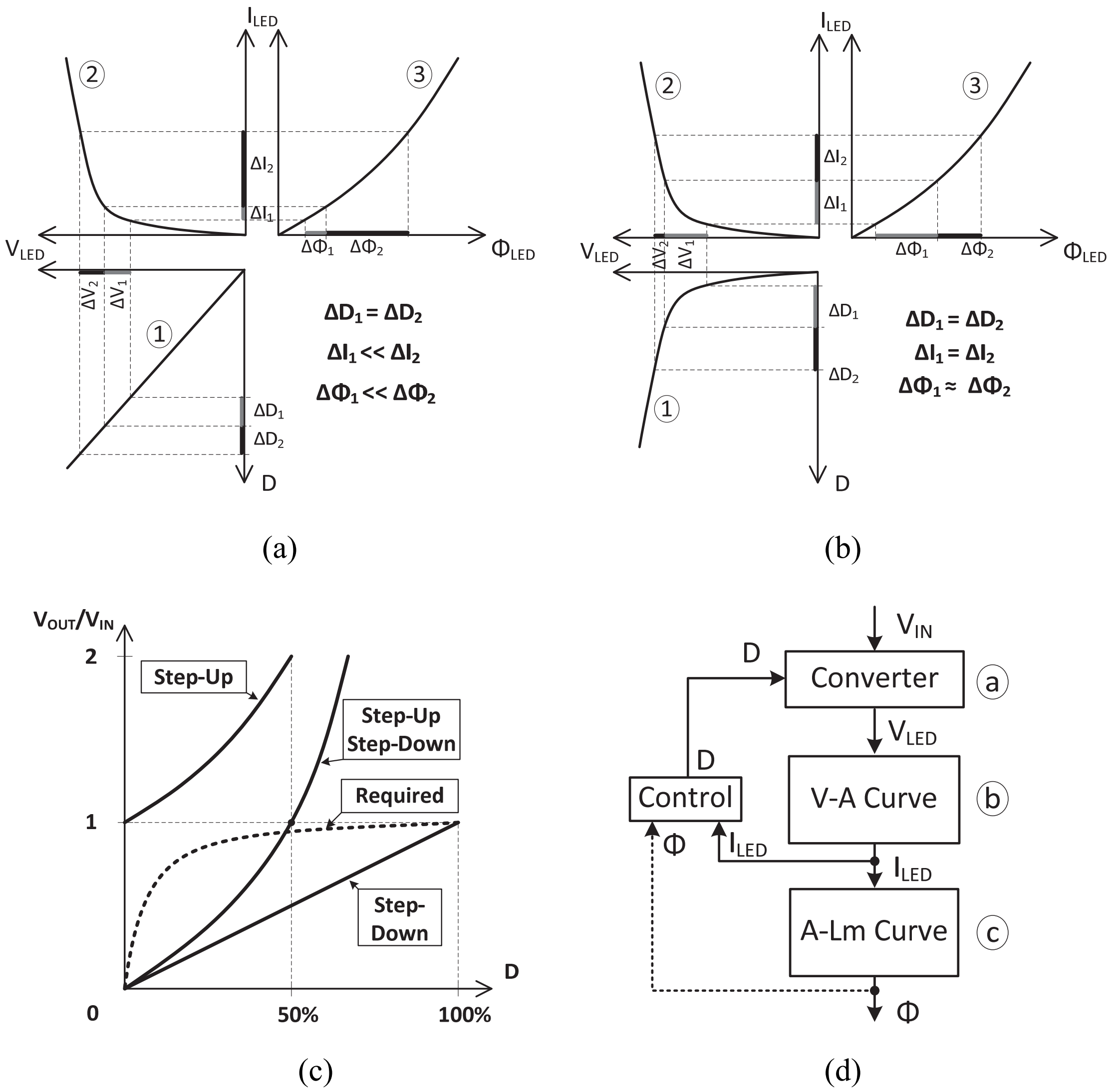

Fig. 3.1 Compensation of nonlinearity: a) relationship between the duty cycle (control parameter) and luminous flux (parameter under control) in case of linear relationship of the converter; b) relationship between the duty cycle and luminous flux in case of nonlinear relationship of the converter c) relationships between the gain of the converter and duty cycle for the conventional topologies as well as relationship required for compensation of LED V-A curve d) parts of the control chain.

To verify this hypothesis, it is necessary to find the converter with an appropriate relationship between the duty cycle and output voltage. Conventional step-up, step-down, and step-up/step-down topologies (the relationships are shown in Fig. 3.1 (c) as solid thick curves) are not suitable for this purpose (the required relationship is shown in Fig. 3.1 (c) as a dashed thick curve). Therefore, the family of tapped-inductor converters has been studied in order to find a suitable solution.

3.2. Family of Tapped Inductor Converters

Like conventional step-up/step-down converters, tapped-inductor converters are classified in three main groups: buck, boost, and buck-boost. Parameter λ has been introduced in order to unify the study of all the converters [94]:

$$\lambda = N1 / N2\,, \tag{3.1}$$

where $N1$ and $N2$ are the numbers of turns of the windings of tapped-inductor. For different topologies designations $N1$ and $N2$ are assigned to different windings (is specified on the schematics of electrical circuit).

Two tapped-inductor buck circuits (Table 3.1) with different relationships between the gain of the converter and duty cycle were discussed in [95].

The relationship between the gain V_{OUT}/V_{IN} and duty cycle D of tapped-inductor buck converter can be found from the expression:

$$\frac{V_{OUT}}{V_{IN}} = \frac{D}{D + (1 - D)\cdot\lambda}\,, \tag{3.2}$$

where V_{IN} is the input voltage of the converter.

The converter with smaller gains at the same duty cycles as conventional buck is called “reducer-buck”, while the converter with higher gains is called “fitter-buck” (Table 3.1). Reducer-buck takes place when $\lambda > 1$, fitter-buck — when $0 < \lambda \leq 1$ (Table 3.1). Gain curves at different duty cycles and parameter λ values are also given in Table 3.1.

Two boost converters as well as two buck-boost converters (Table 3.1) were also discussed in [95].

The relationship between the gain V_{OUT}/V_{IN} and duty cycle D of tapped-inductor boost converter can be found from:

Table 3.1

Summary of the Family of Tapped-Inductor Converters

BUCK		
$0 < \lambda \leq 1$ (“Fitter-Buck”)		$\lambda > 1$ (“Reducer-Buck”)
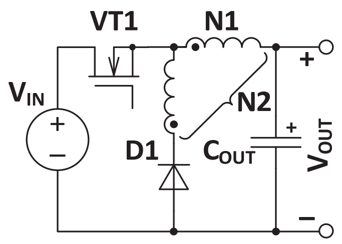	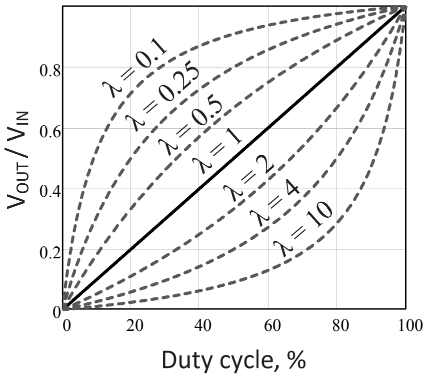	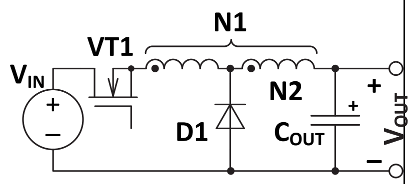
BOOST		
$0 < \lambda \leq 1$ (“Raiser-Boost”)		$\lambda > 1$ (“Fitter-Boost”)
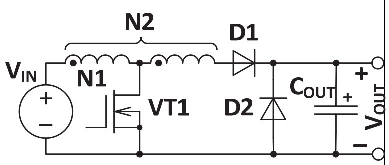	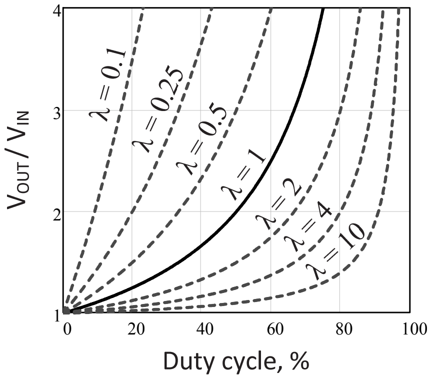	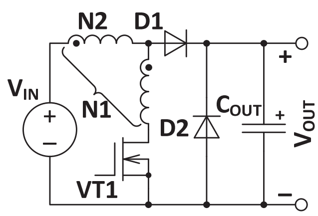
BUCK-BOOST		
$0 < \lambda \leq 1$ (“Raiser-Buck-Boost”)		$\lambda > 1$ (“Reducer-Buck-Boost”)
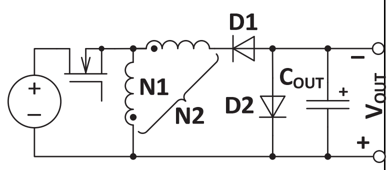	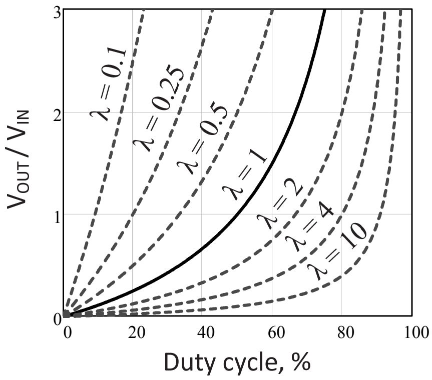	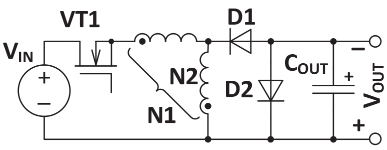

$$\frac{V_{OUT}}{V_{IN}} = \frac{D + (1 - D) \cdot \lambda}{(1 - D) \cdot \lambda}; \tag{3.3}$$

for tapped-inductor buck-boost converter:

$$\frac{V_{OUT}}{V_{IN}} = \frac{D}{(1 - D) \cdot \lambda}. \tag{3.4}$$

The converter with smaller gains at the same duty cycles as conventional boost/buck-boost is called “fitter-boost”/“reducer-buck-boost”, while the converter with higher gains is called “raiser-boost”/“raiser-buck-boost”. Fitter-boost/reducer-buck-boost takes place when $\lambda > 1$, raiser-boost/raiser-buck-boost — when $0 < \lambda \leq 1$ (Table 3.1). Gain curves at different duty cycles and parameter λ values are also given in Table 3.1.

Tapped-inductor based solutions are also available on the market [96], [97], [98]. However, previously tapped-inductor solutions were considered as converters with a high input-to-output voltage step-down ratio or current step-up ratio. The capability of compensation of LED V-A curve has not been studied previously.

It is seen from Fig. 3.1 (c) and Table 3.1 that fitter-buck ($0 < \lambda \leq 1$) tapped-inductor converter is suitable for the compensation of nonlinearity of V-A curve of LED and parameter λ can be used to tune resulting relationship between the duty cycle and luminous flux in control chain. Therefore, this converter is considered more detailed.

Weight and size of the separate converter elements depends on the power losses of switches (determines the size of the heat sink) and necessary capabilities to store energy for energy storages (capacitor and inductor). The estimation of those parameters can be done by the analysis of instantaneous voltage and current curves (Fig. 3.2).

The **power losses** of switches for conventional VF converter topologies were considered in [99], [100]. Power losses ΔP in the switch can be found as the sum of conduction losses ΔP_{on} and switching losses ΔP_{sw}:

$$\Delta P = \Delta P_{on} + \Delta P_{sw}. \tag{3.5}$$

Conduction losses of transistor VT1 depends on average current I_{on} (which is also inductor L1 current) flowing through it during t_{on}. It can be expressed as a relationship with the output current I_{OUT} and duty cycle D, but $I_{on}=I_{OUT}$ if $\lambda=1$ (which is true for conventional buck converter):

$$I_{on} = \frac{I_{OUT}}{D(1-\lambda)+1}. \tag{3.6}$$

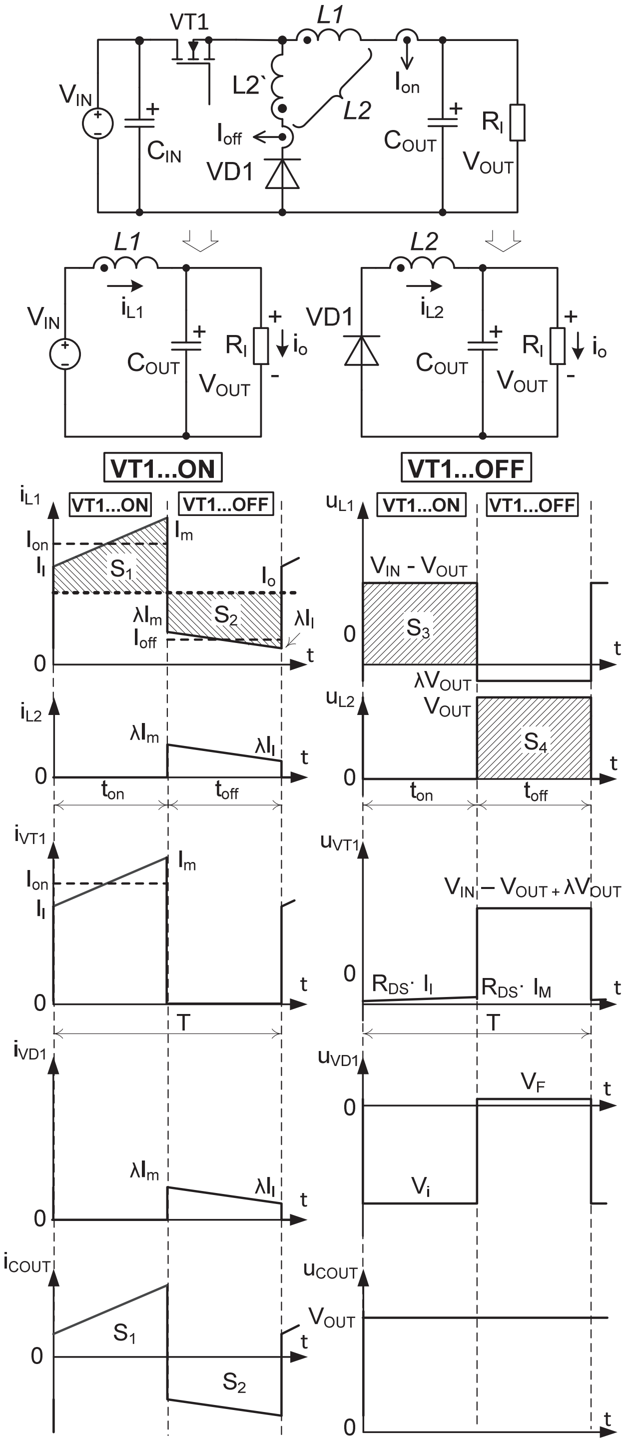

(a) (b)

Fig. 3.2 The analysis of instantaneous voltage and current forms in the separate elements: a) schematics of the fitter-buck tapped-inductor; b) voltage and current waveforms.

Conduction losses of VT1 are equal to product of this current, MOSFET channel resistance R_{Q1on} and duty cycle D:

$$\Delta P_{VT1on} = I_{on}^2 \cdot R_{VT1on} \cdot D = \frac{I_{OUT}^2 \cdot R_{VT1on} \cdot D}{(D(1-\lambda)+1)^2}. \qquad (3.7)$$

In similar way conduction losses of diode VD1 depends on average current I_{off} (which is also inductor L2 current) flowing through it during t_{off} and voltage drop V_{VDon} across it. Taking into account $I_{off} = \lambda I_{on}$, the conduction losses of diode VD1 can be expressed as:

$$\Delta P_{VT1on} = I_{off} \cdot V_{VD1on} \cdot (1-D) = \frac{\lambda I_o \cdot V_{VD1on} \cdot (1-D)}{D(1-\lambda)+1} \qquad (3.8)$$

The description for calculation of switching losses as well as description of MOSFET parameters is given in [101], [102]. Switching losses ΔP_{VT1sw} of the MOSFET transistor depend on-turn on energy losses E_{VT1ton} and turn-off energy losses $E_{VT1toff}$ as well as switching frequency f_{sw}:

$$\Delta P_{VT1sw} = (E_{VT1ton} + E_{VT1toff}) \cdot f_{sw} \qquad (3.9)$$

Turn-on and turn-off energy losses for the worst case scenario can be found taking into account the features of the considered tapped inductor converter (Fig. 3.2):

$$E_{VT1ton} = V_{IN} \cdot I_l \cdot \frac{t_{Irise} + t_{Vfall}}{2} + Q_{rr} \cdot V_{IN}, \qquad (3.10)$$

$$E_{VT1toff} = V_{IN} \cdot I_m \cdot \frac{t_{Vrise} + t_{Ifall}}{2}, \qquad (3.11)$$

where I_l is the current of inductor L1 at the beginning of the switch-on process, I_m is the current of inductor L1 at the end of the switch-on process, Q_{rr} is reverse recovery charge of the diode, t_{Irise} and t_{Ifall} are current rise and fall times that can be found in the datasheet of transistor. Voltage rise time t_{Vrise} and voltage fall time t_{Vfall} are approximately equal to:

$$t_{Vrise} \approx \frac{V_{IN} \cdot R_G \cdot C_{GD}}{V_{Gplateau}}, \qquad (3.12)$$

$$t_{Vfall} \approx \frac{V_{IN} \cdot R_G \cdot C_{GD}}{V_{DR} - V_{Gplateau}}, \qquad (3.13)$$

where R_G is the gate resistor, C_{GD} is the gate to drain capacitance, V_{DR} is the gate driver voltage, but $V_{Gplateau}$ is the gate plateau voltage.

Switching losses of the diode ΔP_{VD1sw} can be found using slightly simplified expression (without taking into account the reverse conductivity of the diode):

$$\Delta P_{VD1sw} \approx \frac{V_{IN} \cdot Q_{rr} \cdot f_{sw}}{2} . \tag{3.14}$$

It is worth mentioning that all these equations (3.5)-(3.14) are true for conventional buck converter at $\lambda = 1$. The comparison of power losses in switches for both tapped-inductor and conventional buck are presented in Appendix G.

Tapped-inductor is the member of the family of the so-called "power inductors", the task of which is energy storage. Also, it can be considered as a transformer. It means the **construction features of the tapped-inductor** are very similar to the flyback transformer.

Expected waveforms of current in both windings of fitter-buck tapped-inductor are shown in Fig. 3.2, and operation principles are the same as in for flyback transformer. Also, it is expected that inductor will operate in CCM (Fig. 3.2).

Ideal magnetic materials cannot store energy, but practical materials store very little. Small non-magnetic (air) gap in series with high permeability magnetic core material is necessary in order to store energy.

There are magnetic core materials with distributed air gap (such as Permalloy powder cores), but they are less appropriate for transformer designs (more preferable in single winding inductor design due to potential EMI problems) [103]. In case of ferrite core material (which is more suitable for DCM) the minimum volume of air gap V_δ to store necessary energy can be found from:

$$V_\delta = A \cdot \delta \geq \frac{L \cdot I_{\max}^2 \cdot \mu_0}{B_{\max}^2} , \tag{3.15}$$

where A is the cross-cut of main magnetic path of the core, δ is the length of air gap, L is required inductance, I_{max} is inductor peak current, μ_0 is permeability of vacuum magnetic constant $\mu_0 = 4\pi \cdot 10^{-7}$ (H/m), but B_{max} is the core material limit for the maximum magnetic flux density ($B_{max} \approx 0.3$ T for usual ferrite materials) [104]. Then the ferrite core can be selected from catalogue knowing the volume of air gap V_δ.

The number of turns N required for inductance L can be found using relationship:

$$N = \sqrt{L / A_L} , \tag{3.16}$$

where A_L is inductance factor specified in manufacturer catalogue for specific magnetic core [103], [104].

In practical calculations with gapped core the reluctance of the magnetic material (with high permeability: μ_r = 3000…100000) can be neglected, because it is very small compared to the air gap reluctance. Therefore, corrected air gap dimensions A_g alone determine the relationship between the inductance and necessary number of turns:

$$N = \sqrt{(L \cdot \delta) / (\mu_0 \cdot A_g)} . \tag{3.17}$$

Corrected air gap dimensions can be found using empirical approximation (adding length of the gap to the core dimensions involved in calculations of the area):

$$A_g \approx (a+\delta) \cdot (b+\delta) , \tag{3.18}$$

where a and b are dimensions of rectangular center-pole of a core (in the similar way the corrected air gap dimensions can be found for cylindrical center-pole of a core). Correction is necessary because intense fringing field adjacent to the gap extends outward beyond the boundaries of the core cross-section [103].

Also, it is worth mentioning that tapped-inductor boost and buck-boost converters (Table 3.1) are not suitable for compensation of nonlinearity of LED load. However, the assessment of capability to compensate nonlinearities of LED for these converters is also given in the following sections.

3.3. Energy Efficient Current Measurement Approach

For tapped-inductor fitter-buck converter it also is possible to minimize power losses in current measurement circuitry and to reduce costs of this circuitry.

The analysis of tapped-inductor waveforms (Fig. 3.2 (b)) shows that the relationship between the output current and the inductor current can be found from expression:

$$I_{OUT} = \left(\frac{I_l + I_m}{2} \right) \cdot D + \left(\frac{\lambda \cdot I_l + \lambda \cdot I_m}{2} \right) \cdot (1 - D) , \tag{3.19}$$

where I_{OUT} is the output current of the converter (i.e. LED current in LED driver application), I_l is current value in inductance L1 at the beginning of transistor VT1 switch on state, I_m is current value in inductance L1 at the end of transistor VT1 switch on state. It is seen from this expression that duty cycle value also should be known to determine output current value. As the optimal value of parameter λ is known for LED driver application ($\lambda = 0.1$), (3.19) can be simplified:

$$I_{OUT} = I_{off} \cdot \left(\frac{D}{\lambda} + 1 - D \right) = I_{off} \cdot (9 \cdot D + 1) \tag{3.20}$$

where I_{off} is an average current value in tapped-inductor during transistor VT1 switch off state:

$$I_{off} = \left(\frac{\lambda \cdot I_l + \lambda \cdot I_m}{2} \right) = \lambda \cdot I_{on} \tag{3.21}$$

Experimental verification of this current measurement approach is given in Appendix H. It is seen from these oscillograms that there is high voltage generated across the secondary winding, especially at smaller duty cycles and at start up process, when full input voltage is applied to primary winding. The appropriate diode D1 should be selected to withstand this voltage and/or additional clamping circuits should be added to prevent other converter elements from high voltage spikes.

3.4. Compensation of Nonlinearity and Improvement of Accuracy

First of all, the parameters of the load connected to the converter play a significant role in a stable performance of the converter. The volt-ampere (V-A) curve of 7 Seoul Semiconductor W724C0 LEDs [105] connected in series has been measured for the analysis of controllability parameters of the tapped inductor converters described above. 50 mA steps at the bottom part (below 600 mA) and 100 mA steps at the upper part (above 600 mA) of the V-A curve have been selected between measurements points (Fig. 3.3). Linear interpolation between the measured points (Fig. 3.3) has been used for the further numerical calculations of the controllability curves (2.12).

Controllability curves (dependency of LED current from the duty cycle of control signal) can be found by combining equations (3.2)-(3.4) with the LED load volt-ampere curve expression (2.8), (2.12) or (2.13). As mentioned previously, the linear interpolation (2.12) of points on the V-A curve of LEDs taken by experimentation was used for further calculations as this expression simplifies the

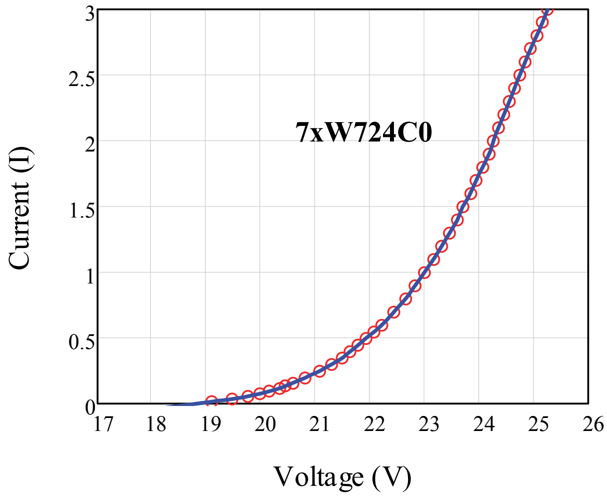

Fig. 3.3 Volt-ampere curve of the LED load used in experiments and for numerical calculations.

calculation process, but the small step between the measurement points allows ensuring a small calculation error. For the tapped-inductor buck converter the resulting controllability expression (transfer function between the duty cycle and output current) is as follows:

$$I_{LED}(D) = I_{LED1} + \frac{\frac{V_{IN} \cdot D}{D + (1-D)\cdot\lambda} - V_{LED1}}{V_{LED2} - V_{LED1}}\left(I_{LED2} - I_{LED1}\right). \tag{3.22}$$

Similarly the controllability expression can be found for tapped-inductor boost converter:

$$I_{LED}(D) = I_{LED1} + \frac{V_{IN} \cdot \frac{D + (1-D)\cdot\lambda}{(1-D)\cdot\lambda} - V_{LED1}}{V_{LED2} - V_{LED1}}\left(I_{LED2} - I_{LED1}\right) \tag{3.23}$$

and tapped-inductor buck-boost converter:

$$I_{LED}(D) = I_{LED1} + \frac{\frac{V_{IN} \cdot D}{(1-D)\cdot\lambda} - V_{LED1}}{V_{LED2} - V_{LED1}}\left(I_{LED2} - I_{LED1}\right) \tag{3.24}$$

The examples of transfer functions between the duty cycle and LED load voltage or current for different topologies of tapped-inductor converters are given in Fig. 3.4 (a).

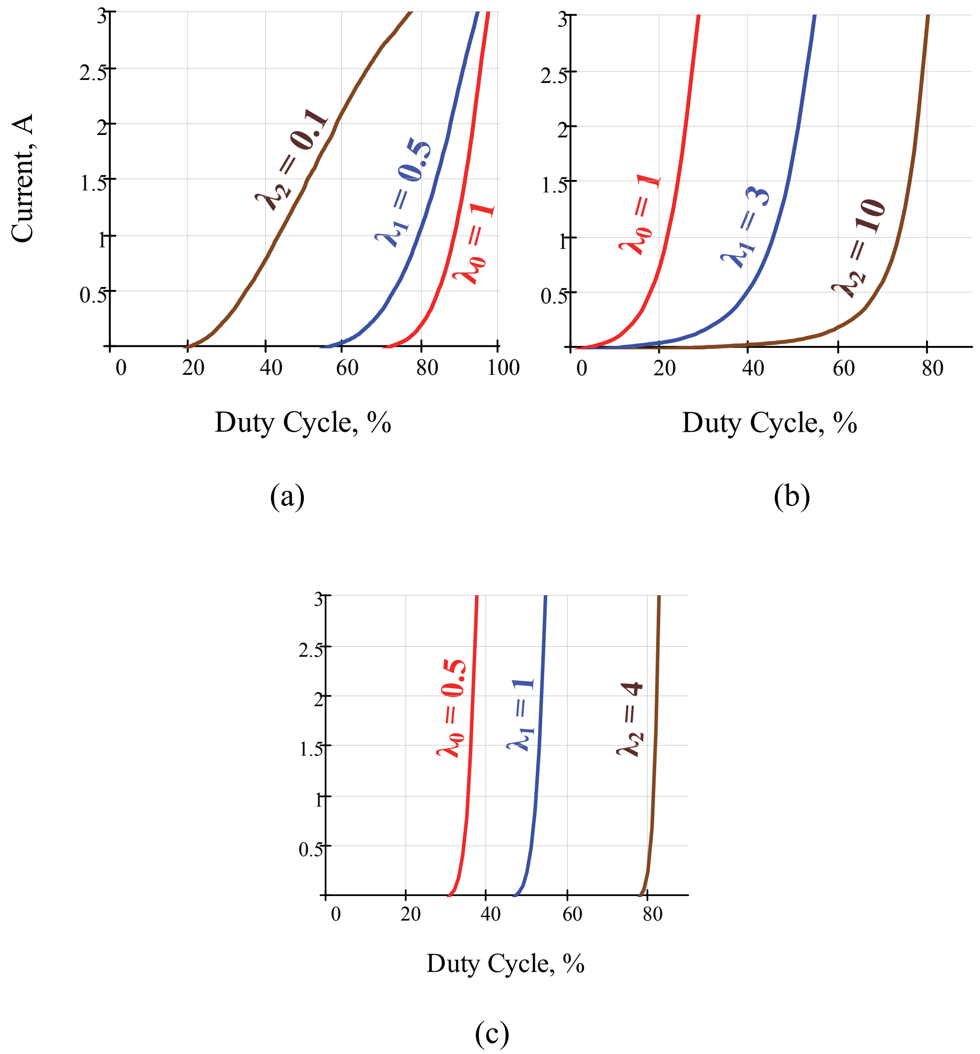

Fig. 3.4 Examples of the transfer functions between the duty cycle and LED load current for tapped-inductor at different λ values: a) buck converter; b) boost converter; c) buck-boost converter.

The analysis of these curves provides insight in the controllability parameters discussed in the first section.

To find out the **optimal value of parameter λ (turns ratio of tapped-inductor)** for each converter topology a few plots with controllability parameter curves at three different input voltages have been constructed. The results are summarized in Fig. 3.5, Fig. 3.6 and Fig. 3.7. This analysis was made using the software for mathematical calculations MathCad.

The analysis of Fig. 3.5 (a), (b) and (c) plots shows that the optimal value of parameter λ for tapped-inductor buck converter from point of view of controllability is approximately 0.1. All the parameters at this point have the best values. Also it is seen from Fig. 3.5 (a), (b) and (c) plots that input voltage of buck converter affects such parameters as practically usable duty cycle span significantly as well as the dynamic range of gain. It is seen that these two parameters are closely related; therefore, are not evaluated for tapped-inductor boost and buck-boost converters. The best results can be achieved at a voltage that is close to the maximum voltage of the LED load.

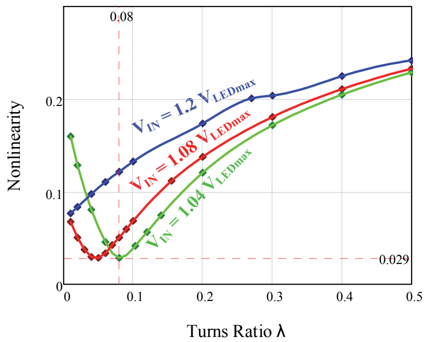

(a)

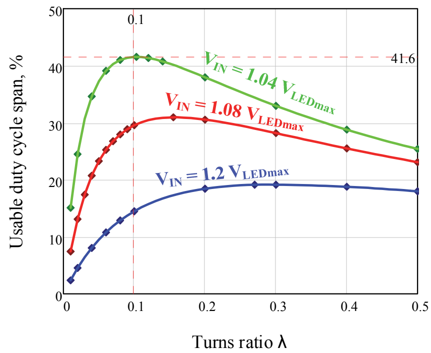

(b)

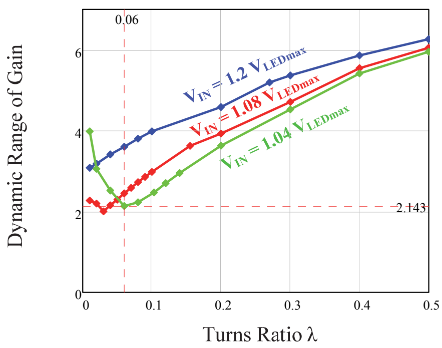

(c)

Fig. 3.5 Controllability parameters of the tapped-inductor buck converter connected to the LED load at different input voltages and tapped-inductor turns ratio λ values: a) nonlinearity; b) usable duty cycle span; c) dynamic range of gain.

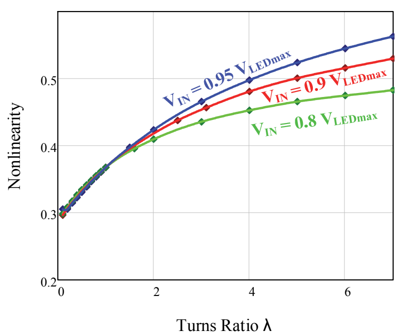

(a)

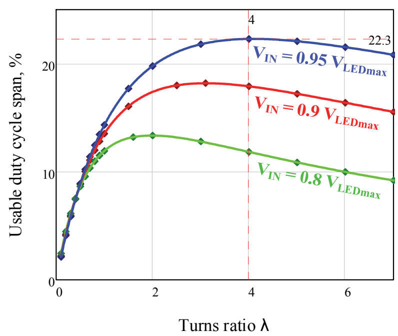

(b)

Fig. 3.6 Controllability parameters of the tapped-inductor boost converter connected to the LED load at different input voltages and tapped-inductor turns ratio λ values: a) nonlinearity; b) usable duty cycle span.

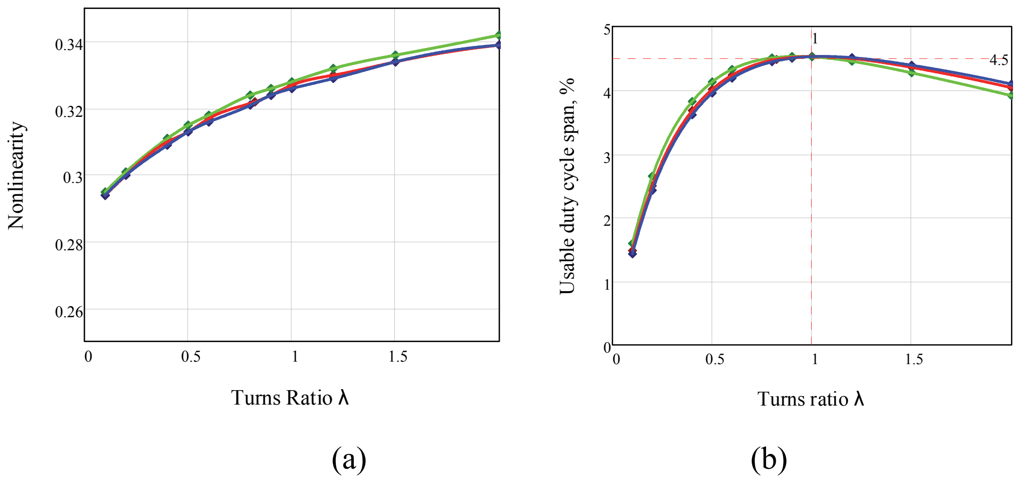

Fig. 3.7 Controllability parameters of the tapped-inductor buck-boost converter connected to the LED load at different input voltages and tapped-inductor turns ratio λ values: a) nonlinearity; b) usable duty cycle span.

For the tapped-inductor boost converter smaller nonlinearity *NL* values appears at smaller λ values (Fig. 3.6 (a)). Usable duty cycle span (Fig. 3.6 (b)) has the best value in the range λ = 2…4. Tapped-inductor boost converter does not have the best values of all the controllability parameters at one point.

A situation is similar with the tapped-inductor buck-boost converter: smaller nonlinearity NL value appears at smaller λ values (Fig. 3.7 (a)), but the usable duty cycle span (Fig. 3.7 (b)) has its best values at $\lambda = 1$ (i.e. conventional buck-boost converter).

To verify the theoretical calculations a laboratory prototypes of fitter-buck ($\lambda = 0.1$) and fitter-boost ($\lambda = 2$) tapped-inductor converter were assembled (in accordance with circuits shown in Table 3.1). The details of these experiments are given in Appendix I.

The results of experiments with the fitter-buck prototype at $V_{in} = 1.04V_{LEDmax}$ input voltage are summarized in Fig. 3.8 (a) and (b). The controllability curve of fitter-buck converter is almost linear (Fig. 3.8 (a)). Usable duty cycle span is more than 65 %, which is approximately 3 times greater in comparison with a conventional buck converter. Therefore, relative inaccuracy of LED current ΔI_{LED} also reduces. Also, the efficiency of fitter-buck is rather high (Fig. 3.8 (b)).

The experiments with the fitter-boost prototype at $V_{in} = 0.95V_{LEDmin}$ are summarized in Fig. 3.9 (a) and (b). The results are not as good as for fitter-buck converter; however, both experiments are good for comparison with numerical calculations (Table 3.2).

It is seen from Table 3.2 that the duty cycle span for the tapped-inductor fitter-buck converter is approximately 3 times greater in comparison with the conventional buck converter, and approximately 2 times greater in comparison with the fitter-boost converter. Thus, using the same control equipment (controller with the same PWM resolution), the accuracy of current regulation can be improved 2…3 times, optimizing turns ratio of the tapped-inductor.

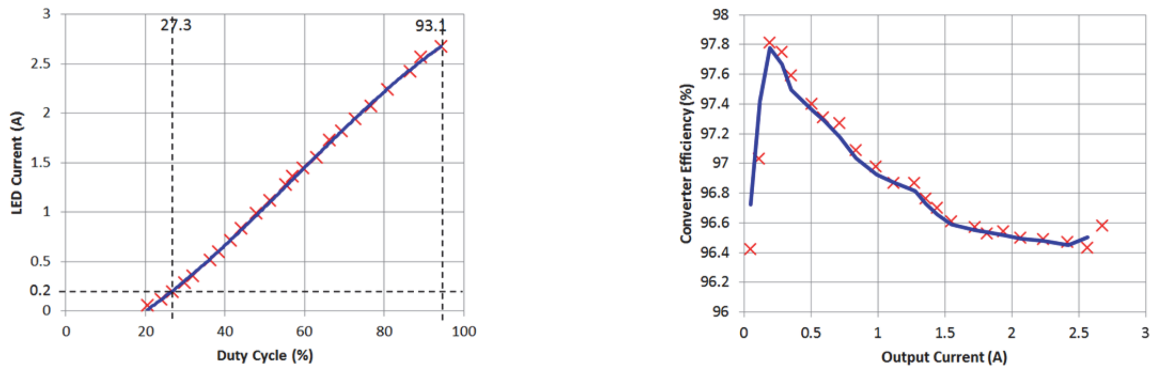

(a) (b)

Fig. 3.8 The results of the experiments with the prototype of fitter-buck ($\lambda = 0.1$) tapped-inductor converter: a) controllability curve; b) efficiency; c) photo of the fitter-buck prototype.

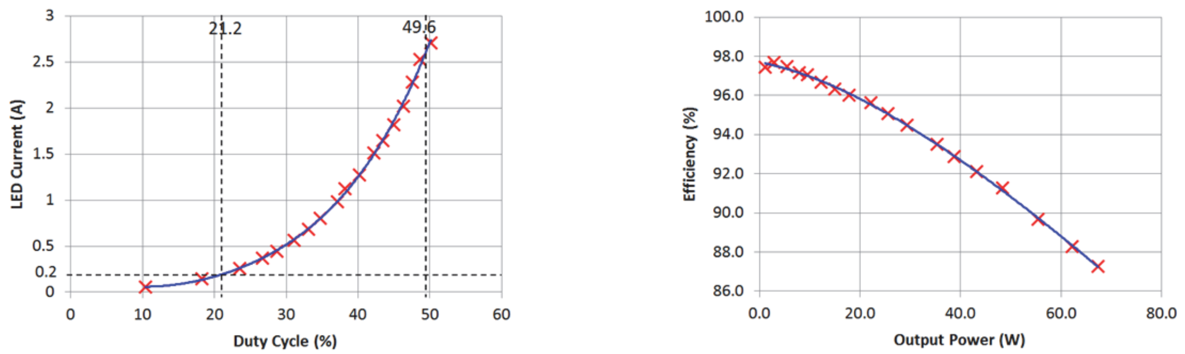

(a) (b)

Fig. 3.9 The results of the experiments with the prototype of fitter-boost ($\lambda = 2$) tapped-inductor converter: a) controllability curve; b) efficiency; f) photo of the fitter-boost prototype.

Table 3.2

Comparison of Theoretical and Experimental Results

	Topology	**Nonlinearity NL, %**	**D_{SPAN}, %**	**ΔI_{LED}, %**
Theoretical	Fitter-Buck (λ=0.1)	4	42	4
	Fitter-Boost (λ=2)	42	20	14
	Conventional buck (λ=1)	25	16	14
Experimental	Fitter-Buck (λ=0.1)	2	67	2
	Fitter-Boost (λ=2)	35	29	10
	Conventional buck (λ=1)	20	20	8

3.5. Discontinuous Conduction Mode for Compensation of Nonlinearity

Another way to compensate nonlinearity of LED V-A curve — use of a discontinuous conduction mode (DCM) of the conventional buck converter — was considered in [106].

The converter operates in a discontinuous mode when low current is drawn by the load, and in continuous mode at higher load current. There is also a boundary point between CCM and

DCM when the inductor current falls to zero exactly at the end of the commutation cycle. This boundary depends on many parameters such as switching frequency f_{sw}, inductance L, duty cycle D and the load. For DCM operation of the buck converter the following criteria should be fulfilled [107], [108]

$$\frac{V_{out}}{V_{IN}} = \begin{cases} D \quad if \quad \dfrac{2L \cdot f_{sw}}{R} < (1-D) \\ \dfrac{2}{1+\sqrt{1+\left(\dfrac{8L \cdot f_{sw}}{R}\right) \Big/ D^2}} \quad otherwise \end{cases}, \tag{3.25}$$

where R is the resistance of resistive load, connected to the converter. Several relationships calculated using (3.25) are given in Fig. 3.10. The same resistance and switching frequency have been used in these calculations, but different inductance values.

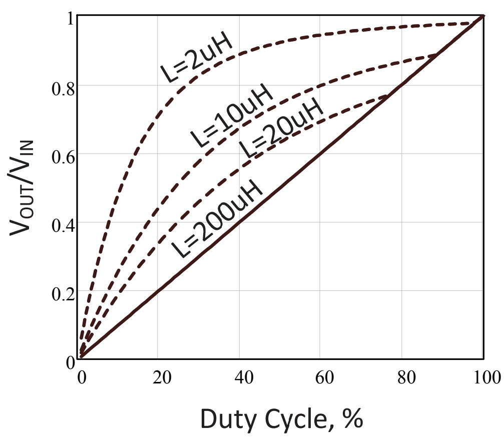

Fig. 3.10 CCM and DCM operation of the buck converter at the same resistive load, but different inductance values.

It is seen from Fig. 3.10 that the buck converter with the lower inductance value L of the main choke allows achieving the relationship required for the compensation of nonlinearity of LEDs, as was shown in Fig. 3.1 (c). However, LED is not resistive load, but the generalized idea is to move the boundary line between CCM and DCM, so that V-A curve of LEDs is mostly located in DCM operation region of the driver. It is expected that the output voltage of the driver increased in DCM will make reduce duty cycles for the same value of the output voltage and current that, in turn, will make the span of duty cycles wider and the control of the driver — easier (Fig. 3.11). The operation of the driver in CCM is shown in Fig. 3.11 (a). Then the operation points of the lamp are defined by horizontal CCM lines, but the range of the duty cycle values of the driver is narrow (from 76 % to 93 %). In contrast, Fig. 3.11 (b) reflects the operation of the driver in DCM. Then the same values of the voltage and current are achieved at lower values of the duty cycle, but its range is wider (from 12 % to 79 %). The expected performance (analytical calculations) in CCM and DCM is shown in Fig. 3.12 (a). Results of experiments are summarized in Fig. 3.12 (b), but the details of these experiments are given in Appendix J.

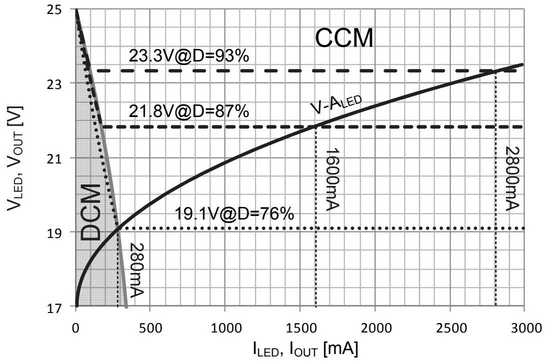

(a)

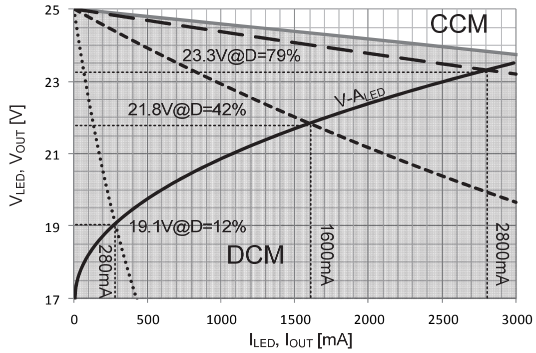

(b)

Fig. 3.11 Calculated operation V-A curves of buck LED driver (VIN = 25 V, load — 7 × W724C 23.2 V × 2.8 A ≈ 70 W): a) completely in CCM; b) completely in DCM.

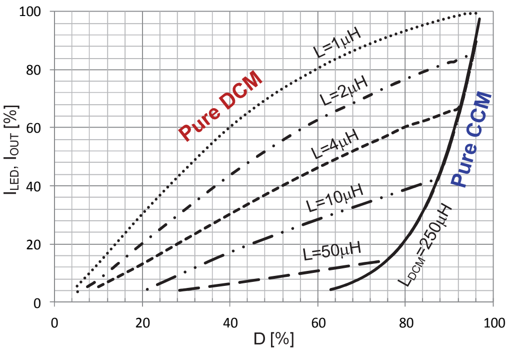

(a)

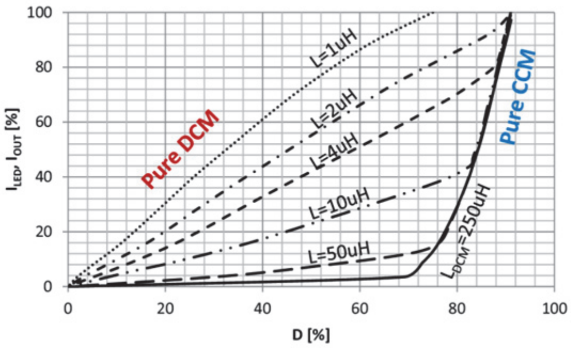

(b)

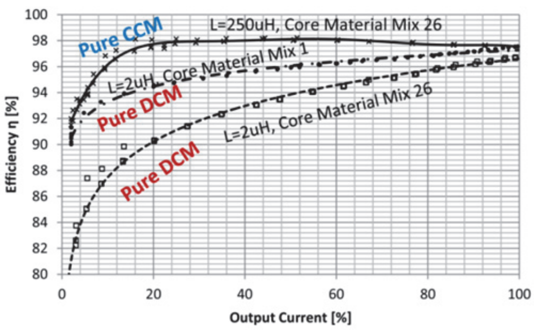

(c)

Fig. 3.12 Regulation and efficiency curves of LED lamp (buck converter) taken in CCM and DCM: a) simulated regulation curves; b) measured regulation curves; c) efficiency at CCM and DCM and different inductor core materials.

The controllability parameters defined in the introduction section were also calculated for analytical calculations, as well as for data obtained from experiments. These controllability parameters are summarized in Table 3.3 and Table 3.4. In these tables the pure CCM operation appears at inductance value *L* = 250 uH, while pure DCM operation appears at inductance value *L* = 2 uH (for experimental data) or *L* = 1 uH (for analytical calculations).

During the study [106] it was found that the use of DCM allows achieving better controllability parameters. However, it was also found that DCM has great impact on the efficiency Fig. 3.12 (c). The estimation of power losses is given in Appendix K.

Table 3.3

Simulated Parameters of Controllability of LED Lamp

L, μH	G_{LEDmin}	G_{LEDmax}	RG	NL, %	G_a
1	**0.53**	**1.61**	**3.03**	**13.2**	**1.15**
2	0.66	5.37	8.14	6.48	0.94
4	0.73	5.37	7.36	2.10	0.77
10	0.51	5.37	10.53	0.44	0.53
50	0.22	5.37	24.41	0.46	0.23
250	1.20	5.37	4.48	17.7	2.97

Table 3.4

Measured Parameters of Controllability of LED Lamp

L, μH	G_{LEDmin}	G_{LEDmax}	RG	NL, %	G_a
1	0.74	1.66	2.24	8.1	1.32
2	**0.92**	**1.25**	**1.36**	**1.9**	**1.10**
4	0.74	7.26	9.81	5.2	0.94
10	0.45	7.26	16.13	3.2	0.5
50	0.24	7.26	30.25	1.8	0.20
250	2.11	7.26	2.79	19.6	4.49

As can be seen from Fig. 3.12 (c) and Appendix K, the choice of inductor core is critical for the converters operating in DCM. It has a great impact on the efficiency. It can be concluded from these curves that the overall efficiency of the converter is higher in CCM; however, the efficiency in DCM can also be improved by proper choice of the inductor size and core material.

3.6. Summary

Two different approaches to compensate nonlinearity of LED load were discussed in this section…

Tapped-inductor

Inherent properties of fitter-buck converter at particular conditions allow compensating LED load nonlinearity, resulting in more stable operation. By using fitter buck converter it is possible to decrease nonlinearity approximately 4 times and to increase usable span of control parameter approximately 3 times in comparison with conventional buck converter. This allows improving current regulation accuracy at the same PWM controller resolution.

The power losses in the switches of fitter-buck converter are smaller in comparison with conventional buck converter resulting to better efficiency. It also allows increasing switching frequency by approximately 30 %.

DCM

A brief summary of the study of LED drivers operating in DCM was presented in this section. The results of simulation and experiments gave opportunity to compare the controllability of LED buck driver with different values of inductance. Obviously, smaller inductance leads to DCM. In this mode the current and duty cycle spans are more equal, therefore the dynamic range is better (closer to 1). Also, the nonlinearity in DCM is slightly smaller than in CCM. Thus, the DCM is preferable from the point of view controllability. However, the operation in DCM strongly depends on value of the inductor. Core material should be chosen carefully (Fig. 3.12 (c)). Also, the losses are high, but it is possible to reduce them by the optimization of the inductor and output capacitor. At the same time, the size of the converter is smaller due to the smaller size of the inductor. Taking into account all pros and cons, DCM can be carefully recommended for use in LED lamps.

4 DIRECT CURRENT CONTROL

4.1. Introduction

LEDs are current consumers rather than voltage consumers. At the same time, the majority of today's LED drivers are based on voltage fed (VF) converters, which means LED current (luminous flux) is controlled indirectly through applied voltage (volt-ampere V-A stage in Fig. 4.1). In previous studies it has been hypothesized that current fed (CF) converters are more suitable for driving LEDs, as the LED current is regulated in direct way [8], [99], [109]. Also, the circuits for three basic topologies of the current fed converters have been derived [8], [109].

The following subsection contains the summary of the current fed converters considered in the previous studies.

4.2. Summary of the Current Fed Converters

The definition and transformation principles are given in [8].

The circuits of considered current fed converter topologies are summarized in Fig. 4.2.

Current transfer function for the CF buck converter can be written as:

$$I_{OUT} = I_{IN} \times (1 - D), \tag{4.1}$$

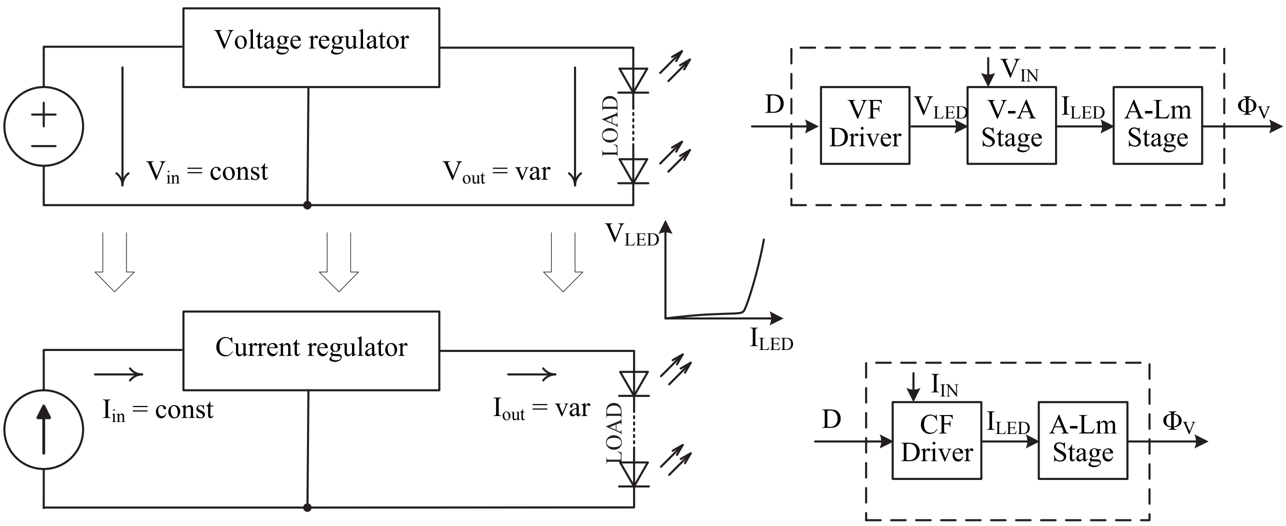

Fig. 4.1 Transition from voltage fed to current fed converters. Functional diagram of the light regulation loops for VF and CF chains.

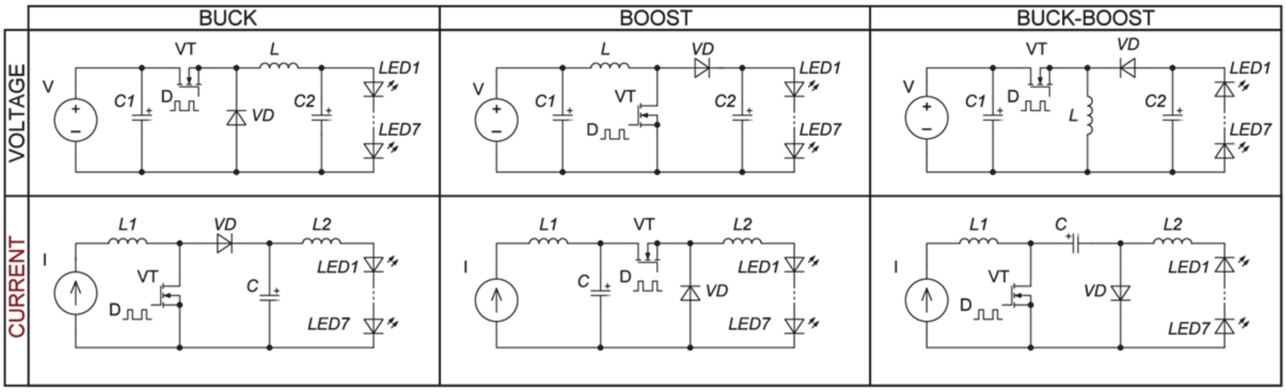

Fig. 4.2 The most widely spread VF converters and their CF versions.

for the CF buck converter:

$$I_{OUTt} = \frac{I_{IN}}{D}, \tag{4.2}$$

but the CF buck boost can be described by the equation

$$I_{OUT} = \frac{-I_{IN} \times (1-D)}{D}. \tag{4.3}$$

These expressions were also defined in [8].

The comparison of controllability of different topologies VF and CF converters are given in Fig. 4.3.

Several advantages of the CF converter over the voltage regulators have been identified for the operation with nonlinear LED load (which is rather current than voltage consumer). Among these advantages:

1) the wider range of usable values of control parameter (duty cycle), which allows increase of resolution;
2) closer to the linear relationship between the control parameter and parameter under control (LED current);
3) reduced value of necessary capacitance, which allows to use ceramic capacitor, thus improving reliability of the driver [110].

The necessity of constant current source at the input has been named the main drawback in [109], [110].

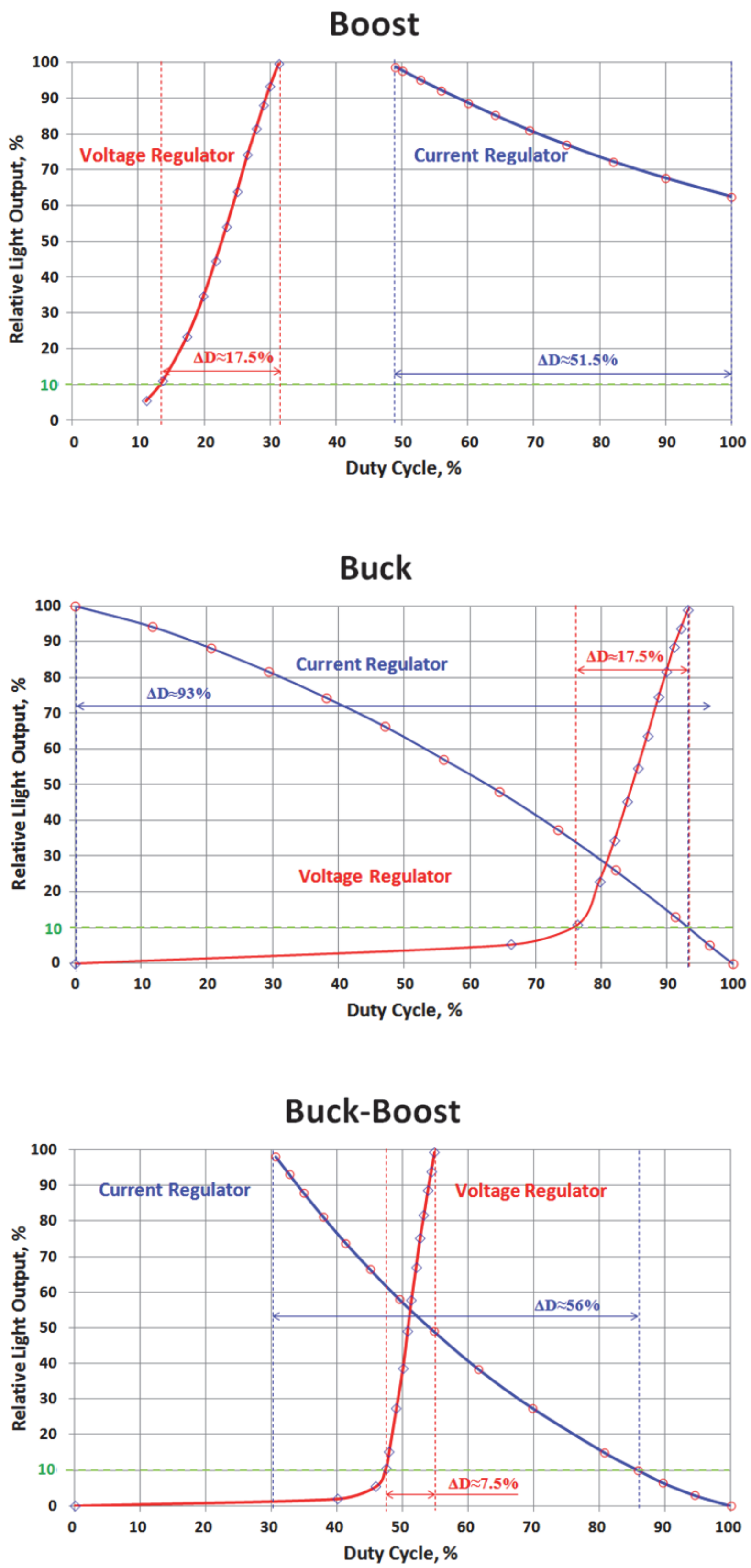

Fig. 4.3 Comparison of controllability curves of different VF and CF topologies

The primary energy source almost always (in many applications) is voltage source. This means that constant current source must be voltage fed converter operating in constant output current mode. The requirements for the constant current source are:

- uninterruptible current at the output
- the capacitor (voltage source) at the output is not allowable to prevent from high short circuit current.

Shaping current in the inductor is most efficient way to create constant current source. Therefore, the inductor current must be input current of the CF driver (inductor must be connected in series with the input of CF driver).

4.3. Non-Inverting Buck-Boost Converter for Direct Current Control

One of the solutions to necessity of constant current source at the input of CF converter was proposed in [111]. In this work non-inverting buck-boost converter has been considered to be the combination of constant current source (CS) and current regulator (CR) as shown in Fig. 4.4.

There are rather many ICs, which are based on this topology and are available on the market, for example [112]. A number of studies have been performed recently to improve different parameters of such circuits. For example, [113] is devoted to optimization of accuracy and energy efficiency of current sensing technique of such ICs, but [114] — optimizes operation of this converter in general purpose applications. However, all these solutions consider the converter to be VF circuit.

The approach presented here is different and considers the topology as a constant current source and current regulator. This may have impact on the values of capacitors and inductors and, therefore, on their weight and size, as well as on the efficiency of the converter. However, the main hypothesis of the research states that by means of this approach it is possible to obtain the regulation curve of the lamp that has high linearity and low averaged gain that, in turn, also provides better accuracy of the regulation and stability of the regulator with a feedback.

According to the [111], transistor VT1 must operate in such a way that average current of inductor L1 is constant (with a variable duty cycle), while the transistor VT2 operates with a constant duty cycle, which determines the value of output current. Transistors can operate either independently or synchronously. In the simplest configuration it is possible to organize a regulation system using only one current feedback in CS stage Fig. 4.4.

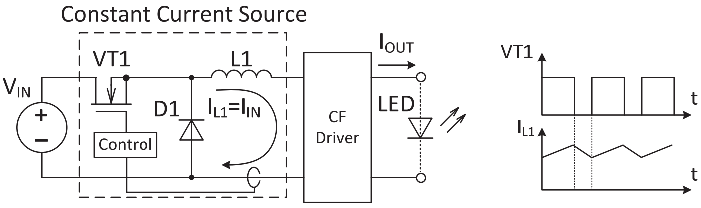

(a)

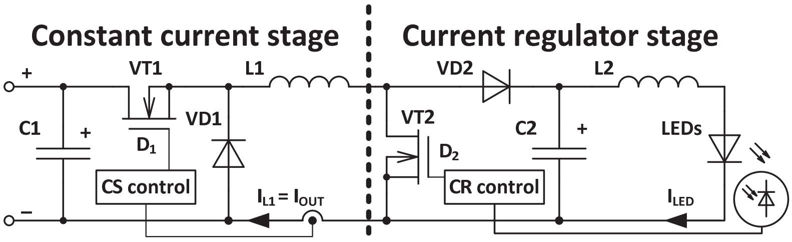

(b)

Fig. 4.4 The concept of direct current control converter: a) combination of constant current source and CF converter; b) principal circuit of non-inverting buck-boost, considered to be the constant current source and current regulator.

The main goal is simplification of control system and reduction of initial costs of the LED lighting system by reduction of application specific integrated circuits.

Several configurations of control system for non-inverting buck-boost converter with independent and synchronous operation of transistors VT1 and VT2 and one current feedback are considered in the following subsections.

4.4. Independent Operation of CC and CR Stages

Both stages of the converter shown in Fig. 4.4 can operate independently with their own switching frequencies f_{sw1}, f_{sw2} and duty cycles D_1 and D_2. The output current is proportional to the duty cycle D_2 of the CR stage, while the constant current at the input is ensured by CS stage operating under constant current controller. There are several different approaches for the current control in CS stage.

Hysteretic Controller

In case of hysteretic controller the output current of the CS stage measured by current sensor is compared with the threshold value. The state of the transistor VT1 is determined by this measured value: the transistor remains open till current threshold value is achieved, then it turns off and the output current decreases. If there is only one threshold value, the controller tends to operate around it at very high frequency (or even in active region of the transistor VT1) causing high power losses. Therefore, hysteretic window is necessary to ensure proper switch mode operation.

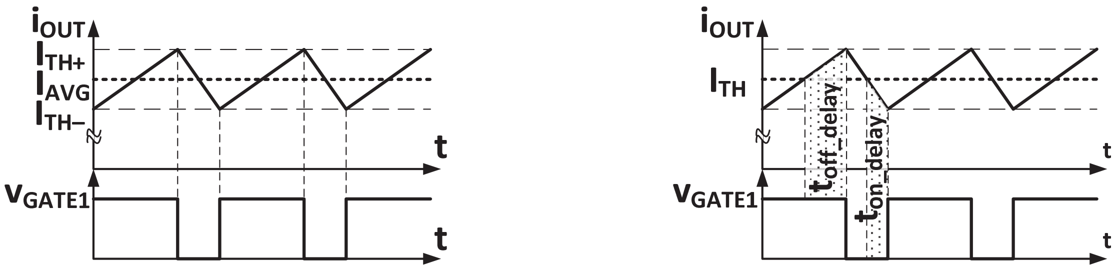

(a) (b)

Fig. 4.5 Operation principles of hysteretic current controller: a) using output current threshold values of upper level I_{TH+} and lower level I_{TH-}; b) using time delays at switch on t_{on_delay} and switch off t_{off_delay} of transistor VT1.

The hysteretic window can be implemented in two ways:

1) by setting two output current threshold values;
2) by setting constant delays at transistor VT1 switch on and switch off (Fig. 4.5).

Constant current source (CS stage) based on buck converter controlled by IRS2541 integrated circuit has been implemented for experimental verification of the performance of hysteretic controller. The hysteretic window of this IC is carried out by constant turn on t_{on_delay} = 320ns and turn off t_{off_delay} = 180ns delays [115].

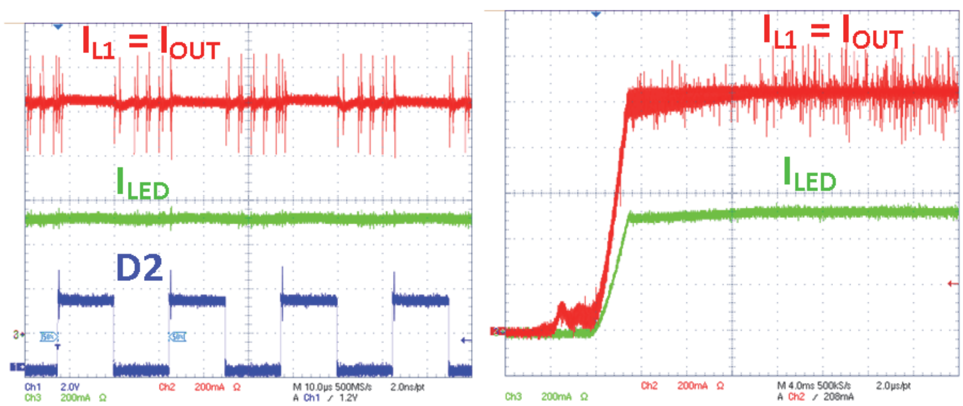

(a) (b)

Fig. 4.6 Operation of non-inverting buck-boost at independent control of CS and CR stages (hysteretic controller for CS stage): a) steady state operation at D2 = 50 %; b) start-up process and further operation at D2 = 50 %

The examples of operation of independently controlled stages of non-inverting buck-boost with hysteretic controller at CS stage are given in Fig. 4.6. For given examples CS stage operates at frequency $f_{sw1} \approx 300$ kHz, while CR stage at frequency $f_{sw2} \approx 40$ kHz.

Frequency Modulation Controllers

In case of frequency modulation (FM) two different approaches are possible: constant pulse frequency modulation (CPFM) and constant pause frequency modulation (CZFM) as shown in Fig. 4.7 (a) and (b). The frequency is variable and depends on the approach: for CPFM the frequency increases at higher duty cycle values, while in case of CZFH it decreases at higher duty cycle values (Fig. 4.7 (d)) [117].

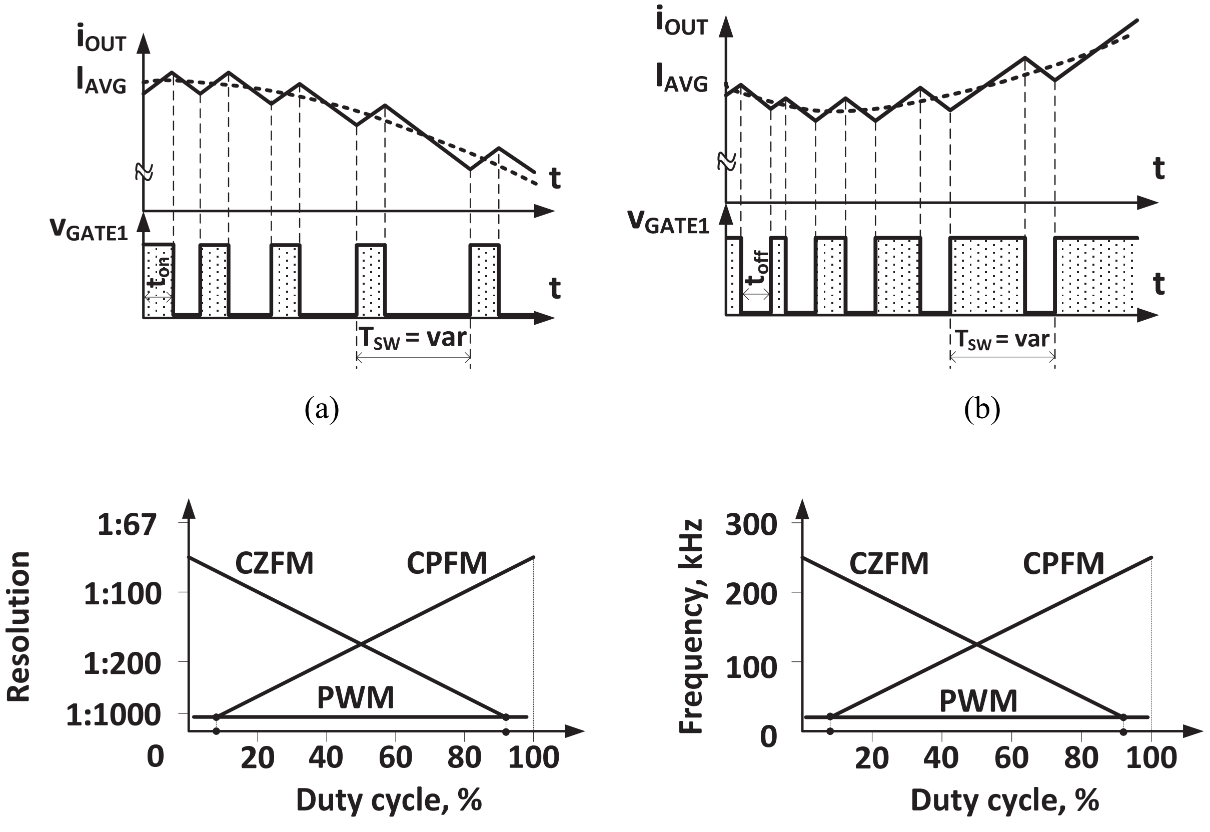

Fig. 4.7 Operation principles of frequency modulation controller: a) constant pulse frequency modulation (CPFM); b) constant pause frequency modulation (CZFM); c) relationship between the resolution and duty cycle; d) relationship between the frequency and duty cycle

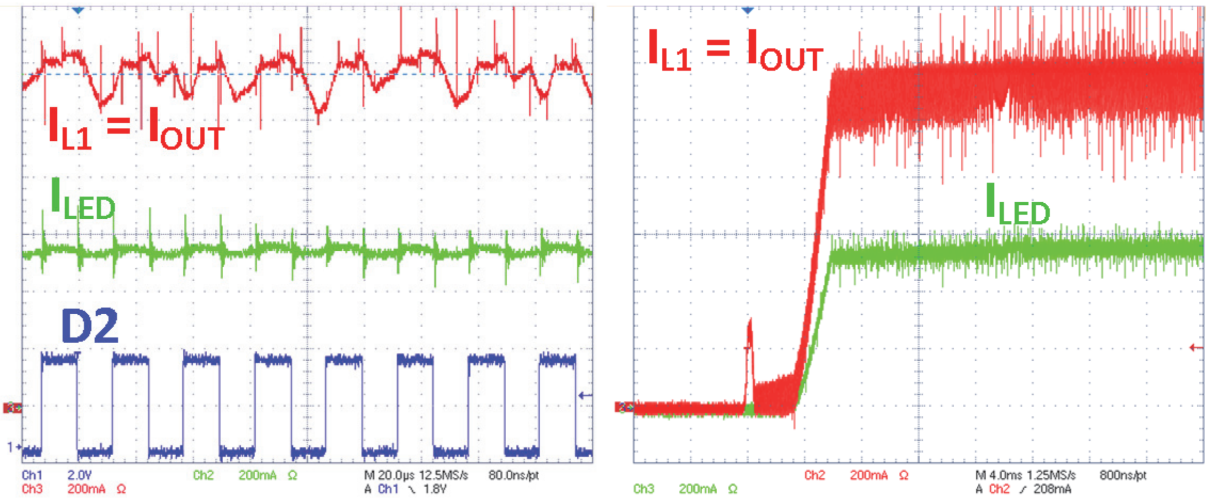

(a) (b)

Fig. 4.8 Operation of non-inverting buck-boost at independent control of CS and CR stages (constant pause controller for CS stage): a) steady state operation at D_2 = 50 %; b) start-up process and further operation at D_2 = 50 %

Also, the resolution in case of FM controller depends from the duty cycle and there is minimum duty cycle value for CPFM and maximum duty cycle value of CZFM (Fig. 4.7 (c)). All this makes FM controller more suitable for stable functionality around one operation points and less suitable for implementation in switch mode converters operating in true constant current mode.

Despite this, constant current source (CS stage) based on buck converter controlled by CPC9909 integrated circuit (IC) has been implemented for experimental verification of the performance of CZFM controller. The constant pause t_{off} = 4µs was set using external resistor in accordance with [118].

The examples of operation of independently controlled stages of non-inverting buck-boost with CZFM controller at CS stage are given in Fig. 4.8. For given examples CS stage operates at frequency $f_{sw1} \approx 240$ kHz, while CR stage at frequency $f_{sw2} \approx 40$ kHz.

Pulse Width Modulation Controller

Pulse wide modulation controller operates at constant frequency. The main advantage of the operation at constant frequency is the reduction of the potential problems with electromagnetic compatibility (EMC) and design of electromagnetic interference (EMI) filter, which is more complicated for broadband frequency range.

For the verification of CS stage operating under PWM controller one of the prototypes discussed in the hardware description section was used. Microcontroller based PWM controller with constant current closed-loop regulation was used.

Experimental verification is summarized in Appendix J.

4.5. Control Algorithm for Synchronous Operation

One of the aims of this research is development of the control algorithm for the LED driver combining voltage source-to-current source converter and current regulator. It is obvious that this control law can be split into two parts — for the current source and for the current regulator. At the same time it is possible to use power balance to obtain the necessary equations.

The static equation of CF buck converter known, for example, from [99] is as follows:

$$i_{LED}(D_2) = I_{\max} \cdot i_{LED}(RO) = I_{L1}(1 - D_2)\,, \tag{4.4}$$

where: D_2 - is the duty cycle of the current regulator, I_{max} -rated current of LEDs, I_{L1} - current in the choke L1, but $i_{LED}(RO)$ is a reversed A-Lm characteristic of LEDs (shown in Fig. 2.7) normalized with respect to the rated current and luminous flux (in which normalized luminous flux measured in [116] is called RO — relative output). The assumption that this curve is linear with slope of 1, as well as $I_{L1} = I_{max}$, gives:

$$D_2 = 1 - RO\,, \tag{4.5}$$

i.e. the more intensive light requires the lower $D1$. The output power on the output side (LEDs side) is equal to:

$$p_{LED}(D_2) = i_{LED}(D_2) \cdot v_{LED}(D_2)\,, \tag{4.6}$$

where $i_{LED}(D_2)$ is found from (4.4)), but can be expressed based on V-A curve. Its simplest approximation (Fig. 2.6 (a)) is linear (2.11).

Combining (4.6) with (4.4), (4.5) and (2.11) produces:

$$p_{LED}(D_2) = V_0 \cdot I_{\max} \cdot RO + R_s \cdot I_{\max}^2 \cdot RO^2\,. \tag{4.7}$$

where: V_0 - is the minimum voltage of LEDs, at which they start emitting light, R_s - their equivalent series resistance.

On the other hand, the input power of the circuit is expressed as a product of input voltage V_{IN} and input current i_{IN}, which is proportional to the duty cycle of the input transistor VT1 - *D1*:

$$p_{IN}(D_1) = V_{IN} \cdot I_{L1} \cdot D_1 = V_{\max} \cdot I_{\max} \cdot D_1 , \tag{4.8}$$

where V_{max} is the maximum LED voltage obtained at the maximum current I_{max}. Then from the power balance $p_{IN} = p_{LED}$ follows:

$$V_{\max} \cdot I_{\max} \cdot D_1 = V_0 \cdot I_{\max} \cdot RO + R_s \cdot I_{\max}^2 \cdot RO^2 \text{ or } D_1 = \frac{V_0}{V_{\max}} \cdot RO + \frac{R_s \cdot I_{\max}}{V_{\max}} \cdot RO^2 . \tag{4.9}$$

Taking into account that LEDs start emitting light at 75 % of their maximum voltage (4.9) can be rewritten as:

$$D_1 \approx 0.75 \cdot RO + 0.25 \cdot RO^2 \text{ or} \tag{4.10}$$

$$D_1 \approx RO \tag{4.11}$$

Equations (4.10), (4.11) and (4.5) show that the non-inverting VF buck-boost circuitry interpreted as a combination of constant source and CF buck regulator has to be controlled with complimentary control signals:

$$D_1 + D_2 \approx 100\% . \tag{4.12}$$

One of them is equal to the relative light output of the lamp, but the other is nearly reverse proportional to it.

Analytical relationships between the relative output and duty cycle of CS (4.10) or CR (4.5) are given in Fig. 4.9. Also, precise control law ($D_1 + D_2$) is represented in this figure. It is seen from Fig. 4.9 that the precise control law based on power balance requires slightly smaller value of sum of duty cycles. It means that the simplified control law version will produce higher current than it is required in central regulation region.

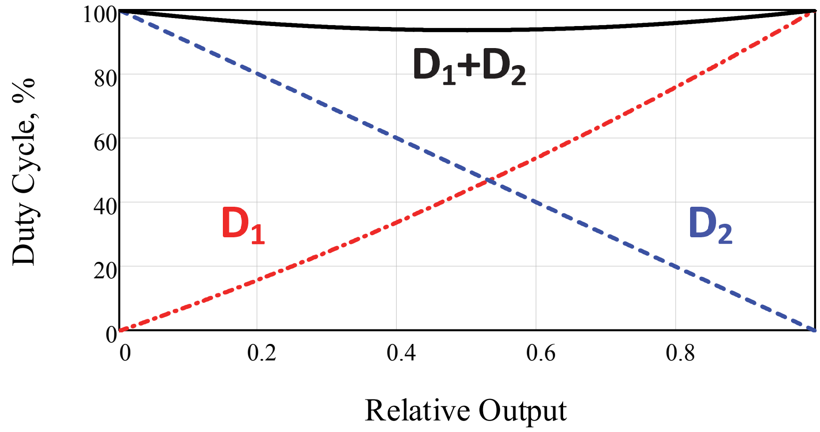

Fig. 4.9 Relationships between the relative output and duty cycle of CS (D_1) or CR (D_2), as well as precise analytical control law $D_1 + D_2$.

Non-inverting buck-boost converter with control defined by (4.5) and (4.11) has been tested experimentally to confirm these considerations. The obtained regulation curves are given in Fig. 4.10 (a).

In general, the expected regulation of the output current is achieved, if condition (4.10) is fulfilled. Also, the current of the CS stage is rather stable within a wide range (40…100 %), as evident from Fig. 4.10 (b).

At the same time, several phenomena can be noticed in this figure:

- there is a certain nonlinearity of the output current and variation of source current;
- the switching cycles of the transistors are synchronized so that the beginning of the on-state for both transistors is the same; then the operation cycle consists of three stages (Fig. 4.11): (I) charge stage, when the input voltage through transistors is applied in positive direction to the internal source inductor L2, (II) neutral stage — when the voltage drop across the inductor is zero or close to that and (III) discharge stage — when the output voltage through diodes is applied to the inductor in reverse direction; two kinds of the neutral stage are possible: at $D_2 < 50$ % it may be tied to ground (IIa) through VT11 and VD22 — Fig. 4.11 (a), or, at $D_2 > 50$ %, it may be placed between almost equal input and output voltages (IIb) by means of VT21 and VD12 — Fig. 4.11 (c); in the case, when $D_2 = 50$ % the neutral stage does not occur — Fig. 4.11 (b);

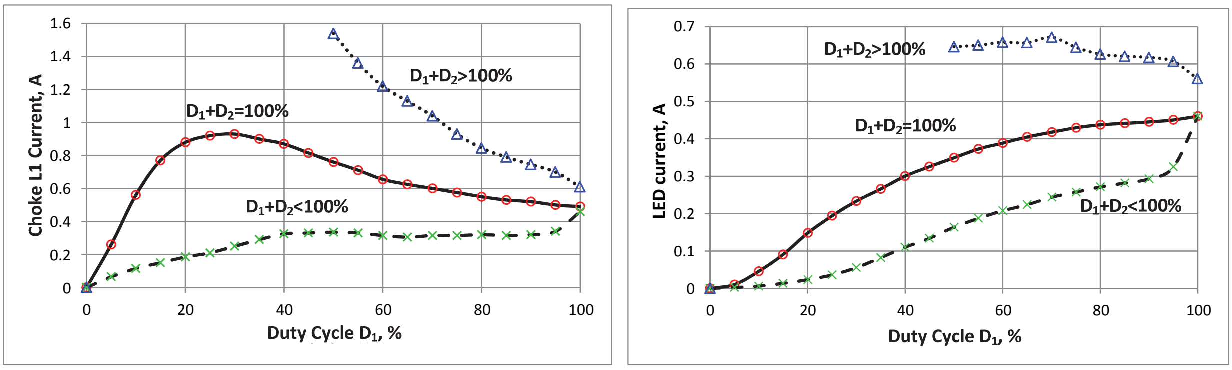

(a) (b)

Fig. 4.10 Source (a) and output (b) current of non-inverting buck-boos converter with applied direct current regulation.

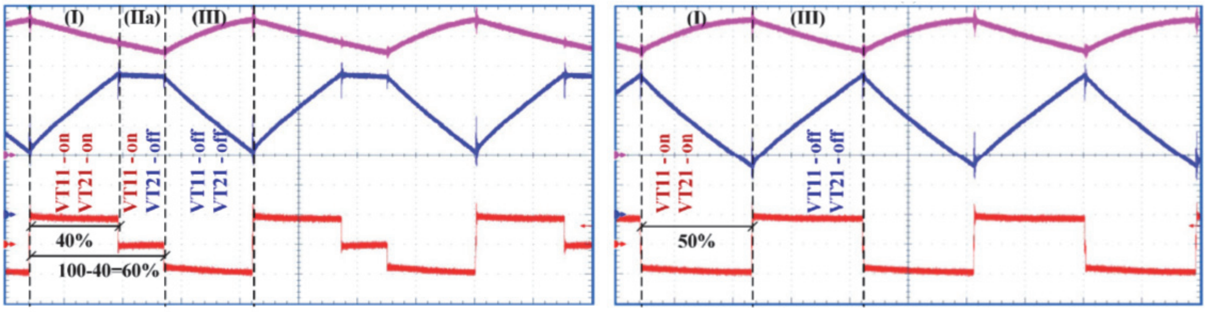

(a) (b)

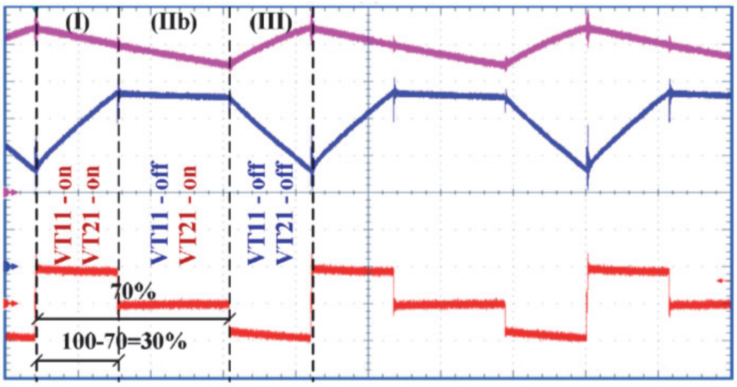

(c)

Fig. 4.11 Source current (blue), voltage (red) and capacitor voltage (magenta) at D2 = 40 % (a), 50 % (b) and 70 % (c). In this figure time scale is 5 μs/div, voltage scale for inductor (red) is 50 V/div, voltage scale for capacitor is 10 V/div, but current scale is 0.2 A/div.

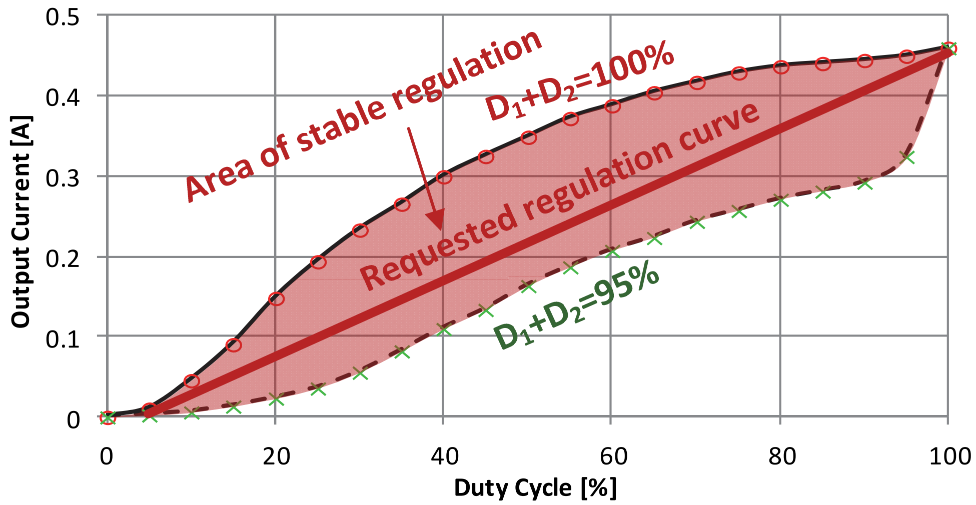

Fig. 4.12 Possible regulation area of tested non-inverting buck-boost converter controlled as combination of current source and current regulator (in this figure duty cycle is D_1).

- the charge stage has to be balanced with the discharge stage, which is possible if (4.10) is valid; therefore, the converter is very sensitive to the charge/discharge unbalance; if $D_1 + D_2 > 1$ the output current and power rise rapidly and the converter is under the risk of damage; if $D_1 + D_2 < 1$ then the converter does not produce the required source and output currents;
- the described above balance rule makes development of control solutions for the converter more complex; however, there is a range of values of the duty cycles (pink area in Fig. 4.12) providing a possibility of a linear regulation curve; the duty cycle itself (whether D_1 or D_2) is the main regulation parameter while the balance $D_1 + D_2$ plays an additional tuning role.

4.6. MCU Based Double Closed Loop Control System

As mentioned previously the main control algorithm for the transistors is (4.10), if the specific operation of the transistors VT1 and VT2 is provided as shown in Fig. 4.11. This ensures that the current of inductor L1 is more or less constant.

Furthermore, the duty cycle D_2 of CR stage can be easily calculated from:

$$D_2 = 1 - I_{SET\_LED} / I_{SET\_CC}\,, \tag{4.13}$$

where I_{SET_LED} is the set point of the current of CR stage, but I_{SET_CC} is the set point of the current of CC stage (set point of maximum current). Combination of (4.10) and (4.13) gives:

$$D_1 \approx I_{SET\_LED} / I_{SET\_CC}\,. \tag{4.14}$$

Therefore, the duty cycles of the transistors VT1 and VT2 can be calculated for the appropriate LED current I_{LED} using (4.13) and (4.14), and fast acting closed loop regulation can be implemented for only one stage (here for CR stage, as it is most critical for proper converter operation) as shown in Fig. 4.13.

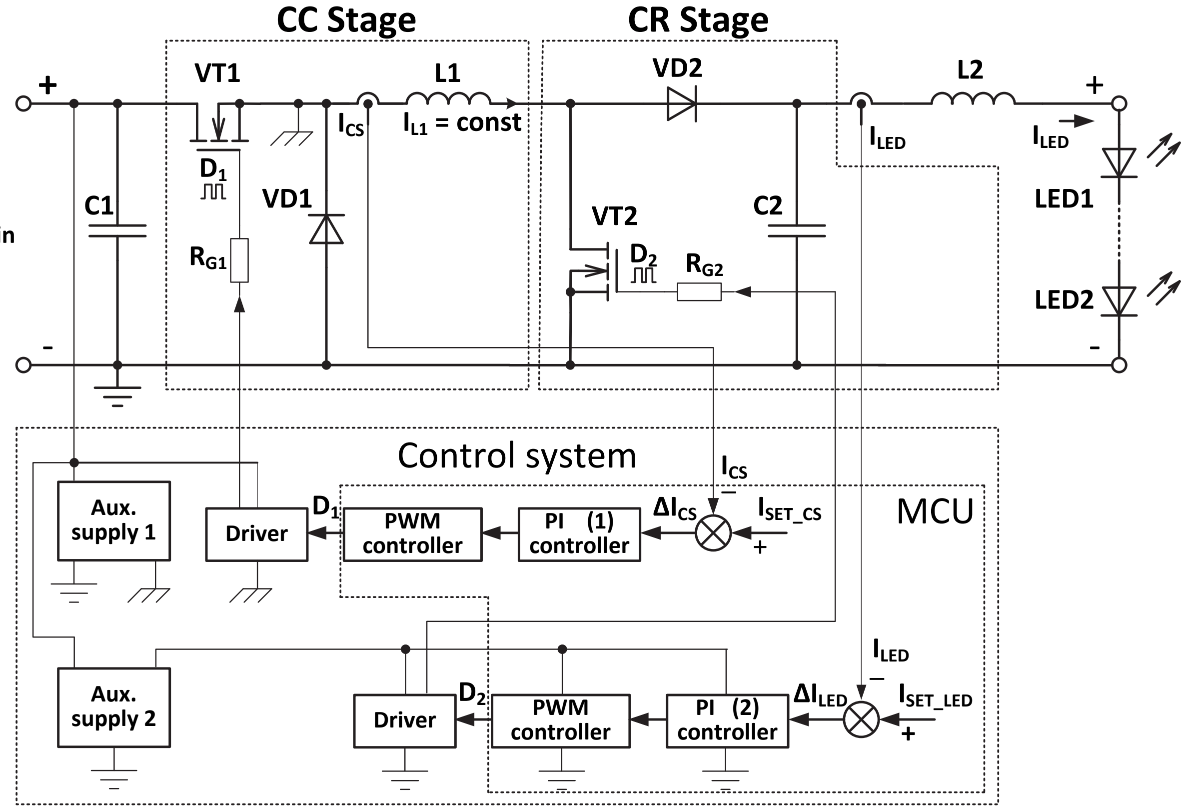

Fig. 4.13 Double closed loop control chain for synchronous operation of CS and CR stages of the non-inverting buck-boost converter based on microcontroller MSP430F2234.

In fact, Fig. 4.13 shows two PI controllers based on microcontroller, where proportional part is taken from the current sensor (actual measurements) while the integral part is calculated (predicted) based on known model (4.14) of the converter.

The control system in accordance with Fig. 4.13 based on MSP430F2234 microcontroller has been implemented for experimental verification of the performance of proposed synchronous operation of both stages of the non-inverting buck-boost converter. Microcontroller code for this configuration of control system is given in Appendix P, and the full electrical circuit for PCB project (OrCAD) is given in Appendix P.

The examples of operation of synchronously controlled stages of non-inverting buck-boost with proposed control method are given in Fig. 4.14. For given examples both stages operate at a constant frequency $f_{sw1} = f_{sw2}$ = 40 kHz.

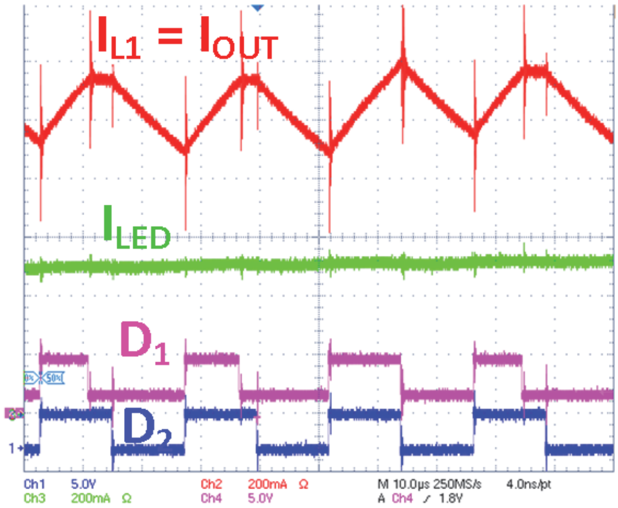

(a)

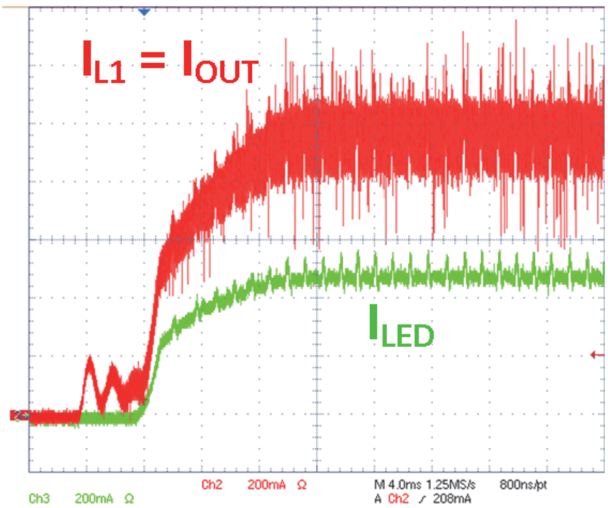

(b)

Fig. 4.14 Operation of non-inverting buck-boost at synchronous control of CS and CR stages: a) steady state operation at $D_2 = 50$ %; b) start-up process and further operation at $D_2 = 50$ %.

4.7. Comparison of Control Approaches

All the experiments have been conducted at similar conditions: input voltage $V_{IN} = 35$ V; LED load of 8 Seoul Semiconductor W724C0 LEDs connected in series.

The comparison in accordance with the control law (4.13) and the efficiency at different approaches is given in Fig. 4.15.

According to the obtained results (Fig. 4.15 (a)), all considered approaches are suitable for implementation of direct current control. However, the hysteretic controller is most suitable for the asynchronous operation under the described conditions. At the same time only the proposed synchronous operation allows eliminating ASIC to implement completely MCU based control system, thus reducing initial costs. It is worth mentioning that synchronous operation also gives good results: it allows achieving higher efficiency (Fig. 4.15 (b)) due to lower switching frequency of CS stage (the same with CR stage).

4.8. n + p Versus p + n Configurations

The non-inverting buck-boost converter (Fig. 4.4) contains the high side transistor VT1 and the low side transistor VT2, which are located on different branches of the bridge. This leads to certain difficulties in organization of the MOSFET driver circuits. In general case (if both are n-type transistors) the power supply of transistor drivers should be isolated from each other. Auxiliary power supply with separate windings can be used for this purpose, as shown in Fig. 4.16 (a).

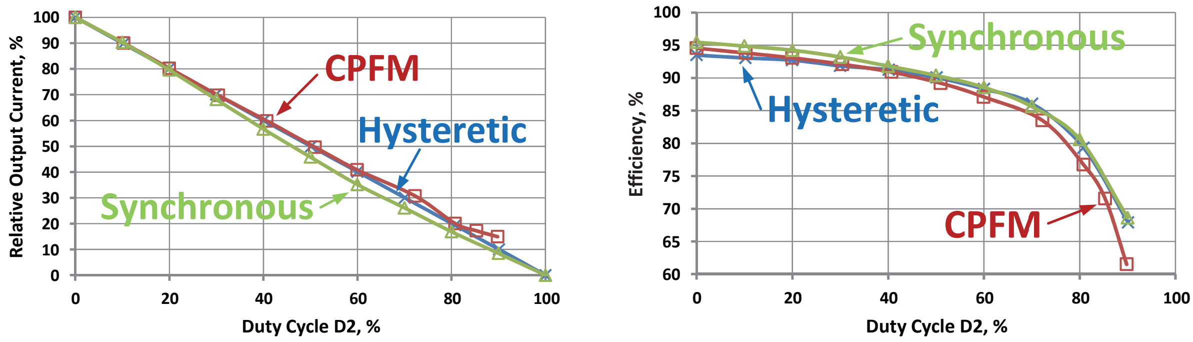

(a) (b)

Fig. 4.15 Performance of non-inverting buck-boost, considered to be the combination of CS and CR stages at different control approaches: a) verification of control law (4.13); b) comparison of efficiencies.

The standard solutions of the problems described above (use of isolation transformer for decoupling of transistor signals or MOSFET drivers with bootstrap capacitor) are not suitable for this converter because of special control technique of the transistors (the value of duty cycle d of the control signal at certain operation point of the converter can reach 100 %).

Use of a galvanically isolated power supply for the MOSFET driver solves the problems described above. Both switches of the converter for the considered case are n-channel field effect transistors (FETs). For this approach it is necessary to use separate small power pulse mode converter with isolation transformer (the general case is shown in Fig. 4.16 (a)).

A ready-made small power (1W) isolated DC-DC power supplies can be used for this purpose. Such power supplies are widely represented on the market. The second option is to use application specific integrated circuits (ASICs) to build isolated power supply for drivers. The benefit in this case is the possibility to provide isolated supply for both drivers by one auxiliary power supply. The main drawbacks are higher initial costs as well as more complicated overall system.

For the clarity of operation principles the current and the voltage waveforms of the inductor L1, as well as control signals of the transistors for this configuration of driver circuits are shown in Fig. 4.16 (b).

The substitution of high side n-type FET by **p-type FET** allows getting rid from obligatory using of auxiliary isolated power supply — this configuration requires sole supply voltage for all needs: power part, drivers and sensors. The supply of p-type FET driver can be implemented on negative linear voltage regulators, as it shown in Fig. 4.16 (c). However, there are higher power

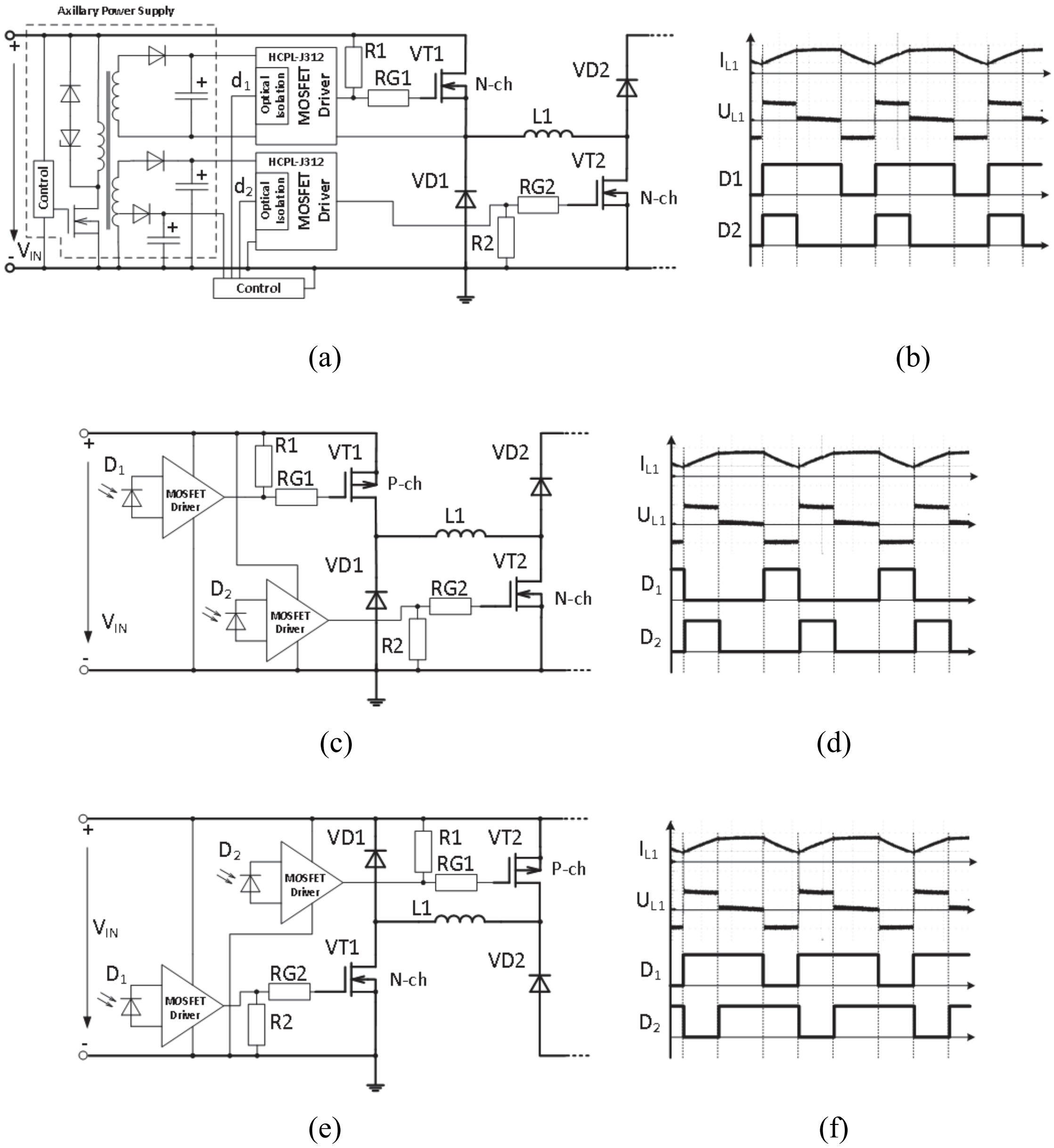

Fig. 4.16 Possible configurations of MOSFET driver circuits for non-inverting buck-boost converter: a) both are n-type transistors; c) p + n configuration; e) n + p configuration; b), d), f) the current and voltage waveforms of inductor L1 and control signals for corresponding configuration.

losses on linear voltage regulators with the increase of input voltage in comparison with small power isolated DC-DC converters (isolated auxiliary power supplies).

At the same time the on-state resistance of p-type FET is higher than that of n-channel MOSFET. Also, for such voltages it is quite realistic to find a proper Schottky diode. Therefore, in such configuration the transistors, especially p-type FET, can be regarded as the main source of conduction losses. Finally, the circuit can be built in two ways: in respect to the ground, as shown in Fig. 4.16 (c) (n + p configuration), and in respect to the positive voltage potential, as shown in Fig. 4.16 (e) (p + n configuration). The current and the voltage waveforms of the inductor L1, as well as control signals of the transistors for these configurations of driver circuits are shown in Fig. 4.16 (d) and (f) respectively. In these cases the logic of the control for p-type transistors will be inverted. The goal of this study was to find the version and on the duty cycles at which the losses of p-type FET are not dominant.

It can be found that p-type FET conducts for a longer time and contributes more losses in the case of ground related converter (Fig. 4.16 (c)), and higher reference command, as well as in the case of positive node related converter (Fig. 4.16 (e) and lower reference command. Therefore, the particular choice depends a lot on the dimming level. Below this hypothesis is verified practically.

The laboratory prototypes of both CF buck driver configurations have been built and tested in the same conditions (The details of these tests are given in Appendix M). A brief efficiency comparison of both configurations is given in Table 4.1. These results allow finding out that the positive node related configuration is slightly more efficient, as expected.

Also, thermal images of the prototypes at different output power were captured (Appendix M). It is quite difficult to clearly assess the element losses using these images because the hottest elements affect nearby elements. However, some conclusions can be drawn:

- At higher output power the main conduction losses of the switches are concentrated in input transistor VT1 (P-FET for the ground related configuration and N-FET for the positive node configuration) and diode VD2. In this case, the smaller transistor on resistance is preferable for VT21;
- At lower output power the main conduction losses of the switches are concentrated in transistor VT2 (N-FET for the ground related configuration and P-FET for the positive node configuration) and diode VD1. In this case, the smaller transistor on resistance is preferable for VT11;
- Among all the switches the diodes are those elements, where the main losses appear.

It is seen from experiments (Appendix M) that the higher power losses of inductor L2 appears at approximately 50 % of maximum output power. In this case the dominant are inductor core losses, which are highly dependent from the current ripple. It means that the current ripple in the inductor L2 has a great impact on the overall efficiency of the considered converter.

Table 4.1

Efficiency Comparison of n + p and p + n Configurations of the Converter

P_{OUT}	$0.25 \cdot P_{max}$	$0.5 \cdot P_{max}$	$0.75 \cdot P_{max}$	P_{max}
n + p configuration	74.0 %	82.9	88.5 %	92.5 %
p + n configuration	71.9 %	81.9 %	87.8 %	92.0 %

However, the impact on the electrical power consumption depends on dimming profile of the analyzed lighting system. The simplest dimming profile for the street lighting allows full exploitation of the maximum light intensity (100 %) during the first (till 24:00) and the last few hours (after 6:00) of system operation, thereby reducing the energy consumption in the middle of the night when a lower level of illumination (70 %) is enough [119]. To find out the operation time of the system at these dimming levels, the data of the sunset and sunrise time for one year (2014) for the location of Latvia [120] has been analyzed. The results are summarizes in Fig. 4.17.

For the sample calculations it was decided to use the known parameters of the park lighting system in Kuldiga, a town in Latvia. One part of this lighting system consists of 24 LED lamps; each lamp provides luminous flux of 4000 lm. Also, we assume that the total efficacy of LEDs and the optics of the considered lamps are equal to 100lm/W. The ballast of the lamp consists of primary power supply (95 % efficient) and LED dimmer considered in the scope of this paper (from Fig. 5: the efficiency of ground related configuration is 92 % at 100 % of maximum output power and 86.8 % at 70 % of maximum output power; the efficiency of positive node related configuration is 92.5 % at 100 % of maximum output power and 87.6 % at 70 % of maximum output power). Taking into account all the parameters discussed above the total electrical consumption to provide required illumination level during one year can be found: 4588kWh for the LED lamp with ground related configuration and 4556kWh for the LED lamp with positive node related configuration, which is 0.7 % savings.

4.9. Summary

According to [109], direct current control approach allows increasing regulation resolution approximately 3 to 6 times in comparison with voltage regulator (buck, boost, and buck-boost). The non-inverting buck-boost converter with proper control can operate as a combination of a current source and current regulator that provides a good opportunity to adjust its output current (and the corresponding LED light) in the wide range of its duty cycle. Therefore, the approach itself is suitable for fluently dimmable LED drivers.

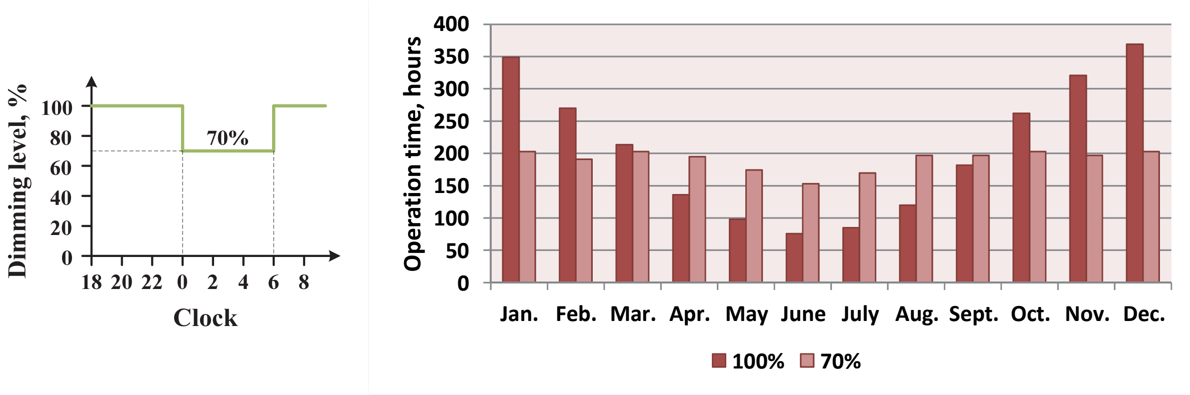

Fig. 4.17 The simplest dimming profile (a) and the operation time of the LED lamps for this profile at different dimming levels during the year (b).

Several control approaches have been studied in this research. According to the obtained results, the hysteretic controller is most suitable for the operation of non-inverting buck-boost converter under described conditions. However, the proposed synchronous operation also gives good results and allows using only microcontroller without additional application specific integrated circuits, thus reducing initial costs.

Also, the different sole supply configurations of the non-inverting buck-boost converter were studied from the point of view of efficiency. The theoretical assumption that the positive node related configuration is more efficient was confirmed during the experiments (Fig. 6.21). Also, experiments show that the inductor core losses significantly affect the total losses of the current source inductor L2 due to current ripple (Table 6.5, Fig. 6.23). The power losses of this inductor can be reduced using more appropriate core material. It is worth mentioning that the significant parameter of the assessment is the lighting profile, where the dimming levels and the operation time at these levels are taken into account. Thus, the same topology and the same element base allow improving the efficiency by choosing the proper configuration for particular application.

At the same time some significant features of the approach that complicate its development have been discovered. First of all, more accurate duty cycle balance equation has to be supported by control system. Secondly, also the balance itself has to be kept carefully — it can be used for additional regulation.

5 CONCLUSIONS

Two main hypotheses have been formulated in the beginning of the Doctoral Thesis:

1. The accuracy of fluent light regulation can be improved by the compensation of nonlinearities of LED (volt-ampere, lumen-ampere curves) with nonlinearity of driver;
2. Direct LED current regulation can be implemented on the basis of non-inverting buck-boost converter.

1. For the confirmation/refutation of the first hypothesis the different converter topologies with nonlinear input-to-output transfer functions have been studied, as well as operation of DC-DC converter in a discontinuous conduction mode.

During these studies it has been found that the fitter-buck converter, which is the member of the family of tapped-inductor converters, is capable of providing the required nonlinear input-to-output transfer function. This transfer function can be tuned by the ratio of winding turns of tapped-inductor $\lambda = N1/N2$. The optimal value of the parameter λ and the operation conditions of the converter have been found in analytical way by evaluation of controllability parameters: nonlinearity, gain, usable duty cycle range, dynamic range, etc. The controllability parameters for tapped-inductor fitter-buck converter are optimal, when the input voltage is slightly higher (5 to 10 %) than output voltage (maximum LED load voltage at full load operation), and the ratio of winding turns of tapped-inductor approximately is equal to $\lambda \approx 0.1$.

The analytical results have been confirmed by the experiments with the built prototype of the tapped-inductor fitter-buck converter: the accuracy of fluent light regulation improves as the dimming resolution increases at least 4 times in comparison with the conventional converter topologies. In addition, the efficiency of this converter is higher or stays at the same level with conventional converter topologies. The efficiency of the tapped-inductor fitter-buck converter can be improved in practical solutions, where output current or inductor current measurements are required for the implementation of closed loop control. The energy efficient inductor current measurement approach can be implemented by placing current sensor in the secondary branch of tapped-inductor, where average current is noticeably smaller than in the primary branch.

Also, it has been found that DC-DC converter operating in discontinuous conduction mode is capable of compensating nonlinearities of LED. Using DCM, it is also possible to increase dimming resolution in comparison with conventional converter topologies. The results have been confirmed both in analytical and practical way, like in the case with the tapped-inductor fitter-buck converter. However, the efficiency of the DC-DC converter operating in DCM suffers from the higher peak-to-average currents and higher losses in inductor cores. The efficiency and operation stability can be improved by careful selection of material for the inductor core.

In this way, the first hypothesis has been fully confirmed during these studies. This approach not only improves the accuracy of fluent light regulation, but also gives an opportunity to increase the efficiency.

2. For the confirmation of the second hypothesis non-inverting buck-boost converter has been considered. In accordance with [8], the constant current source is necessary at the input of the current fed (CF) converter for the proper operation. It has been found that the simplest as well as the most efficient way to make the constant current source is to form constant current in the inductor. Therefore, non-inverting buck-boost converter can be considered the simplest combination of constant current source (CS) and current regulator (CR), which in this case is current fed buck converter.

Different control approaches and hardware configuration for the non-inverting buck-boost converter have been studied in the scope of the present research. Also, the main control algorithm has been developed ($D1 + D2 \approx 100$ %).

It has been found that the non-inverting buck-boost converter operating under the proposed control approach (adhering to the main rule) allows achieving direct current control, thus increasing dimming resolution in comparison with the conventional converter topologies. Efficiency of this converter is slightly worse than of conventional converters. However, this efficiency difference can be minimized by the proper selection of the hardware configuration of the non-inverting buck-boost converter depending on the dimming profile of the lighting system.

Thus, also the second hypothesis has been confirmed in the present Doctoral Thesis.

Further research is related to the development of smart lighting systems. In the framework of the research the energy efficient LED drivers with convenient dimming function have been considered. However, these drivers are capable of operating directly only in low voltage DC applications (portable devices, automotive lighting, nanogrids for households of the future). At the same time AC power grids are still the most common energy transmission systems, also in households. Thus, development of the ballast, which incorporates single stage primary converter from the AC grid side with one of the proposed converters, is still topical.

Also, the heart of the smart lighting systems is the main controller, and the lamps must interact with this controller. The choice and integration of appropriate communication modules and sensors in the ballast is the task for the near future.

AUTHOR'S PUBLICATIONS

1. A. Avotinsh and **O. Tetervenoks**, "Illumination Measurement Stand for Artificial Light Sources," in *Proceedings of 10th International Symposium "Topical Problems in the Field of Electrical and Power Engineering. Doctoral School of Energy and Geotechnology II,"* 2011, pp. 250-254.
2. **O. Tetervenoks** and A. Avotinsh, "Implementation of Wireless Communication for LED Luminary Light Efficiency Evaluation Stand," in *7th International Conference-Workshop "Compatibility and Power Electronics" (CPE 2011): Student Forum*, 2011, pp. 72-76.
3. I. Milashevski, **O. Tetervenoks**, and I. Galkin, "Assessment of Energy Efficient LED Ballasts Based on their Weight and Size," *Scientific Journal of Riga Technical University. Power and Electrical Engineering*, vol. 29, no. -1. pp. 105-112, 2011.
4. I. Milashevski, **O. Tetervenoks**, and I. Galkin, "A Concept of Laboratory Testbench for Investigation of LED Dimmers," *Tech. Electrodyn.*, vol. Special, no. Part 2, pp. 136-141, 2011.
5. **O. Tetervenoks** and A. Avotinsh, "Design and Optimization of Light Efficiency Evaluation Stand. Technical Electrodynamics," *Tech. Electrodyn.*, vol. Special, no. Part 2, pp. 142-147, 2011.
6. **O. Tetervenoks**, I. Galkin, and I. Milashevski, "Study of High Brightness RGB Light — Emitting Diode Color Control Systems," in *11th International Symposium "Topical Problems in the Field of Electrical and Power Engineering. Doctoral School of Energy and Geotechnology II,"* 2012, pp. 168-171.
7. I. Galkin, I. Milashevski, and **O. Tetervenoks**, "Comparative study of steady-state performance of LED drivers at different modulation techniques," in *2011 7th International Conference — Workshop Compatibility and Power Electronics, CPE 2011 - Conference Proceedings*, 2011, pp. 382-387.
8. I. Galkin, I. Milashevski, and **O. Tetervenoks**, "Comparative Estimation of Efficiency of LED Dimmers at Different Modulation Techniques," in *Proceedings of the 14th European Conference on Power Electronics and Applications (EPE2011)*, 2011, pp. 1-9.
9. **O. Tetervenoks**, "Finding Requirements for Ballasts of Colored LED Matrices," in *Proceedings of 12th International Symposium "Topical Problems in the Field of Electrical and Power Engineering. Doctoral School of Energy and Geotechnology II,"* 2012, pp. 52-55.
10. I. Galkin, **O. Tetervenoks**, and I. Milashevski, "Weight and size estimation of energy efficient LED ballasts," *Elektron. ir Elektrotechnika*, no. 4, pp. 55-60, 2012.
11. I. Milashevski, **O. Tetervenok**, and A. Suzdalenko, "Comparative study of LED ballasts for different light regulation techniques," in *15th International Power Electronics and Motion Control Conference and Exposition, EPE — PEMC 2012 ECCE Europe*, 2012.
12. **O. Tetervenoks** and I. Galkin, "LED luminary evaluation stand ambient light sensor provided data processing," in *15th International Power Electronics and Motion Control Conference and Exposition, EPE — PEMC 2012 ECCE Europe*, 2012.
13. I. Milashevski, I. Galkin, and **O. Tetervenok**s, "Assessment of buck converter powered by current or voltage sources for LEDs luminary," in *Proceedings of the Biennial Baltic Electronics Conference, BEC*, 2012, pp. 239-242.
14. **O. Tetervenoks** and I. Galkin, "Evaluation of efficacy of light sources combined of different color LEDs," in *Proceedings of the Biennial Baltic Electronics Conference, BEC*, 2012, pp. 231-234.
15. **O. Tetervenoks** and I. Galkin, "Evaluation of Efficacy of Colored LED Matrices," *Tech. Electrodyn.*, vol. Special, no. Part 3, pp. 22-26, 2012.

16. **O. Tetervenoks**, I. Galkin, and J. Armas, “Autonomous Power Supply System for Light Sensor of Illumination Measurement Test Bench,” *Electr. Control Commun. Eng.*, vol. 1, no. 1, pp. 30-35, 2012.

17. **O. Tetervenoks**, I. Galkin, and A. Avotins, “Illumination Detection for LED Dimming Process Efficiency Evaluation,” *Electron. Electr. Eng.*, vol. 19, no. 1, 2013.

18. I. Milashevski, **O. Tetervenoks**, and I. Galkin, “Choice of Light Regulation Technique for Distributed Lighting,” *Tech. Electrodyn.*, vol. Special, no. Part 2, pp. 74-78, 2012.

19. **O. Tetervenoks**, “Choice of the Optimal Power of Distributed Lighting System Unit,” in *Digest Book and Electronic Proceedings of the 53rd International Scientific Conference Dedicated to the 150th Anniversary of Riga Technical University. Section of Power and Electrical Engineering*, 2012, pp. 89-91.

20. I. Galkin, **O. Tetervenoks**, and I. Milashevski, “Comparative study of steady-state performance of voltage and current fed dimmable LED drivers,” in *International Conference — Workshop Compatibility in Power Electronics , CPE*, 2013, pp. 292-297.

21. **O. Tetervenoks**, “Estimation of controllability and power losses of tapped-inductor converter used as dimmable driver for light-emitting diodes,” in *International Conference — Workshop Compatibility in Power Electronics , CPE*, 2013, pp. 150-155.

22. I. Galkin, **O. Tetervenoks**, and I. Milashevski, “Static Losses and Controllability of Current Fed Dimmable LED Drivers,” in *Proceedings of the 15th European Conference on Power Electronics and Applications (EPE 2013)*, 2013, p. P.1-P.10.

23. **O. Tetervenoks** and I. Galkin, “Choice of the MOSFET Drivers for the Converter Utilized as Dimmable LED Driver,” *Energy Saving. Power Eng. Energy Audit.*, vol. 1, no. 8, pp. 202-207, 2013.

24. **O. Tetervenoks**, “Analysis of Constant Output Power Operation of Tapped-Inductor Based LED Driver,” in *Digest Book and Electronic Proceedings of the 53rd International Scientific Conference Dedicated to the 150th Anniversary of Riga Technical University. Section of Power and Electrical Engineering*, 2013, pp. 17-19.

APPENDICES

A. Abbreviations

AC - alternating current;

ADC — analog-to-digital converter;

ASIC — application specific integrated circuit;

ASSIST — Alliance for Solid — State Illumination Systems and Technologies;

BCM — boundary conduction mode;

BMS — building management system;

CCT — correlated color temperature;

CCM — continuous conduction mode;

CF — current fed;

CIE — International Commission on Illumination (Commission Internationale de l'Eclairage);

CR — current regulator;

CRI — color rendering index;

CS — constant current source;

CQS — color quality scale;

DAC — digital-to-analog converter;

DC — direct current;

DCM — discontinuous conduction mode;

EMC — electromagnetic compatibility;

EMI — electromagnetic interference;

GAI — gamut area index;

HID — high-intensity discharge lamps;

HPMV — high-pressure mercury vapor discharge lamps;

HPS — high-pressure sodium lamps;

IC — integrated circuit;

IEC — International Electrotechnical Commission;

IFS — instantaneous flicker sensation;

IR — infrared;

LPS — low-pressure sodium lamps;

LED — light-emitting diode;

LRC — Lighting Research Center;

MCU — microcontroller unit;

MH — metal halide lamps;

MOCVD — metalorganic chemical vapor deposition;

MOSFET — metal-oxide semiconductor field-effect transistor;

NIST — National Institute of Standards and Technology

PF — power factor;

PFC — power factor corrector;

PWM — pulse width modulation;

RGB — refers to the colors: red, green, blue;

RLO — relative light output;

RMS — root mean square;

RO — relative output;

SSL — solid state lighting;

SMPS — switch mode power supply;

TFEL — thin film electroluminescent display;

TRIAC — triode for alternating current;

UV — ultraviolet;

VF — voltage fed

B. Glossary

Additive color — color obtained by mixing of two or more different colors (colored light sources). Red, green, and blue are primaries in additive color mixing. Additive color is in contrast with subtractive color.

Colorimetry — the science of color measurement, which is used to quantify and describe physically the human color perception.

Dimming — luminous flux regulation of the light source.

Epitaxy — the deposition of a crystalline overlayer on a crystalline substrate.

Efficacy (luminous efficacy) — in lighting it refers to the light amount (in lumens) produced by the light source as a ratio to the power consumption (in watts) of this light source (the ratio of total produced light amount to the input electrical power).

Efficiency (electrical efficiency) - the ratio of useful output power to the total input power.

Heterostructure — the combination of multiple heterojunctions together in a semiconductor device. A heterojunction is the interface that occurs between two layers or regions of dissimilar crystalline semiconductors. These semiconducting materials have unequal band gaps as opposed to a homojunction.

Homoepitaxy — a kind of epitaxy performed with only one material, in which a crystalline film is grown on a substrate or film of the same material.

Monochromatic LED — LED that emits a narrow bandwidth of light.

Off-line power supply — a power supply in which the AC line voltage is rectified and filtered without using a line frequency isolation transformer [121].

Quantum well — heterostructure with sufficiently thin layers, in which quantum interference effects begin to appear prominently in the motion of the electrons [122], [123].

Substrate — the physical material upon which a semiconductor device, e.g. a photovoltaic cell or an integrated circuit, is applied.

Subtractive color — color obtained by subtracting (filtering, absorbing) part of light spectra from white light. It is used in printing, where primaries are cyan, magenta and yellow.

Wafer (in electronics) — a thin slice of semiconductor material used in electronics for the fabrication of integrated circuits and in photovoltaics.

C. Common Configuration of the Testbench

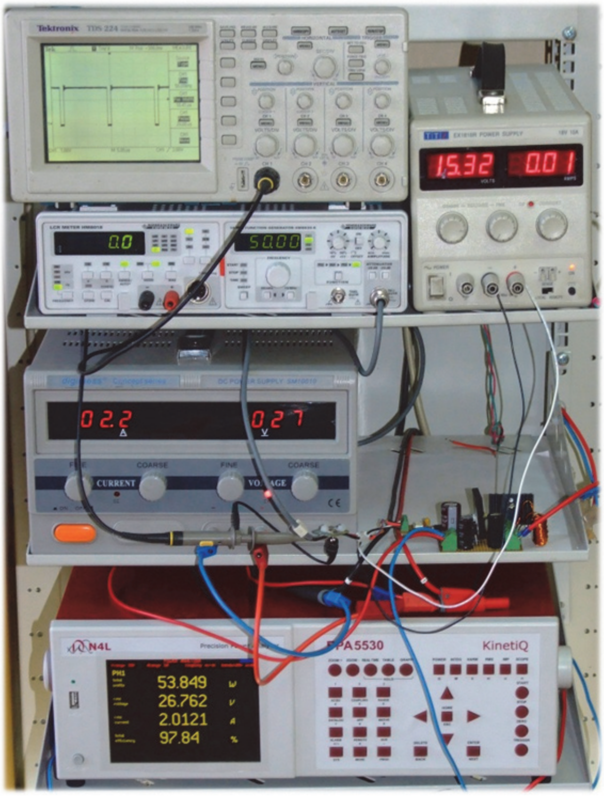

(a)

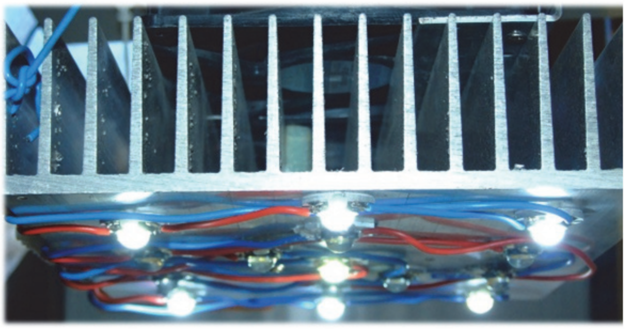

(b)

(c)

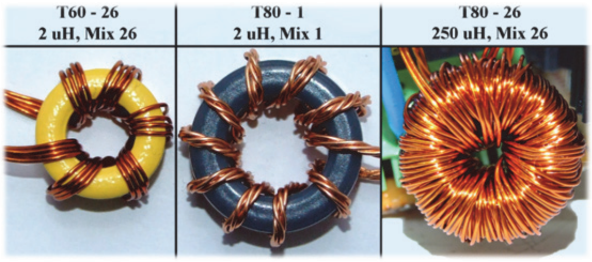

(d)

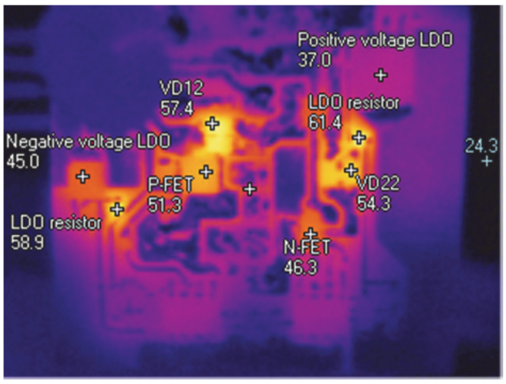

(e)

Fig. 6.1 Common configuration of the testbench: a) measurement equipment; b) LED lamp; c) converter prototype; d) parts under the test; e) example of thermal image of the prototype.

D. Light and Human Vision

Light nature can be described in several different ways, but in lighting it is most commonly considered as a direct beam of rays (for optics) and as electromagnetic waves (for representation of colorimetric parameters of light source).

Electromagnetic wave source (light source) emits a radiant flux Φ_e, which is equal to the area enclosed by its spectral distribution curve $\Phi_e(\lambda)$ as it shown in Fig. 6.2:

$$\Phi_e = \int_0^\infty \Phi_e(\lambda) d\lambda \,. \tag{6.1}$$

The physical quantity of radiant flux is watt [W]. However, radiant flux is obtained by integrating spectral distribution curve in whole wavelength range, while the light is only visible (by human eye) part of electromagnetic waves, therefore radiant flux is not appropriate quantity to represent visible light [17], [124].

Human eye is capable of perceiving electromagnetic waves in quite a narrow range (approximately from 380 nm to 780 nm), which is closely related to the specifics of the human eye. The light-sensitive part of the eye (in particular central region of retina) consists of light-sensitive rod cells and cone cells. Rod cells are sensitive in whole visible spectrum and are more sensitive than cone cells. Cone cells have three different types, which are sensitive in the red, green, and blue spectral range. Thus, depending on luminance level human eye has different vision regimes, which are summarized in Fig. 6.3 [17], [124], [125].

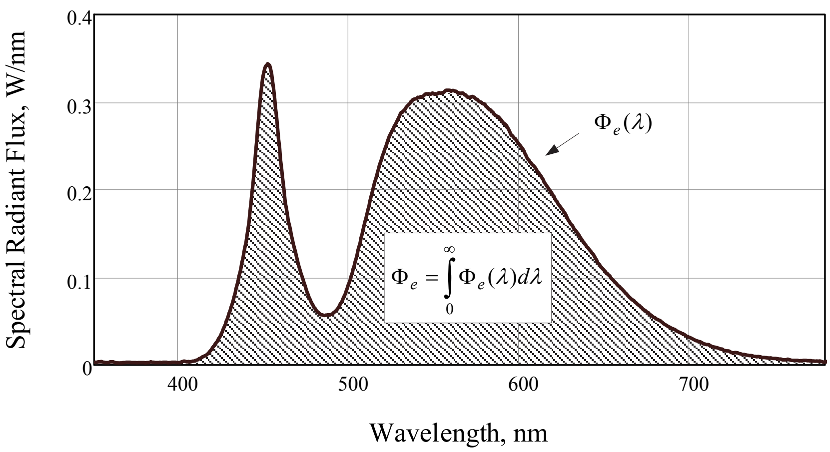

Fig. 6.2 Example of spectral radiant flux distribution curve of white LED.

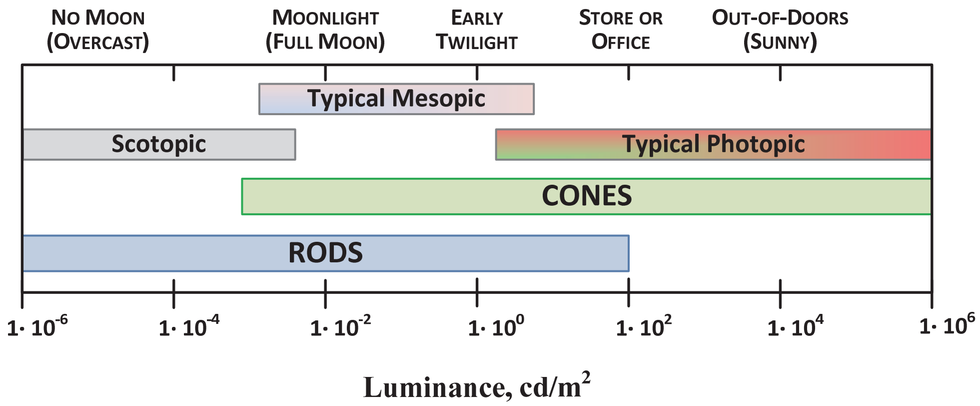

Fig. 6.3 Different vision regimes of the human eye depending on luminance level [125].

Cones are responsible for photopic vision at a high ambient light level (during daylight conditions). In this regime eye is capable of distinguishing colors. At a low ambient light level (during night) rods are responsible for scotopic vision. In this vision regime eye is capable of distinguishing different gray levels. There is also a third type of human eye vision — mesopic. This type relates to light levels between the photopic and scotopic vision regimes (Fig. 6.3). Sensitivity of the eye at photopic and scotopic vision regimes in whole visible range of spectra is shown in Fig. 6.4 [17]. Photopic vision is usually considered for the purposes of lighting applications.

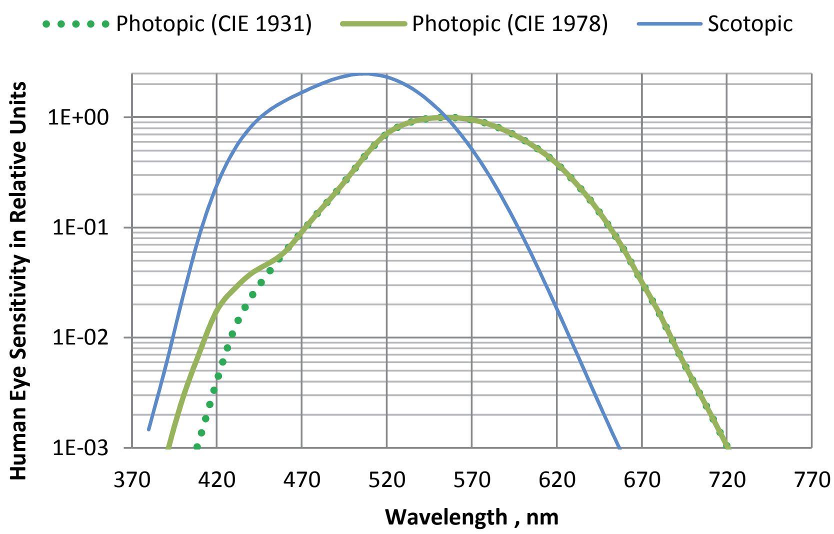

Fig. 6.4 Sensitivity of the human eye at photopic and scotopic vision regimes [126], [127].

Green doted curve in Fig. 6.4 is the relative luminous efficiency function *V(λ)* of photopic vision. It was introduced in 1924 by the International Commission on Illumination (CIE) for point-like source where the viewer angle is 2° (CIE 1931 *V(λ)* function, which is the current photometric standard in the United States). A modified *V(λ)* function was introduced by Judd and

Vos in 1978 (CIE 1978 $V(\lambda)$ function, solid green curve in Fig. 6.4). Values on the Fig. 6.4 are normalized with respect to the maximum luminous efficacy factor for the photopic vision K_m = 683 lm/W. Maximum luminous efficacy factor and the luminous efficiency function $V(\lambda)$ is used to convert radiant flux to the luminous flux

$$\Phi_v = K_m \int_{380}^{780} \Phi_e(\lambda) V(\lambda) d\lambda \,. \tag{6.2}$$

The maximum luminous efficacy factor for the scotopic vision is equal to 1700 lm/W [17], [124], [126].

There are two quantities of measuring optical properties and capability of the light source to convert applied power to the light: luminous efficacy of optical radiation and luminous efficiency of a light source. Luminous efficacy is the ratio of luminous flux emitted by the source to the radiant flux of the same source:

$$\eta_{efficacy} = \frac{\Phi_v}{\Phi_e} = \frac{683 \dfrac{lm}{W} \int_{380}^{780} \Phi_e(\lambda) V(\lambda) d\lambda}{\int_{0}^{\infty} \Phi_e(\lambda) d\lambda} \,. \tag{6.3}$$

Luminous efficiency is the ratio of luminous flux emitted by the source to the electrical power P_{el} applied to this source:

$$\eta_{efficiency} = \frac{\Phi_v}{P_{el}} = \frac{683 \dfrac{lm}{W} \int_{380}^{780} \Phi_e(\lambda) V(\lambda) d\lambda}{V_F \cdot I_F} \,, \tag{6.4}$$

where V_F and I_F are forward voltage and current of LED [17], [124], [126]. The units of both these quantities are lumens per watt lm/W, therefore it is important always to clarify which one is used for comparison.

The color perception is closely related to photopic vision of human eye. The human eye cannot distinguish between all the combinations of visible light but it tends to group various spectra in colors.

For the representation of colorimetric data the color space of International Commission on Illumination (CIE) are usually used. In 1931 CIE standard observer colorimetric functions $\bar{x}(\lambda)$, $\bar{y}(\lambda)$ and $\bar{z}(\lambda)$ (Fig. 6.5 (a)) were defined from primaries, which were obtained by transformation of Wright's and Guild's experimental data mean results. One of primaries was forced to be equal to photopic luminous efficiency function ($\bar{y}(\lambda) = V(\lambda)$). Other two imaginary functions were chosen so that they produce no luminance response [128], [129].

The multiplication of standard observer colorimetric functions by the amount of energy in the stimulus (energy pattern of spectral distribution of light source) at each wavelength and integrating across the spectrum gives tristimulus values of given stimulus:

$$X = k\int_{\lambda} P(\lambda)\bar{x}(\lambda)d\lambda \tag{6.5}$$

$$Y = k\int_{\lambda} P(\lambda)\bar{y}(\lambda)d\lambda \tag{6.6}$$

$$Z = k\int_{\lambda} P(\lambda)\bar{z}(\lambda)d\lambda \tag{6.7}$$

where *X, Y, Z* are the tristimulus values, *P(λ)* is the stimulus spectral power distribution, and *k* is the normalization constant. CIE XYZ color space is device independent [129], [18].

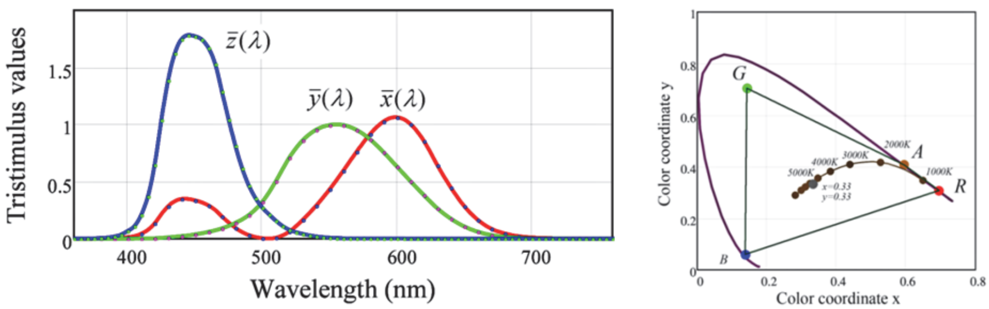

(a) (b)

Fig. 6.5 Color perception: a) tristimulus values of standard observer color matching functions (CIE 1931) [127]; b) chromaticity diagram.

Chromaticity diagram is used to get convenient representation of colors. It is a two-dimensional projection of a three-dimensional tristimulus space and should be used with great care [129]. The transformation for this projection is defined by equations

$$x = \frac{X}{X+Y+Z}, \tag{6.8}$$

$$y = \frac{Y}{X+Y+Z} \text{ and} \tag{6.9}$$

$$z = \frac{Z}{X+Y+Z} \text{ or } z = 1 - x - y \quad (6.10)$$

where x and y are the coordinates of chromaticity diagrams. Third coordinate z can always be obtained from the other two [17].

This transformation operation removes luminance information, thus for full specification of colored stimulus, one of the tristimulus values should be specified in addition to two chromaticity coordinates (usually Y tristimulus value, as it represents luminance information) [129], [18]. Example of CIE 1931 (x, y) chromaticity diagram is given in Fig. 6.5 (b).

E. Special Approaches of Pulse Mode Light Regulation Technique

Pulse mode light regulation technique is most interesting from the point of view of the stroboscopic effect. In the simplest case the light output of LED lamp is varying at a relatively high frequency between no light output and maximum light output. The average light output is regulated by the duty cycle *D* (Fig. 6.6 (a)) and can be found from

$$AVG = R_{\max} \cdot D \cdot 100\% = D \cdot 100\% \ , \tag{6.11}$$

but the flicker index in accordance with (2.4) and Fig. 6.6 (a) can be expressed as

$$I = (1 - D) \cdot 100\% \,. \tag{6.12}$$

In [130], [131] the bi-level pulse mode light regulation of LED lamp has been described. Two power sources are used providing two light output levels R_{max} and R_{min} (Fig. 6.6 (b)). This method allows increase in efficacy of dimming process as well as reduction of the stroboscopic effect. For bi-level regulation average light output can be found from

$$AVG = D \cdot R_{\max} + R_{\min}(1 - D)\,, \tag{6.13}$$

but the flicker index according to (2.4) and Fig. 6.6 (b) can be written as

$$I = \frac{(R_{\max} - R_{\min}) \cdot (1 - D)}{R_{\max} + R_{\min} \cdot \left(\dfrac{1}{D} - 1\right)}\,. \tag{6.14}$$

The stroboscopic effect can also be reduced by using of several LED matrices with interleaved control signals [132] as shown in Fig. 6.6 (c).

The relative light output for interleaved regulation method can be found from (6.11), but the flicker index from (6.14) taking into account the overlaps. Dependence of the flicker index from the relative light output at different pulse mode regulation techniques discussed above is shown in Fig. 6.7.

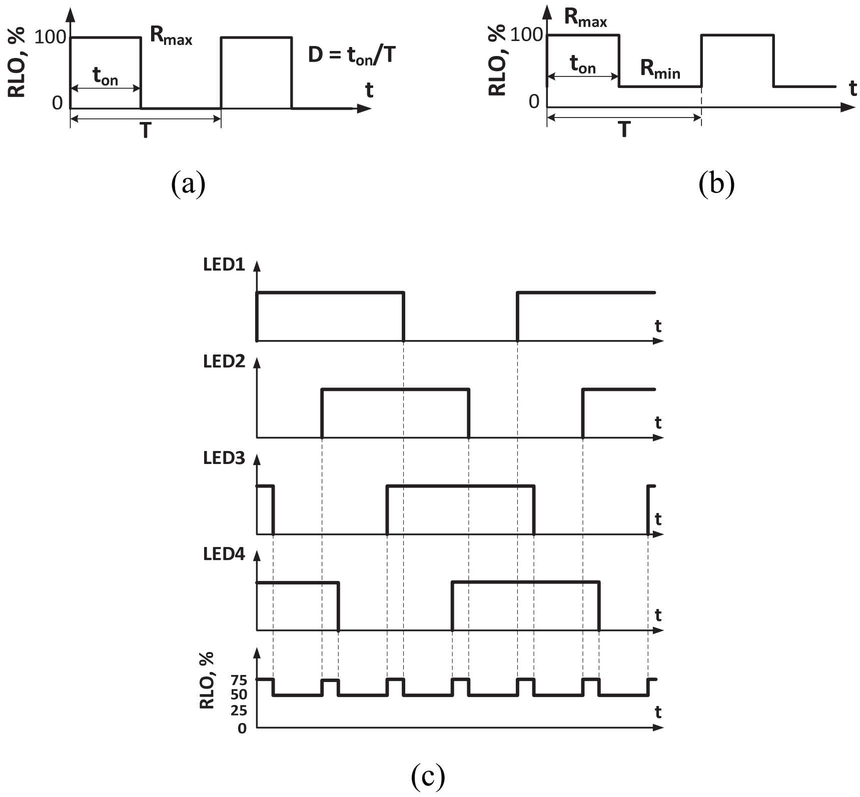

Fig. 6.6 Different kind of LED lamp pulse mode light regulation methods: a) standard PWM; b) bi-level regulation; c) interleaved regulation.

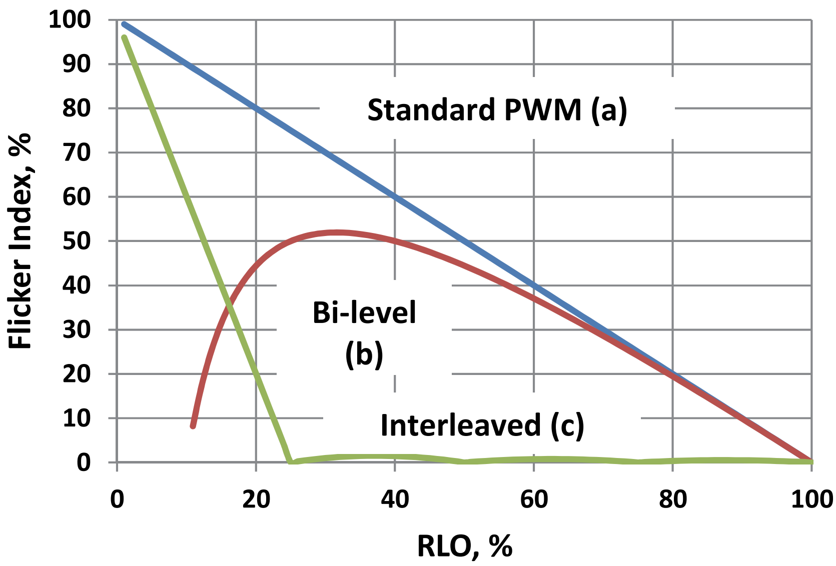

Fig. 6.7 Dependence of flicker index from relative light output at different pulse mode light regulation techniques: a) standard PWM; b) Bi-level (R_{min} = 10 %); c) interleaved (4 levels).

F. Experimental Assessment of Light Fluctuations

Almost all of the amplified **photodetectors** available on the market have an integrated filter to reduce influence of light fluctuations at frequency of power grid. At the same time LED lamps are the least inertial and are capable to create light fluctuations at high frequencies; therefore, it was decided to build photodetector with the ability to determine light fluctuations at higher frequencies.

Photodiode TEMD6200FX01 (with small diode capacitance for improved performance) and low noise 50MHz operational amplifier LTC6244HV were chosen as main elements of photodetector. The principal circuit of photodetector is given in Fig. 6.8 (a). Printed circuit board was placed in metal box to minimize influence of ambient noise (Fig. 6.8 (b) and (c)).

The **experimental setup** consists of LED lamp under study, photodetector, digital oscilloscope with the capability of data acquisition, and box with dark walls where to place lamp and sensor (to minimize interference of ambient light).

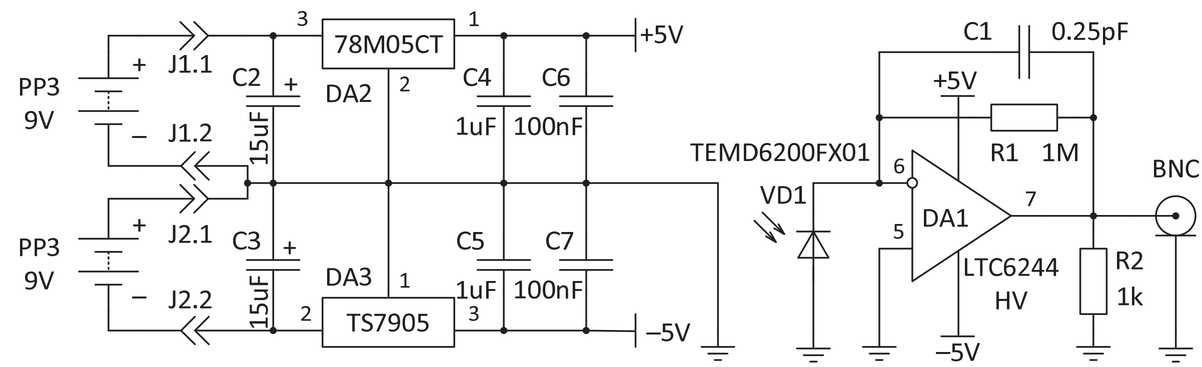

(a)

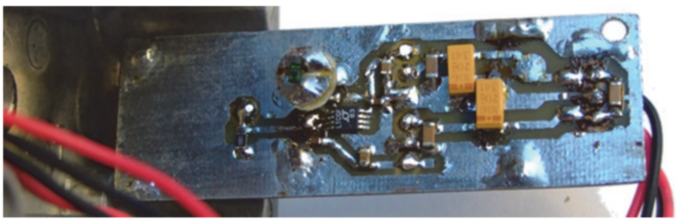

(b)

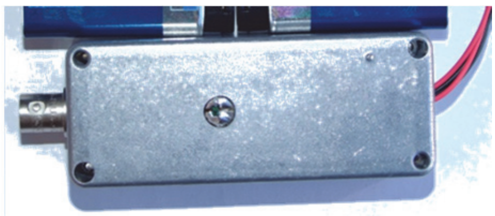

(c)

Fig. 6.8 Photodetector used in experiments: a) principal circuit; b) printed circuit board of photodetector c) assembled.

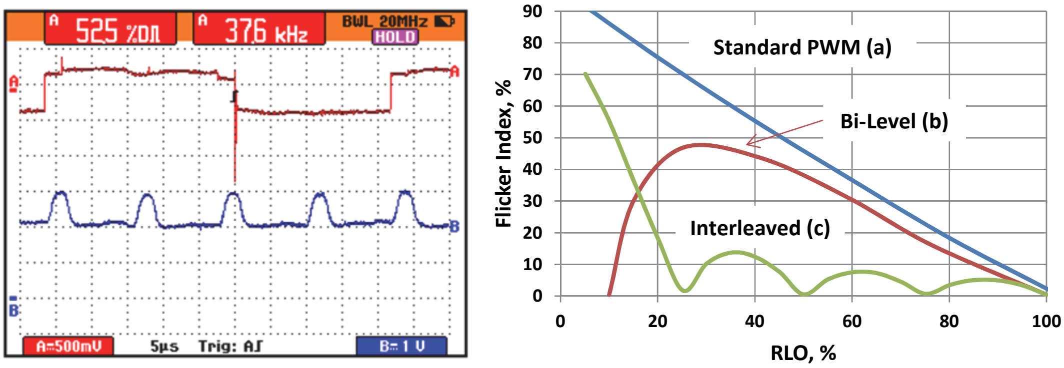

(a) (b)

Fig. 6.9 Results of experiments: a) example of data from the photodetector (channel B) at ≈55 % of RLO in case of 4-level interleaved regulation approach; b) the results of flicker index measurements at different pulse mode light regulation techniques.

The measurements for different pulse mode light regulation techniques have been taken at different RLO values in whole regulation range with 5 % step. The operation frequency for all the techniques during all the experiments was the same — 20 kHz. The example of data taken from photodetector in case of 4-level interleaved regulation approach at ≈55 % RLO is shown in Fig. 6.9 (a). The data of experiments has been analyzed using (2.6) and (2.7) and the results are summarized in Fig. 6.9 (b). The experimental results are in good agreement with the analytical part confirming the correctness of calculations.

The relationship between the percent flicker/flicker index, flicker frequency and the acceptability of the stroboscopic effect is given in [32]. According to this relationship and Fig. 6.9 (b), the acceptable level of the stroboscopic effect for standard PWM and bi-level approach can be achieved at operation frequencies higher than 1.5 kHz almost regardless of the flicker index at frequencies above 750 Hz for 2-level approach, and at frequencies above 400Hz for 4-level approach.

The similar relationship for percent likelihood of detection of the stroboscopic effect is also given in [32]. If we consider 5 % to 100 % RLO range, the operation frequency must be above 10 kHz for standard PWM approach to achieve less than 20 % of likelihood of flicker detection in whole regulation range, above 5 kHz for bi-level approach, and above 2 kHz for 4-level interleaved approach. Also, it is worth mentioning that in case of standard PWM there is only one point in the whole RLO range with 0 % of the likelihood of flicker detection, 2 such points in case of bi-level approach, and 4 such points in case of 4-level interleaved approach (Fig. 6.9 (b)), which may be useful in applications with very stringent light quality requirements (for instance, photo and video studio equipment, lighting in exhibition areas etc.).

G. Calculation of Power Losses for Tapped-Inductor Fitter-Buck Converter

The load characteristics were taken into account during the construction of these curves. It is seen from Fig. 6.10 that power losses of the switches of tapped-inductor converter are smaller in comparison with the conventional buck. The maximum power dissipation of the transistor without the heat sink (minimal weight and size) is equal to $\Delta P_{VT1max} = (175\text{-}45) / 62 = 2.1$ W at 45 °C ambient temperature. The maximum power dissipation of the diode is equal to $\Delta P_{VT1max} = (175 - 45) / 75 = 1.7$ W. In this case the switching frequency is the limiting parameter. For conventional buck converter the maximum allowable switching frequency at described conditions approximately is equal to 220 kHz. For tapped-inductor converter this frequency approximately is equal to 280 kHz.

These calculations were performed for the devices specified in Table 6.1 using their technical specification [135], [136]. All the calculations were performed in *MathCad*.

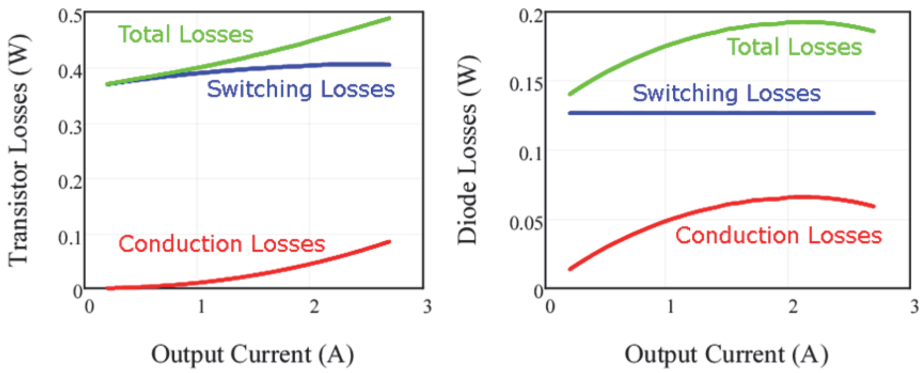

(a)

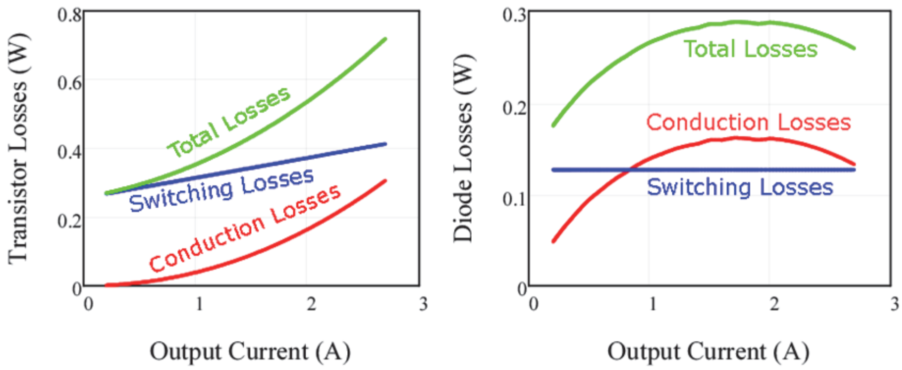

(b)

Fig. 6.10 The comparison of power losses in switches at the same conditions (the same load, switching devices, inductor L1 inductance and the switching frequency 50 kHz): a) tapped-inductor converter ($\lambda = 0.1$); b) conventional buck (λ=1).

H. Experimental Verification of Current Measurement Approach for Tapped-Inductor Fitter-Buck Converter

In order to verify the described above current measurement approach a series of experiments were conducted. From the similar oscillograms as in Fig. 6.11 average tapped-inductor current values at transistor VT1 switch on I_{on} and switch off I_{off} states were found from the instantaneous current values at the beginning and the end of switching process (I_l, I_m, λI_l, λI_m). The results are summarized in Fig. 6.12. Two curves are given in this figure for comparison: experimentally obtained relationship between the average current in the primary winding (inductance L1) during the on-state of transistor VT1 to the output current and the same dependency calculated from measurements of current in the secondary winding (inductance L2`) during off-state using (3.20).

Slight discrepancy between the measured and calculated curves is seen in Fig. 6.12 that can be explained by measurement inaccuracy caused by the precision of measurement equipment.

The moment for the current measurement should also be chosen with care, as the oscillations appears in the primary winding at the beginning of on-state of transistor VT1 as well as in the secondary winding at the beginning of off-state of transistor VT1 (Fig. 6.11).

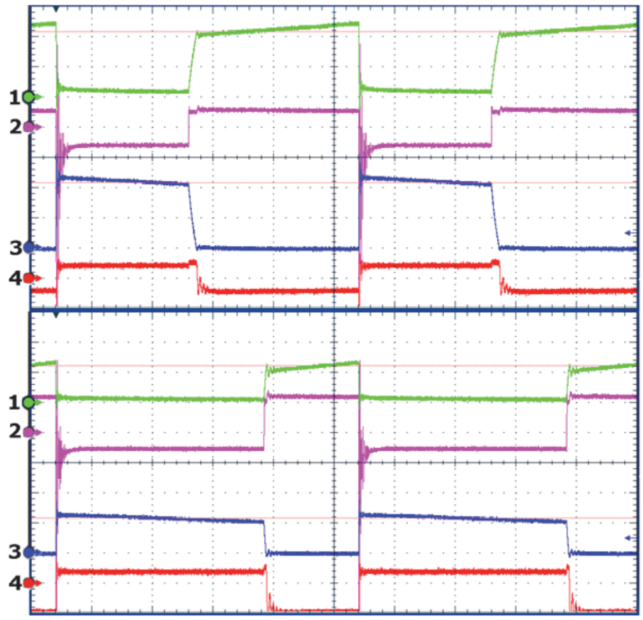

(a) (b)

Fig. 6.11 Measured waveforms of tappet-inductor at $V_{in} = 28$ V input voltage of the converter and operating frequency 25 kHz. For both graphs: 1) current form in the primary winding with inductance L1 (2 A/div); 2) voltage across the primary winding (5 V/div); 3) current form in the secondary winding with inductance L2` (200 mA/div); 4) voltage across the secondary winding (50 V/div). Graph (a): converter operating at full load ($P_{out} \approx 30$ W, D = 56 %). Graph (b): converter operating at 1/3 of full load ($P_{out} \approx 10$ W, D = 30 %).

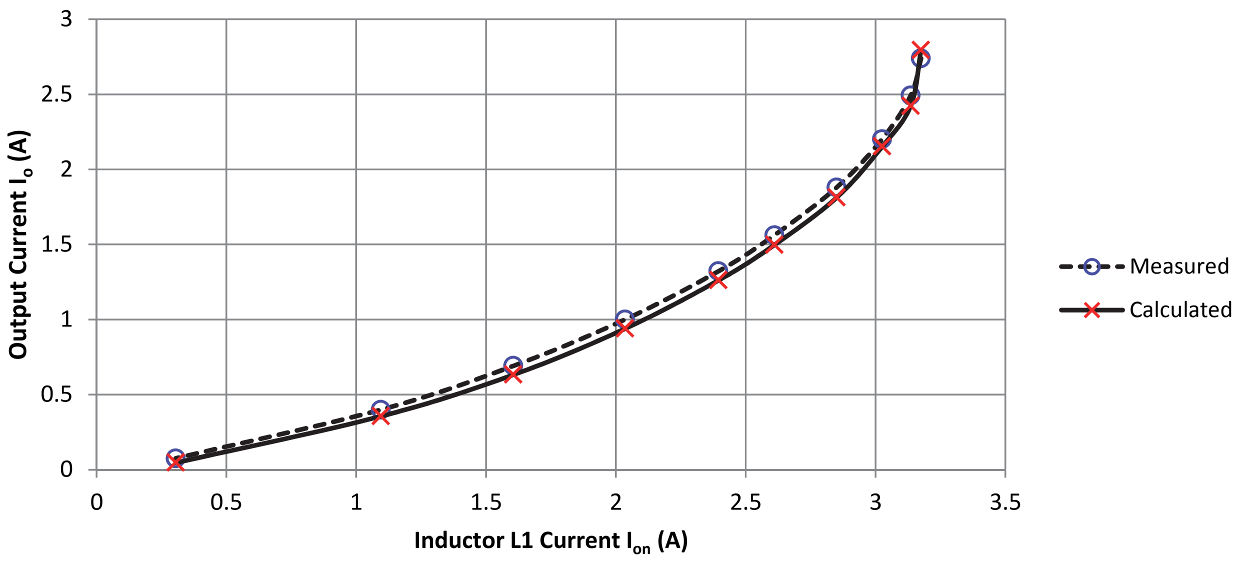

Fig. 6.12 Relationship between the output current and average current I_{on} in the primary winding of tapped-inductor: comparison of the measured and calculated values of output current of the converter.

For the described current measurement approach microprocessor based regulation system is more suitable, because the duty cycle value should be known to determine (to calculate) output current. For the better precision current measurement samples should be taken in the middle or at the end of transistor VT1 switch off state.

I. Experimental Verification for Tapped-Inductor Converters

The component list of the prototypes is given in Table 6.1.

As usual the load of the converter prototype is 7 Seoul Semiconductor W724C0 LEDs connected in (Fig. 3.3).

The results of experiments with the fitter-buck prototype at $V_{in} = 1.04V_{LEDmax}$ input voltage are summarized in Fig. 3.8 (a) and (b). The controllability curve of fitter-buck converter is almost linear (Fig. 3.8 (a)). Usable duty cycle span is more than 65 %, which is approximately 4 times greater in comparison with the conventional buck converter. Therefore, also relative inaccuracy of LED current ΔI_{LED} reduces. Also, the efficiency of fitter-buck is rather high (Fig. 3.8 (b)).

The experiments with the fitter-boost prototype at $V_{in} = 0.95V_{LEDmin}$ are summarized in Fig. 3.9 (a) and (b). The results are not as good as for the fitter-buck converter; however, both experiments are good for comparison with numerical calculations (Table 3.2).

Photos of booth converter prototypes are given in Fig. 6.13

Table 6.1

Bill of Material for Experimental Prototypes

Component		Fitter-Buck	Fitter-Boost
Transistor		IRF540N (MOSFET), 100 V, 33 A, 44 mΩ	
Diode/s		MUR860, 600 V, 8 A	2 × MUR860, 600 V, 8 A
Input Capacitor		Electrolytic 1000 μF, 35 V	
Output Capacitor		Electrolytic 470 μF, 63 V	
Tapped-Inductor	Core	ETD29, EPCOS, N97 material, 0.6mm air gap	
	Windings	N1 = 23, N2 = 230, λ = 0.1	N1 = 98, N2 = 49, λ = 2

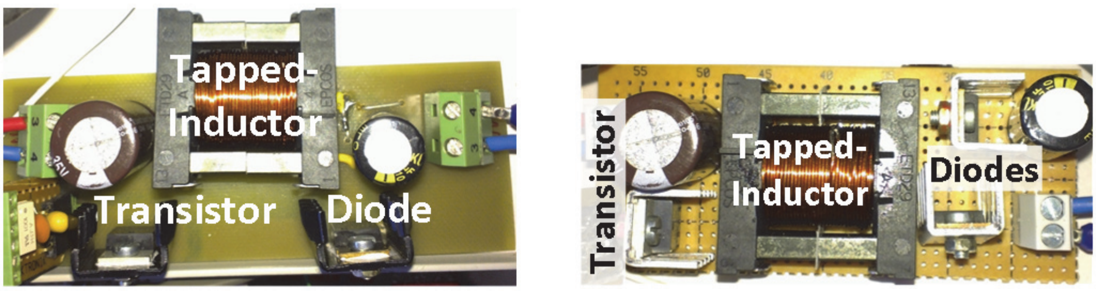

(a) (b)

Fig. 6.13 Photos of the prototypes: a) for fitter-buck; b) for fitter-boost.

J. Experimental Verification of Discontinuous Conduction Mode for Compensation of Nonlinearity

A series of experiments have been conducted in order to verify the previously listed assumptions and simulation results. A buck converter with 25 V on its input intended for a 70 W LED load has been assembled (in particular the load contains 7 W724C LED of total power 23.2 V x 2.8 A ≈ 70 W). The component list of the converter prototype is given in Table 6.2. The converter has been tested with different values of inductance (1, 2, 4, 10, 50 and 250 μH). The results of these tests are summarized in Fig. 3.12 (b) and Table 3.4.

Table 6.2

Components Used in Experiments

Component	Manufacturer	Part #	Main Parameters
Transistor	NXP Semiconductor	IRF540N	V_{DS}=100V, R_{DS}=77mΩ
Diode	ON Semiconductor	MUR860	V_{RR}=600V, V_F=1.2V
Output capacitor	Nichicon	UPW1J471MHD	C=470uF, R_{ESR}=0.13Ω
Inductor Core 1	Micrometals	T60-26	Size T60, μ_0=75
Inductor Core 2	Micrometals	T80-26	Size T80, μ_0=75
Inductor Core 3	Micrometals	T80-1	Size T80, μ_0=20

Fig. 6.14 Elements of experimental setup: a) converter prototype; b) inductors used in measurements of the efficiency and losses.

K. Experimental Estimation of Losses in DCM Operation

The analytical evaluation of power losses of the inductor were presented in [106] using the information from [137]-[139].

A series of experiments were conducted to evaluate power loss distribution between the main elements of the converter in CCM and DCM operation modes. It is seen from Fig. 3.12 (b) that pure DCM operation of converter can be practically achieved at 2μH inductance; therefore 250μH and 2μH inductances were selected for practical measurements in pure CCM and pure DCM operation accordingly.

It was decided to approximately estimate these losses by the difference ΔT between the ambient temperature T_a and temperature of each component using thermal camera.

Thermal image of the converter operating in DCM at full output power is shown in Fig. 6.15 as an example. For approximate estimation of power losses the curves that represent dependency between component temperature and dissipated power were measured (Fig. 6.16 (a)). They were made by applying known power to the components and then measuring their temperature.

The next step of this experiment was the analysis of thermal images of the converter at different operation modes and output powers. The results of this analysis are summarized in Table 6.3.

Table 6.3 shows that the distribution of losses among the components in CCM is quite uniform in the whole output current range. In DCM the inductor is the main source of losses which can be reduced by a proper choice of the core material.

The measured power losses of the converter at different operation modes and output powers are summarized in Fig. 6.16 (b). Overall efficiency of the converter is shown in Fig. 3.12 (b).

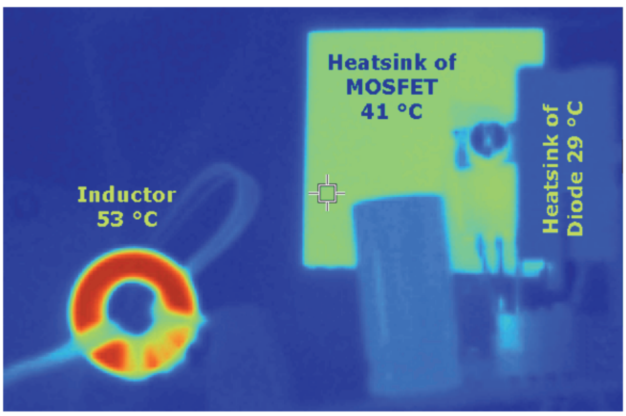

Fig. 6.15 Thermal image of inductor (53°C), diode (29°C) and transistor (41°C) in DCM (D≈100 %, I_{LED}=2.7A, inductor core T60-26).

Table 6.3

Measured Distribution of Power Losses of Buck Converter in CCM and DCM

I_{out}, %	ΔP_{total}, W	η, %	Transistor		Diode		Inductor	
			ΔT, °C	ΔP, W	ΔT, °C	ΔP, W	ΔT, °C	ΔP, W
Pure CCM, L = 250uH, Inductor Core Material Mix 26								
33	0.4	97.9	6	0.2	9	0.3	8	0.2
67	0.9	97.9	8	0.2	11	0.4	11	0.2
100	1.7	97.5	12	0.4	12	0.4	15	0.4
Pure DCM, L = 2uH, Inductor Core Material Mix 26								
33	1.8	92.3	9	0.3	4	0.1	29	0.9
67	2.6	95.0	16	0.6	7	0.2	36	1.2
100	2.8	96.7	19	0.8	7	0.2	31	1.0
Pure DCM, L = 2uH, Inductor Core Material Mix 1								
33	1.1	95.2	11	0.4	5	0.1	9	0.3
67	1.9	96.5	17	0.7	6	0.2	11	0.4
100	2.2	97.6	19	0.8	6	0.2	10	0.3

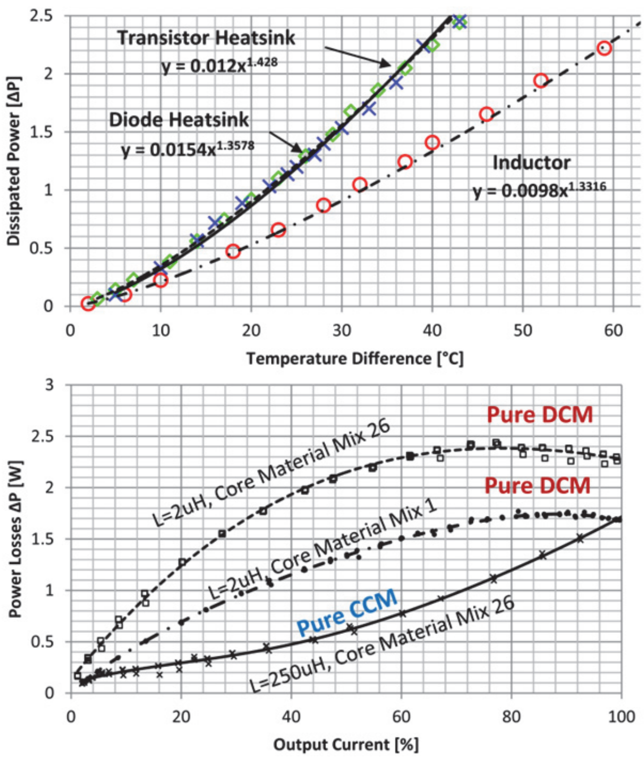

(a) (b)

Fig. 6.16 Estimation of power losses: a) Relationships between the power dissipation in components and their temperature; b) losses of converter in CCM and DCM.

L. Experimental Verification of Non-Inverting Buck-Boost Operating with Independent CS and CR stages with PWM controller

Functional diagram of control loop is shown in Fig. 6.17. In this control loop the output current set point value is compared with the actual output current value. The difference of them is the error, which increases or decreases initial duty cycle to adjust output current (Fig. 6.17). Microcontroller code for this configuration of control system is given in Appendix N. Results of experiments at different output powers are given in Fig. 6.18.

The results from Fig. 6.18 show unstable operation of non-inverting buck-boost under independent control of CS and CR stages (MCU based PWM controller with one current feedback in control loop for CS stage). Experiments showed that the transient processes (start-up, load change) are also very unstable for this configuration.

The problem is that voltage at the input of CF driver changes in wide range (from 0 to maximum forward voltage of the connected LED string). This causes continuous operation with large error in control loop, which affects the actual value of output current. Integral part of PID controller would not be capable to compensate this error so fast (at least several switching cycles are necessary for these calculations).

Therefore, the problem can be solved by calculating initial duty cycle simultaneously from the expression of buck converter $D = V_{OUT}/V_{IN}$ using input and output voltage of the converter. In simplified version it can be assumed that the input voltage is constant (in the most cases in practice). Therefore, only the value of output voltage can be used for initial duty cycle calculations (dashed parts of circuit shown in Fig. 6.17). Microcontroller code for this configuration of control system is given in Appendix O. Results of experiments at different output powers are given in Fig. 6.19.

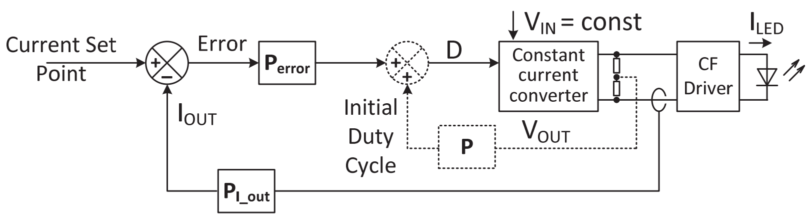

Fig. 6.17 Functional diagram of control loop for considered constant current: initial duty cycle depends on the ratio of output and input voltages (simplified version, suitable for practical implementation).

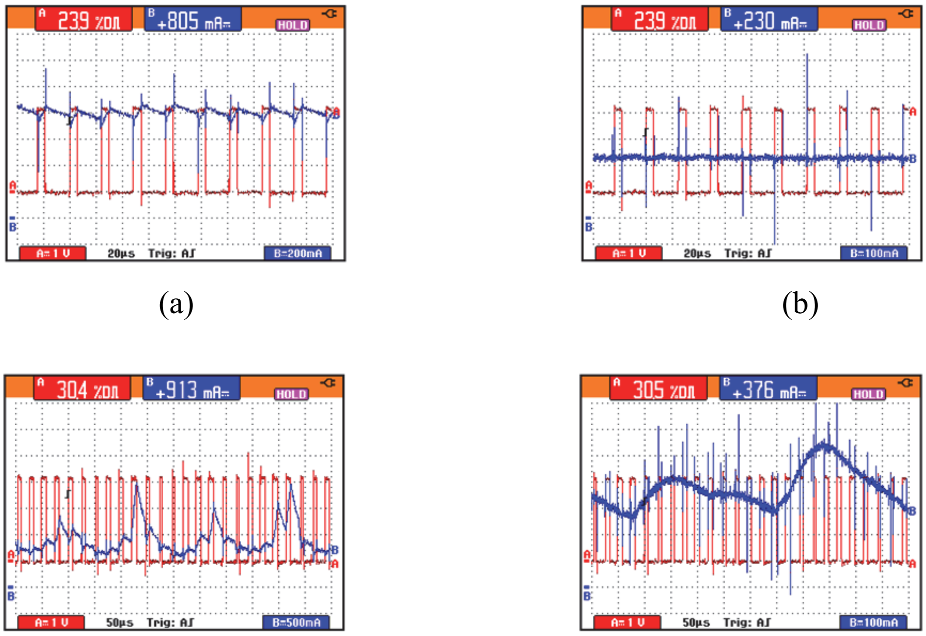

(a) (b)

(c) (d)

Fig. 6.18 Performance of the non-inverting buck-boost at independent control of CS and CR stages (MCU based PWM controller with one current feedback in control loop for CS stage): a) duty cycle and current waveform of CS stage at lower output power; b) current waveform of CR stage at lower output power; c) duty cycle and current waveform of CS stage at higher output power; d) current waveform of CR at higher output power;

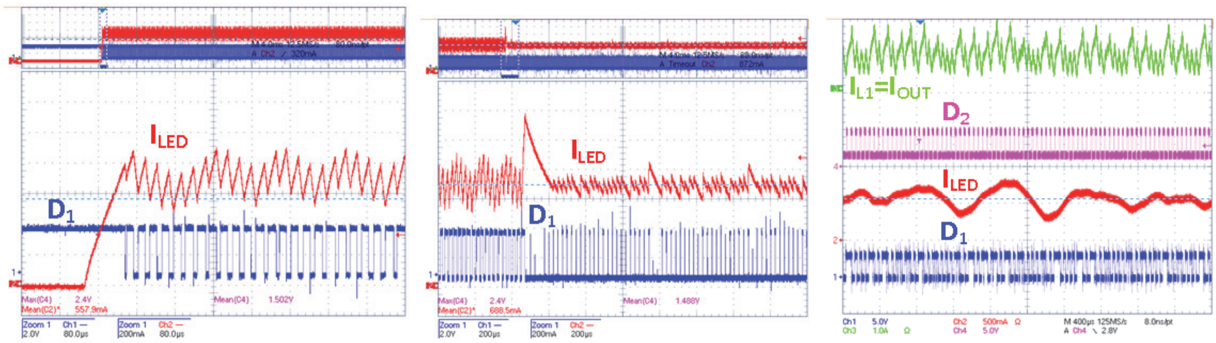

(a) (b) (c)

Fig. 6.19 Performance of the non-inverting buck-boost at independent control of CS and CR stages (MCU based PWM controller with current feedback and voltage feedback in control loop for CS stage): a) transient process from no load to full load; b) transient process from full load to short circuit; c) operation at small output power

The results of these experiments show good performance at higher output power levels. Also, transient processes are stable for this configuration (Fig. 6.19 (a) and (b)). However, this configuration becomes less stable at lower output power (Fig. 6.19 (c)).

M. Experimental Verification of p + n and n + p Configurations of Non-Inverting Buck-Boost

The laboratory prototypes of both CF buck driver configurations have been tested (Fig. 6.20) in the same conditions: the same input voltage, LED load, switching frequency (100kHz). Both prototypes consist of the same elements (Table 6.4).

The results are summarized in Fig. 6.21. It is seen from Fig. 6.21 (a) that the efficiency of both configurations is quite similar. However, the enlarged scale (Fig. 6.21 b) allows finding out that the positive node related configuration is slightly more efficient, as expected.

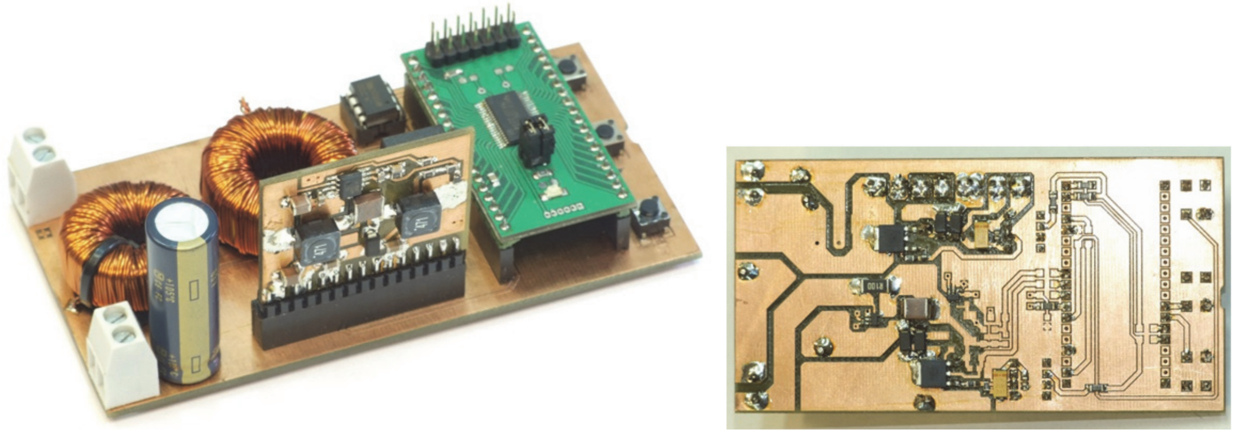

(a) (b)

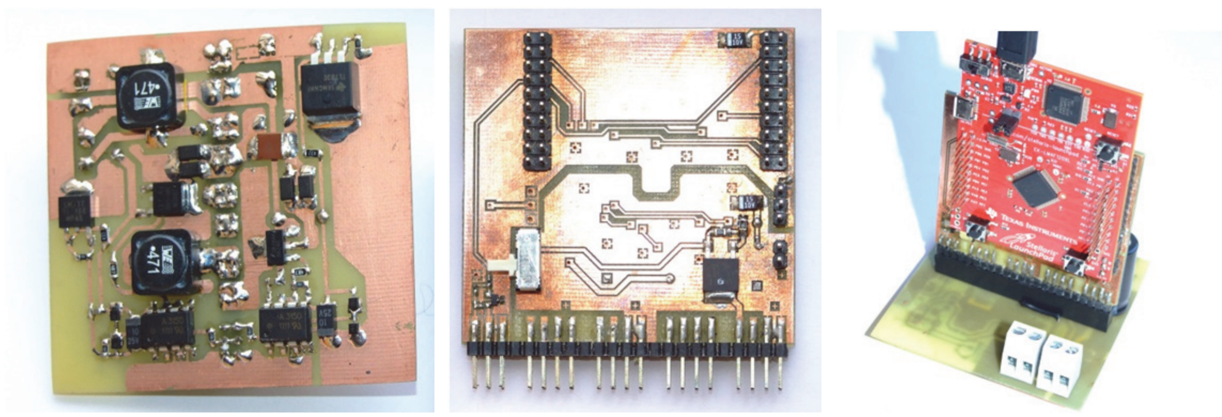

(a) (b) (c)

Fig. 6.20 Prototypes of different type configurations of non-inverting buck-boost converter: a) both N-FET transistors and galvanically isolated driver supply-assembled system; b) bottom view of the main board; c) configuration with P-FET transistor-power board; d) extension board; e) assembled system.

Table 6.4

Main Elements of the Prototypes

Component	Ref. designator	Description, parameters
Capacitor	C1	Ceramic, 10 uF, 100 V
Capacitor	C2	Aluminum electrolytic, 220 uF, 100 V
Inductor	L1	Micrometals T80-26 toroid core, 330 uH, 68 mΩ
Inductor	L2	Micrometals T80-26 toroid core, 480 uH, 112 mΩ
Diode	VD12, VD22	STPS2150A, 150V, 2A
Transistor (N-FET)	VT21, VT11	FDT86246, N-Channel, 150 V, 2 A, 236 mΩ
Transistor (P-FET)	VT21, VT11	IRFR9120N, P-Channel, 100 V, 6.6 A, 480 mΩ

Thermal images of the prototypes at different output power were captured. From the point of view of power losses in semiconductor switches the most interesting are the points near the maximum and minimum output power: in Fig. 6.22 are shown thermal images of the prototypes operating at 30 % and 70 % of maximum output power.

Also, the thermal images of both inductors L1 and L1 were captured. The results are summarized in Table 6.5. The temperature of inductor L1 is stable over whole regulation range (at different current values); therefore, it can be concluded that the conduction losses are small in comparison with the core losses.

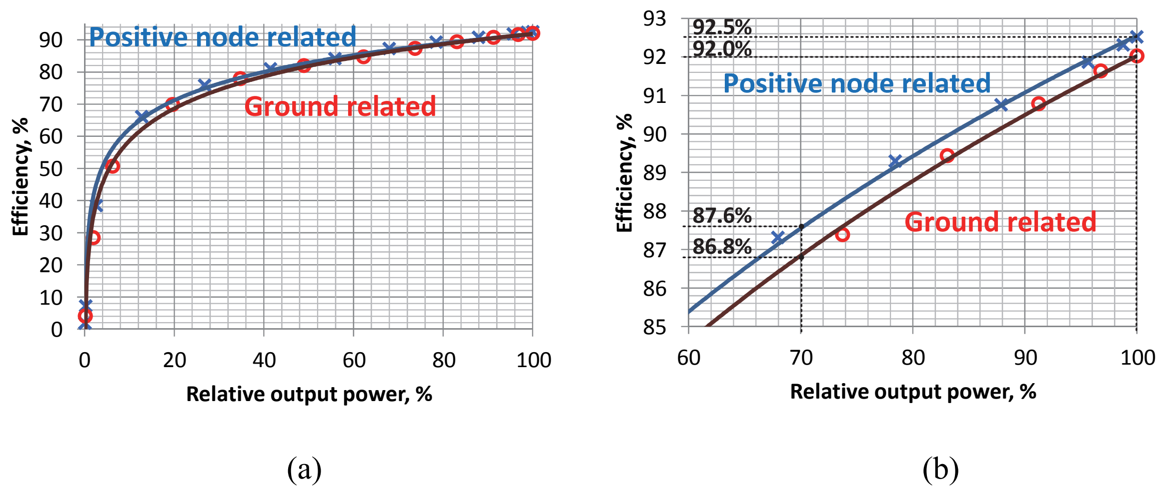

Fig. 6.21 Efficiency of the considered CF buck driver for both configurations: (a) over whole regulation range; (b) enlarged scale at higher output power.

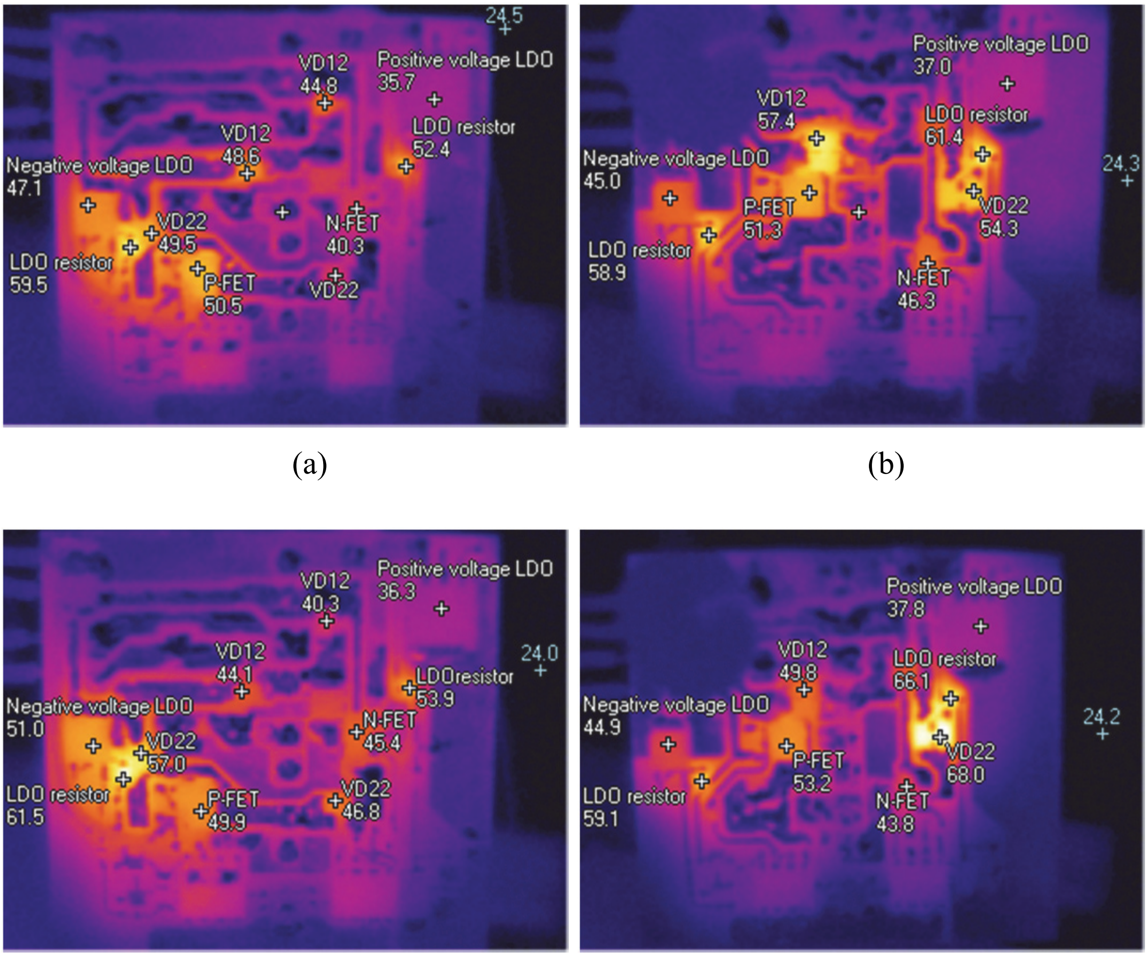

Fig. 6.22 Thermal images of the prototypes: a) ground related configuration at 70 % of maximum output power; b) positive node related configuration at 70 % of maximum output power; c) ground related configuration at 30 % of maximum output power; d) positive node related configuration at 30 % of maximum output power.

It is seen from Table 6.5 that the higher power losses of inductor L2 appears at approximately 50 % of maximum output power. In this case the dominant are inductor core losses, which are highly dependent from the ripple current. The total power losses of the prototype and the current ripple

Table 6.5

Temperature of Inductors L1 and L2 at Different Output Power

Relative output power, %	99	80	50	30
Temperature of L1, °C	30	31	31	30
Temperature of L2, °C	32	37	42	37

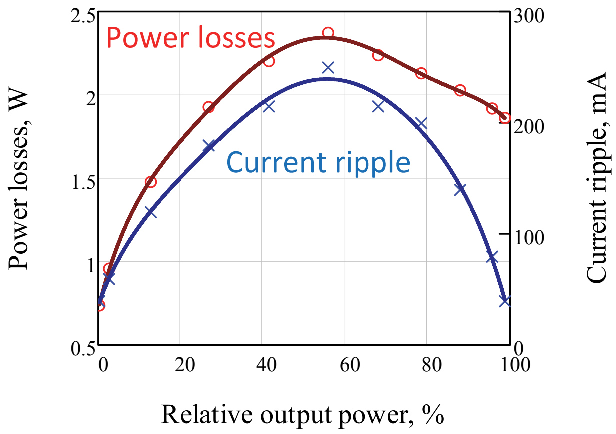

Fig. 6.23 Total power losses and the current ripple of the positive node related prototype at different output power levels.

(peak-to-peak value) are placed in one plot in Fig. 6.23 to show the relationship of these waveforms. This figure shows that the current ripple in the inductor L2 also has a great impact on the overall efficiency of the considered converter.

N. MSP430F2232 Assembler Code for Asynchronous Control of Non-Inverting Buck-Boost (Single Closed Loop with CS Stage Current Feedback)

```
;******************************************************************************
;
;            MSP430F22x4
;         -----------------
;     /|\|                 |-
;      | |                 |
;      --|RST              |-
;        |                 |
;     >---|P2.0/A0P4.1|--> PWM1
;     >---|PB2.7       |
;      >---|PB2.6      |
;
;
;******************************************************************************
#include "msp430x22x2.h"

;-------------------------------------------------------------------------------
        RSEG    CSTACK              ; Define stack segment
;-------------------------------------------------------------------------------
        RSEG    CODE                ; Assemble to Flash memory
;-------------------------------------------------------------------------------
RESET      mov.w   #SFE(CSTACK),SP        ; Initialize stackpointer
StopWDT    mov.w   #WDTPW+WDTHOLD,&WDTCTL  ; Stop WDT

        CLR.B   &DCOCTL               ; Select lowest DCOx
                                      ; and MODx settings
        BIC.B   #RSEL3+RSEL2+RSEL1+RSEL0,&BCSCTL1 ; Select range 7
        BIS.B   #RSEL3+RSEL2+RSEL1+RSEL0,&BCSCTL1 ; Select range 7
        BIS.B   #DCO2+DCO1,&DCOCTL     ; Select max DCO tap

        mov     #700, R12              ; R12 - set point
        mov     #0, R11                ; Temp register

        mov.b   #00000110b, &P4DIR     ; PWM output setup P4.1
        mov.b   #00000010b, &P4SEL     ; PWM output setup P4.1

        bis.b   #00000100b, &P4OUT         ; P-ch FET gate control bic - no output

        call    #Delay
ButConf    bic.b   #11000000b, &P2DIR     ; P2.7, P2.6 as input
        bic.b   #11000000b, &P2SEL         ; P2.7, P2.6 disable secondary functions
        bis.b   #11000000b, &P2IES     ; high-to-low transition
        bis.b   #11000000b, &P2IE      ; Interupt enable on P2.7, P2.6

        mov.w   #0001101000010000b, &TBCTL  ; Timer B control register
;               |||| ||||||
;               |||| ||||++  Mode control -> Up/down mode
;               |||| ||++  Input divider -> /1
;               |||| ++  Clock source select -> SMCLK
;               ||++  Counter length -> 8-bit
;               ++  TBCLx group -> Each TBCLx latch loads independently

        mov.w   #255, &TBCCR0          ; Set 0 capture/compare register
        mov.w   #254, &TBCCR1          ; Set 1 capture/compare register

        bic.w   #1100000100000000b, &TBCCTL0 ; Capture/compare register
;              ||     |
;              ||     +  Capture mode -> Compare
;              ++  No capture

        bic.w   #1100000100000000b, &TBCCTL1 ; Capture/compare register
;              ||     |
;              ||     +  Capture mode -> Compare
;              ++  No capture

        bis.w   #0000010001000000b, &TBCCTL1 ; Capture/compare register
;                   || |||
;                   || +++  Output mode -> Toggle/set
;                   ++  Compare latch load -> when TBR counts to TBCL0 or 0
        mov     #5,  R10
        call    #Delay
D_startup     dec     R10
              jnz     D_startup

        ;-----------------------------------------------------------------------------------------------
----
SetupADC10    mov.w     #ADC10SHT_2+ADC10ON+ADC10IE,&ADC10CTL0  ; 16x, enable int.
        ;         mov.w   #ADC10ON+ADC10IE,&ADC10CTL0 ; 4x, enable int.
        bis.b   #00000001b,&ADC10AE0       ; P2.0 ADC10 option select
;       bis     #INCH0, &ADC10CTL1         ; P2.1 ADC10 option select
                                           ;
        bis.w   #ENC+ADC10SC,&ADC10CTL0 ; Start sampling/conversion
        bis.w   #CPUOFF+GIE,SR         ; LPM0, ADC10_ISR will force exit
        nop
;       bic.b   #01h,&P1OUT            ; P1.0 = 0
;       cmp.w   #01FFh,&ADC10MEM       ; ADC10MEM = A0 > 0.5AVcc?
;       jlo     Mainloop               ; Again
;       bis.b   #01h,&P1OUT            ; P1.0 = 1
;       jmp     Mainloop               ; Again
                                       ;

;-------------------------------------------------------------------------------
; time delay
;-------------------------------------------------------------------------------
Delay       mov    #20,    R14
D1          mov    #50000,    R15
D2          dec    R15
            jnz    D2
            dec    R14
            jnz    D1

            ret
;-------------------------------------------------------------------------------
P2_INTR;  Exit LPM0 on reti when any button is pressed
;-------------------------------------------------------------------------------
            mov.b  &P2IN, R13            ; copy P2 input state
            bit    #0000000010000000b, R13  ; test: P2.7 interrupt pending?
            jnz    P2_6_int              ; go to increase procedure, if no P2.7 interrupt pending
            mov    #700, R12
            jmp    OUT_P2_int

P2_6_int    bit    #0000000001000000b, R13  ; test: P2.6 interrupt pending?
            jnz        OUT_P2_int              ; out of interrupt procedure, if no P2.6 interrupt pending
            mov    #900, R12             ;

OUT_P2_int
            reti
;-------------------------------------------------------------------------------
ADC10_ISR;  Exit LPM0 on reti
;-------------------------------------------------------------------------------
           mov    &ADC10MEM, R11
           sub    R12, R11
           RRA    R11
           RRA    R11
           add    &TBCCR1, R11

           cmp    #254, R11
           jge    OUT_ADC_ih

           cmp    #2, R11
           jl     OUT_ADC_il
           mov    R11,   &TBCCR1
           jmp    OUT_ADC_i

OUT_ADC_ih  mov    #254,   &TBCCR1
           jmp    $+6
OUT_ADC_il  mov    #2,   &TBCCR1

OUT_ADC_i          bis.w          #ENC+ADC10SC,&ADC10CTL0    ;    Start sampling/conversion
           reti                       ;
;-------------------------------------------------------------------------------
           COMMON  INTVEC             ; Interrupt Vectors
;-------------------------------------------------------------------------------
           ORG     PORT2_VECTOR
           DW      P2_INTR
           ORG     ADC10_VECTOR        ; ADC10 Vector
           DW      ADC10_ISR
           ORG     RESET_VECTOR        ; POR, ext. Reset
           DW      RESET
           END
```

O. MSP430F2232 Assembler Code for Asynchronous Control of Non-Inverting Buck-Boost (Double Closed Loop: CS Stage Current and Voltage Feedbacks)

```
;******************************************************************************
;            MSP430F22x4
;         -----------------
;      /|\|                |-
;       | |                |
;       --|RST             |-
;         |                |
;    >---|P2.0/A0P4.1|--> PWM1
;    >---|PB2.7    P4.2|→PWM2
;    >---|PB2.6          |
;
;
;******************************************************************************
#include "msp430x22x4.h"
;-------------------------------------------------------------------------------
        RSEG    CSTACK                  ; Define stack segment
;-------------------------------------------------------------------------------
        RSEG    CODE                    ; Assemble to Flash memory
;-------------------------------------------------------------------------------
RESET       mov.w   #SFE(CSTACK),SP         ; Initialize stackpointer
StopWDT     mov.w   #WDTPW+WDTHOLD,&WDTCTL  ; Stop WDT

        CLR.B   &DCOCTL                 ; Select lowest DCOx
                                        ; and MODx settings
        BIS.B   #RSEL3+RSEL2+RSEL1+RSEL0,&BCSCTL1 ;Select range 7
        BIS.B   #DCO2+DCO1+DCO0,&DCOCTL     ; Select max DCO tap

        mov     #480, R10               ; current set point (~0.7A)

        mov.b   #00000010b, &P4DIR      ; PWM output setup P4.1
        mov.b   #00000010b, &P4SEL      ; PWM output setup P4.1

        bic.b   #00000100b, &P4OUT      ; P-ch FET gate control

        call    #Delay

        mov.w   #0001001000010000b, &TBCTL  ; Timer B control register
;               |||| ||||||
;               |||| ||||++  Mode control -> Up mode
;               |||| ||++  Input divider -> /1
;               |||| ++  Clock source select -> SMCLK
;               ||++  Counter length -> 10-bit
;               ++  TBCLx group -> Each TBCLx latch loads independently


        bic.w   #1100000100000000b, &TBCCTL0 ; Capture/compare register
;              ||     |
;              ||     +  Capture mode -> Compare
;              ++  No capture


        mov.w   #0000010011000000b, &TBCCTL1 ; Capture/compare register
;                  || |||
;                  || +++  Output mode -> Toggle/set
;                  ++  Compare latch load -> when TBR counts to TBCL0 or 0



        mov.w   #511, &TBCCR0           ; Set 0 capture/compare register
        mov.w   #0, &TBCCR1             ; Set 1 capture/compare register

        call    #Delay
         ;-------------------------------------------------------------------------------
SetupADC10   mov.w     #ADC10SHT_2+ADC10ON+ADC10IE,  &ADC10CTL0  ;
16x, enable int.
             mov.w   #INCH_1+CONSEQ_1 ,&ADC10CTL1           ; select A0
and A1 (sequence of these channels)
             mov.w                #ADC10SHT_2+MSC+ADC10ON+ADC10IE,
&ADC10CTL0 ;
             bis.b     #00000011b,&ADC10AE0              ;  P2.0,  P2.1  ADC10
option select
             mov.b   #02h,&ADC10DTC1         ; 2 conversions

         Mainloop    bic.w   #ENC,&ADC10CTL0         ;
         busy_test   bit     #BUSY,&ADC10CTL1        ; ADC10 core inactive?
             mov.w   #0200h,&ADC10SA         ; Data buffer start

             bis.w                #ENC+ADC10SC,&ADC10CTL0       ;       Start
sampling/conversion
             bis.w    #CPUOFF+GIE,SR            ; LPM0, ADC10_ISR will force
exit
             nop

             mov      &0200h,  R8             ; data from A1(P2.1) voltage (PWM
base)
             rra     R8
             mov     &0202h,  R9            ; data from A0 (P2.0) current
             rra     R9
             inv     R9
             inc     R9                     ; Negative current value
             add     R10,     R9            ; R9 -- current error
             add     R9,      R8
             cmp     #1,      R8
             jge     TP2
             mov     #1,      R8
TP2          cmp     #511,    R8
             jl      c_p_ADC
             mov     510,     R8
c_p_ADC      mov     R8,  &TBCCR1
             jmp     Mainloop               ; Again

;-------------------------------------------------------------------------------
; time delay
;-------------------------------------------------------------------------------
Delay        mov    #20,    R14
D1           mov    #50000,    R15
D2           dec    R15
             jnz    D2
             dec    R14
             jnz    D1

             ret

;-------------------------------------------------------------------------------
ADC10_ISR;  Exit LPM0 on reti
;-------------------------------------------------------------------------------
             bic.w   #CPUOFF,0(SP)          ; Exit LPM0 on reti
             reti                           ;
                                            ;
;-------------------------------------------------------------------------------
             COMMON  INTVEC                 ; Interrupt Vectors
;-------------------------------------------------------------------------------
             ORG     ADC10_VECTOR           ; ADC10 Vector
             DW      ADC10_ISR
             ORG     RESET_VECTOR           ; POR, ext. Reset
             DW      RESET
             END
```

P. MSP430F2232 Assembler Code for Synchronous Control of Non-Inverting Buck-Boost (Double Closed Loop: CS Stage Current and Voltage Feedbacks)

```
;******************************************************************************
;
;
;
;            MSP430F22x4
;         -----------------
;     /|\|              |-
;      | |              |
;      --|RST           |-
;        |              |
;   >---|P2.0/A0P4.1|--> PWM1
;     >---|PB2.7       |→PWM2
;     >---|PB2.6           |
;
;
;******************************************************************************
#include "msp430x22x4.h"
;------------------------------------------------------------------------------
        RSEG    CSTACK                  ; Define stack segment
;------------------------------------------------------------------------------
        RSEG    CODE                    ; Assemble to Flash memory
;------------------------------------------------------------------------------
RESET       mov.w   #SFE(CSTACK),SP         ; Initialize stackpointer
StopWDT     mov.w   #WDTPW+WDTHOLD,&WDTCTL  ; Stop WDT

        BIS.B   #RSEL3+RSEL2+RSEL1+RSEL0,&BCSCTL1 ; Select range 7
        BIS.B   #DCO2+DCO1+DCO0,&DCOCTL     ; Select max DCO tap

        clr     R9                      ; Initial values for
        clr     R6
        clr     R5
        mov     #230, R10               ; current set point (~0.7A)
        mov     #1, R11                 ; current output level 255/511

        mov.b   #00000110b, &P4DIR          ; PWM output setup P4.1, P4.2
        mov.b   #00000110b, &P4SEL          ; PWM output setup P4.1, P4.2

        bis.b   #10010000b, &P1DIR          ; for debugging
        bic.b   #10000000b, &P1OUT          ; for debugging
        bis.b   #00010000b, &P1SEL          ; for debugging


        call    #Delay

        mov.w   #0001001000010000b, &TBCTL  ; Timer B control register
;                  |||| ||||||
;                  |||| ||||++  Mode control -> Up mode
;                  |||| ||++  Input divider -> /1
;                  |||| ++  Clock source select -> SMCLK
;                  ||++  Counter length -> 10-bit
;                  ++  TBCLx group -> Each TBCLx latch loads independently


        bic.w   #1100000100000000b, &TBCCTL0 ; Capture/compare register
;               ||     |
;               ||     +  Capture mode -> Compare
;               ++  No capture


        mov.w   #0000010011000000b, &TBCCTL1 ; Capture/compare register
;                    || |||
;                    || +++  Output mode -> Toggle/set
;                    ++  Compare latch load -> when TBR counts to TBCL0 or 0

        mov.w   #0000010011000000b, &TBCCTL2 ; Capture/compare register
;                    || |||
;                    || +++  Output mode -> Toggle/set
;                    ++  Compare latch load -> when TBR counts to TBCL0 or 0

        mov.w   #511, &TBCCR0               ; Set 0 capture/compare register
        mov.w   #0, &TBCCR1               ; Set 1 capture/compare register
        mov.w   #0, &TBCCR2               ; Set 1 capture/compare register

        call    #Delay
;------------------------------------------------------------------------------
SetupADC10
          mov.w       #ADC10SHT_2+ADC10ON+ADC10IE,&ADC10CTL0   ;   16x,
enable int.
          bis.b   #00000001b,&ADC10AE0          ; P2.0 ADC10 option select
          mov.w   #ADC10SHT_2+MSC+ADC10ON+ADC10IE, &ADC10CTL0 ;
int.

Mainloop    bic.w   #ENC,&ADC10CTL0         ;
busy_test   bit     #BUSY,&ADC10CTL1        ; ADC10 core inactive?

        bis.w   #ENC+ADC10SC,&ADC10CTL0 ; Start sampling/conversion

        bic.b   #10000000b, &P1OUT          ; for debugging

        bis.w   #CPUOFF+GIE,SR          ; LPM0, ADC10_ISR will force exit
        nop

        mov     &ADC10MEM,   R6         ; data rom A0 (P2.0) current
        add     R6,     R5
        mov     R5,     R9
        mov     R6,     R5

        rra     R9
        rra     R9
        inv     R9
        inc     R9                      ; Negative current value
        add     R10,     R9             ; R9 -- current error
        rla     R9

c_p_ADC
        mov     #511,    R7
        subc    R11,     R7
        add     R11,     R9
        cmp     #2,      R9
        jge     TP3
        mov     #1,      R9
TP3         mov     R7,  &TBCCR2
        mov     R9,  &TBCCR1
        jmp     Mainloop                ; Again

;------------------------------------------------------------------------------
; time delay
;------------------------------------------------------------------------------
Delay       mov     #20,    R14
D1          mov     #50000,    R15
D2          dec     R15
         jnz     D2
         dec     R14
         jnz     D1

         ret
;------------------------------------------------------------------------------
ADC10_ISR;  Exit LPM0 on reti
;------------------------------------------------------------------------------
         bic.w   #CPUOFF,0(SP)          ; Exit LPM0 on reti

         bis.b   #10000000b, &P1OUT      ; for debugging

         reti                           ;
                    ;
;------------------------------------------------------------------------------
        COMMON  INTVEC                  ; Interrupt Vectors
;------------------------------------------------------------------------------
        ORG     ADC10_VECTOR            ; ADC10 Vector
        DW      ADC10_ISR
        ORG     RESET_VECTOR            ; POR, ext. Reset
        DW      RESET
        END
```

Q. Electrical Circuit of the Prototype of Non-Inverting Buck-Boost (OrCAD Project)

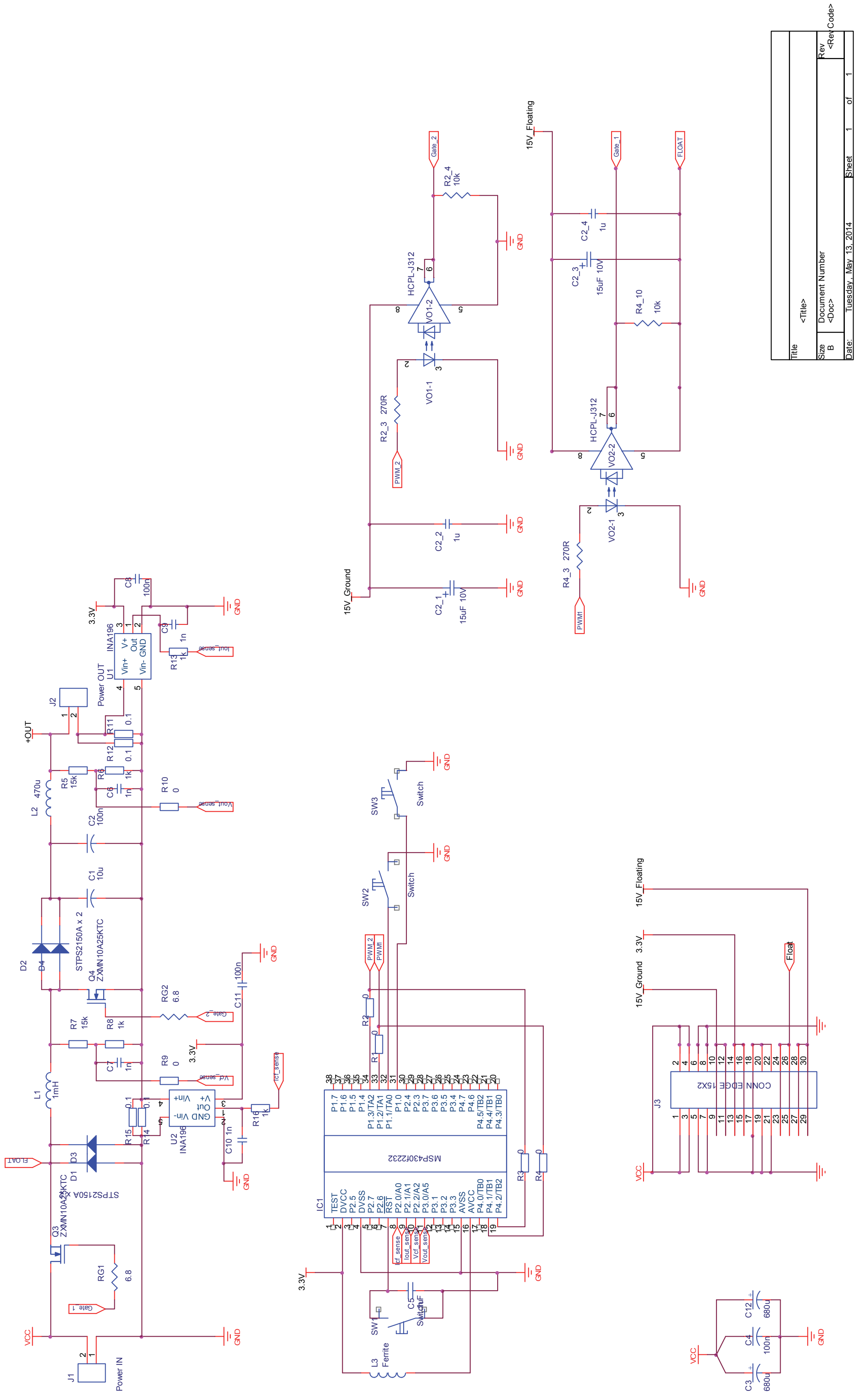

REFERENCES

[1] A. Žakauskas, M. S. Shur, and R. Gaska, *Introduction to Solid — State Lighting*. New York: John Willey, 2002.

[2] European Commission, "Directive 2009/125/EC of the European Parliament and of the Council of 21 October 2009 establishing a framework for the setting of ecodesign requirements for energy-related products," *Off. J. Eur. Union*, pp. 10-35, 2009.

[3] U.S. Government Printing Office, "Energy Independence and Security Act of 2007," *Security*, vol. Public Law, pp. 1-311, 2007.

[4] Cree Inc., "Cree First to Break 300 Lumens-Per-Watt Barrier," *Cree press releases*, 2014. [Online]. Available: http://www.cree.com/News-and-Events/Cree-News/Press-Releases/2014/March/300LPW-LED — barrier. [Accessed: 27-Sep-2014].

[5] IEA, "World Energy Outlook 2011," *Outlook*, 2011.

[6] L. Ribickis and A. Avotiņš, *Apgaismošanas tehnoloģijas*. Rīga: RTU, 2007.

[7] Cree Inc., "LED Lighting Catalog," 2014. [Online]. Available: http://www.cree.com/Lighting/Document — Library. [Accessed: 02-Sep-2014].

[8] I. Milashevski, *Research and Development of Electronic Ballasts for Smart Lighting Systems with Light Emitting Diodes, Thesis on Power Engineering*. Tallinn: TUT Press, 2012.

[9] A. Suzdalenko, I. Milashevski, and I. Galkin, "Comparative study of smart lighting grids with LEDs operated with concentrated, localized or distributed control," in *SPEEDAM 2012 — 21st International Symposium on Power Electronics, Electrical Drives, Automation and Motion*, 2012, pp. 1437-1441.

[10] A. Suzdalenko and I. Galkin, "Choice of power and control hardware for smart LED luminary," in *BEC 2010 - 2010 12th Biennial Baltic Electronics Conference, Proceedings of the 12th Biennial Baltic Electronics Conference*, 2010, pp. 331-334.

[11] A. Suzdalenko and I. Galkin, "Investigation of power supply methods for intelligent LED luminary," in *Proceedings of EPE-PEMC 2010 - 14th International Power Electronics and Motion Control Conference*, 2010.

[12] S. Bhardwaj, T. Özçelebi, and J. Lukkien, "Smart lighting using LED luminaries," in *2010 8th IEEE International Conference on Pervasive Computing and Communications Workshops, PERCOM Workshops 2010*, 2010, pp. 654-659.

[13] M. C. Kinn, "Proposed components for the design of a smart nano-grid for a domestic electrical system that operates at below 50V DC," in *IEEE PES Innovative Smart Grid Technologies Conference Europe*, 2011.

[14] Perry J. and National Semiconductor, "Designing LED Lighting Systems for Optimal Light Output," *Power Electronics Technology*, 2011. [Online]. Available: www.powerelectronics.com. [Accessed: 15-Feb-2015].

[15] LEDinside, "Cree's New SiC Technology Lowers High-Power LED Costs," *Technical article from a media platform for LED and LED lighting*, 2014. [Online]. Available: http://www.ledinside.com/news/2014/10/cree_develops_new_sic_technology_to_lowers_high_power_led_costs. [Accessed: 15-Feb-2015].

[16] Cree Inc., “The new Cree SC5 Technology Platform,” *Cree SC5 Technology Platform promotion page*. [Online]. Available: http://www.cree.com/sc5. [Accessed: 15-Feb-2015].

[17] E. F. Schubert, *Light-Emitting Diodes*, Second Edi. New York: Cambridge University Press, 2006.

[18] J. Schanda, *Colorimetry: Understanding the CIE System*. Willey, 2007.

[19] International Commission on Illumination (CIE), “Chromaticity Difference Specification for Light Sources,” *Technical note CIE TN 001:2014.*, 2014. [Online]. Available: http://files.cie.co.at/738_CIE_TN_001-2014.pdf. [Accessed: 18-Sep-2014].

[20] N. Ohta and A. Robertson, *Colorimetry: Fundamentals and Applications*. Willey, 2005.

[21] Cree Inc., “LED Color Mixing: Basics and Background,” *Technical article CLD-AP38, Rev. 1A*. [Online]. Available: http://cree.com/xlamp_app_notes/color_mixing. [Accessed: 15-Sep-2014].

[22] American National Standards Institute, “Specifications for the Chromaticity of Solid State Lighting Products,” ANSI C78.377-2008, 2008.

[23] International Commission on Illumination (CIE), “CIE International Lighting Vocabulary,” CIE S 017/E:2011, 2011.

[24] D. Erdmann, “Color Rendering Index (CRI).” [Online]. Available: http://www.ianiro.com/media/formato2/ianiro_517.pdf. [Accessed: 29-Nov-2014].

[25] International Commission on Illumination (CIE), “Color Rendering of White LED Light Sources,” Technical Report 177:2007, 2007.

[26] U.S. Department of Energy Energy Efficiency and Renewable Energy, “LED Measurement Series: Color Rendering Index and LEDs,” PNNL-SA-56891, 2008.

[27] Y. Ohno, “Color Quality of White LEDs,” in *III-Nitride based Light Emitting Diodes and Applications*, T.-Y. Seong, J. Han, H. Amano, and H. Morkoc, Eds. Berlin: Springer DE, 2013, pp. 349-371.

[28] Osram Opto Semiconductors, “Light and Color Methods of Achieving High CRI with LEDs,” *Webinar materials OS SSL MK*, 2011. [Online]. Available: http://ledlight.osram-os.com/wp-content/uploads/2012/02/OSRAM-OS_WEBINAR_HighCRI_06-26-12.pdf. [Accessed: 29-Nov-2014].

[29] “ASSIST alliance develops new metric for color properties in retail lighting,” *LEDs Magazine*, Jun-2010. [Online]. Available: http://www.ledsmagazine.com/articles/2010/06/assist-alliance-develops-new-metric-for-color-properties-in-retail-lighting.html. [Accessed: 30-Nov-2014].

[30] Lighting Research Center, “Guide to Light and Color in Retail Merchandising,” *ASSIST Recommends...*, 2010. [Online]. Available: www.lrc.rpi.edu/programs/solidstate/assist/pdf/AR — ColorGuideforRetailLighting — March2010.pdf. [Accessed: 30-Nov-2014].

[31] Lighting Research Center, “Recommendations for Specifying Color Properties of Light Sources for Retail Merchandising,” *ASSIST Recommends...*, 2010. [Online]. Available: http://www.lrc.rpi.edu/programs/solidstate/assist/pdf/AR — SpecifyColorRec — March2010.pdf. [Accessed: 30-Nov-2014].

[32] Lighting Research Center, “Flicker Parameters for Reducing Stroboscopic Effects from Solid-state Lighting Systems,” *ASSIST Recommends...*, 2012. [Online]. Available: http://www.lrc.rpi.edu/programs/solidstate/assist/pdf/AR-Flicker.pdf. [Accessed: 03-Jul-2014].

[33] C. Allefeld, P. Pütz, K. Kastner, and J. Wackermann, “Flicker-light induced visual phenomena: Frequency dependence and specificity of whole percepts and percept features,” *Conscious. Cogn.*, vol. 20, no. 4, pp. 1344-1362, 2011.

[34] International Electrotechnical Commission, “Electromagnetic compatibility (EMC) — Part 4-15: Testing and measurement techniques — Flickermeter — Functional and design specifications,” *IEC 61000-4-15*, 2010.

[35] D. Gallo, C. Landi, R. Langella, and A. Testa, “Implementation of a test system for advanced calibration and performance analysis of flickermeters,” *IEEE Trans. Instrum. Meas.*, vol. 53, no. 4, pp. 1078-1085, 2004.

[36] D. Gallo, C. Landi, and N. Pasquino, “An Instrument for the Objective Measurement of Light Flicker,” in *2005 IEEE Instrumentationand Measurement Technology Conference Proceedings*, vol. 3, pp. 1942-1947.

[37] Engineering Society of North America, “Measurement of Light and Other Radiant Energy,” in *IESNA Lighting Handbook: Reference & Application*, 9th ed., M. S. Rea, Ed. New York, 2000, p. 1000.

[38] G. Held, *Introduction to Light Emitting Diode Technology and Applications*. Auerbach Publications, 2008.

[39] M. Godlewski, M. Skrobot, E. Guziewicz, and M. R. Phillips, “Color tuning of white light emission from thin films of ZnSe,” *J. Lumin.*, vol. 125, no. 1-2, pp. 85-91, 2007.

[40] Lithonia Lighting and RTLED, “White Paper: Binning and LED. What is Binning with respect to LEDs?,” *version 1.0*, 2010. [Online]. Available: http://lithonia.acuitybrands.com/Files/RTLED_Files/RTLED_WPaper_BinningandLED.pdf. [Accessed: 13-Mar-2014].

[41] S. Phatak, “Manufacturing LEDs on large diameter substrates: What’s the holdup?,” *LEDs Magazine*, 2013. [Online]. Available: http://www.ledsmagazine.com/articles/print/volume-10/issue-2.html. [Accessed: 13-Mar-2014].

[42] Philips, “Breakthrough luminance, design flexibility and optical control for Illumination solutions,” *LUXEON Z and LUXEON Z ES Datasheet DS120 20130517*, 2013. [Online]. Available: http://www.philipslumileds.com/products/luxeon-z. [Accessed: 19-Jul-2013].

[43] Cree Inc., “Cree Xlamp® XP-G leds,” *product family datasheet*. [Online]. Available: http://www.cree.com. [Accessed: 19-Jun-2013].

[44] J. Cooper, “Driving LED lamps — some simple design guidelines,” *LEDs Magazine*, 2007. [Online]. Available: http://www.ledsmagazine.com/articles/print/volume-4/issue-8.html. [Accessed: 13-Mar-2014].

[45] S. M. Baddela and D. S. Zinger, “Parallel connected LEDs operated at high to improve current sharing,” *Conf. Rec. 2004 IEEE Ind. Appl. Conf. 2004. 39th IAS Annu. Meet.*, vol. 3, 2004.

[46] G. Sauerländer, D. Hente, H. Radermacher, E. Waffenschmidt, and J. Jacobs, "Driver electronics for LEDs," in *Conference Record — IAS Annual Meeting (IEEE Industry Applications Society)*, 2006, vol. 5, pp. 2621-2626.

[47] M. Schmid, D. Kuebrich, M. Weiland, and T. Duerbaum, "Evaluation on the efficiency of power LEDs driven with currents typical to switch mode power supplies," in *Conference Record — IAS Annual Meeting (IEEE Industry Applications Society)*, 2007, pp. 1135-1140.

[48] J. Zhang, J. Wang, and X. Wu, "A capacitor-isolated LED driver with inherent current balance capability," *IEEE Trans. Ind. Electron.*, vol. 59, no. 4, pp. 1708-1716, 2012.

[49] J. Wang, J. Zhang, X. Huang, and L. Xu, "A family of capacitive current balancing methods for multi-output LED drivers," in *Conference Proceedings — IEEE Applied Power Electronics Conference and Exposition — APEC*, 2011, pp. 2040-2046.

[50] W. Thomas and J. Pforr, "A novel low-cost current-sharing method for automotive LED — lighting systems," *2009 13th Eur. Conf. Power Electron. Appl.*, 2009.

[51] Y.-L. Lin, H.-J. Chiu, Y.-K. Lo, C.-M. Leng, and Q. T. Nha, "LED driver with a combined energy transfer inductor for current balancing," in *2014 International Conference on Intelligent Green Building and Smart Grid (IGBSG)*, 2014, pp. 1-4.

[52] R. Zhang and H. Chung, "Use of Daisy-Chained Transformers for Current-Balancing Multiple LED Strings," *IEEE Trans. Power Electron.*, vol. 29, no. 3, pp. 1418-1433, 2014.

[53] R. Zhang and H. Shu-Hung Chung, "Transformer — isolated resonant driver for parallel strings with robust balancing and stabilization of individual LED current," *IEEE Trans. Power Electron.*, vol. 29, no. 7, pp. 3694-3708, 2014.

[54] S. Winder, *Power Supplies for LED Drivers*. Newnes, 2008.

[55] Infineon, "SIPMOS Small-Signal-Transistor," *BSS159N datasheet, Rev.2.2*, 2009. [Online]. Available: http://www.infineon.com. [Accessed: 12-Sep-2014].

[56] Texas Instruments, "LM117/LM317A/LM317-N Three-Terminal Adjustable Regulator," *Technical datasheet SNVS774O*. [Online]. Available: http://www.ti.com/lit/ds/symlink/lm117.pdf. [Accessed: 12-Sep-2014].

[57] B. Johanson and J. Lee, "Solutions for Today's Low-Power LED Lighting Trends," *Fairchild*, 2011. [Online]. Available: https://www.fairchildsemi.com/technical-articles/. [Accessed: 12-Oct-2014].

[58] International Electrotechnical Commission, "Electromagnetic compatibility (EMC) — Part 3-2: Limits-Limits for harmonic current emissions (equipment input current ≤ 16 A per phase)," *EN61000-3-2*, 2014.

[59] H. J. Chiu, Y. K. Lo, J. T. Chen, S. J. Cheng, C. Y. Lin, and S. C. Mou, "A high-efficiency dimmable LED driver for low-power lighting applications," in *IEEE Transactions on Industrial Electronics*, 2010, vol. 57, no. 2, pp. 735-743.

[60] P. Athalye, M. Harris, and G. Negley, "A two-stage LED driver for high-performance high-voltage LED fixtures," in *Conference Proceedings — IEEE Applied Power Electronics Conference and Exposition — APEC*, 2012, pp. 2385-2391.

[61] D. Gacio, J. M. Alonso, A. J. Calleja, J. García, and M. Rico — Secades, "A universal-input single-stag2e high-power-factor power supply for HB — LEDs based on integrated buckflyback converter," *IEEE Trans. Ind. Electron.*, vol. 58, no. 2, pp. 589-599, 2011.

[62] J. M. Alonso, J. Viña, D. G. Vaquero, G. Martínez, and R. Osorio, "Analysis and design of the integrated double buck-boost converter as a high-power-factor driver for power-led lamps," *IEEE Trans. Ind. Electron.*, vol. 59, no. 4, pp. 1689-1697, 2012.

[63] Y. X. Qin, H. S. H. Chung, D. Y. Lin, and S. Y. R. Hui, "Current source ballast for high power lighting emitting diodes without electrolytic capacitor," in *Proceedings — 34th Annual Conference of the IEEE Industrial Electronics Society, IECON 2008*, 2008, pp. 1968-1973.

[64] M. Arias, D. G. Lamar, F. F. Linera, D. Balocco, A. Aguissa Diallo, and J. Sebastián, "Design of a soft-switching asymmetrical half-bridge converter as second stage of an LED driver for street lighting application," *IEEE Trans. Power Electron.*, vol. 27, no. 3, pp. 1608-1621, 2012.

[65] L. G. L. Gu, X. R. X. Ruan, M. X. M. Xu, and K. Y. K. Yao, "Means of Eliminating Electrolytic Capacitor in AC/DC Power Supplies for LED Lightings," *IEEE Trans. Power Electron.*, vol. 24, no. 5, 2009.

[66] H. Ma, W. Yu, C. Zheng, J. S. Lai, Q. Feng, and B. Y. Chen, "A universal-input high-power-factor PFC pre-regulator without electrolytic capacitor for PWM dimming LED lighting application," in *IEEE Energy Conversion Congress and Exposition: Energy Conversion Innovation for a Clean Energy Future, ECCE 2011, Proceedings*, 2011, pp. 2288-2295.

[67] T. Jiang, H. Zeng, J. Zhang, and Z. Qian, "A primary side feedforward control scheme for low power LED driver compatible with triac dimmer," in *Conference Proceedings — IEEE Applied Power Electronics Conference and Exposition - APEC*, 2012, pp. 963-968.

[68] X. Qu, S. C. Wong, and C. K. Tse, "Resonance-assisted buck converter for offline driving of power LED replacement lamps," *IEEE Trans. Power Electron.*, vol. 26, no. 2, pp. 532-540, 2011.

[69] C. Chun-An, C. Chien-Hsuan, C. Hung-Liang, and C. Tsung-Yuan, "A single-stage high-PF driver for supplying a T8-type LED lamp," in *2014 International Power Electronics Conference (IPEC — Hiroshima 2014 ECCE — ASIA)*, 2014, pp. 2523-2528.

[70] K. Shu — Kong and D. D.-C. Lu, "A High Step-Down Transformerless Single-Stage Single-Switch AC/DC Converter," *IEEE Trans. Power Electron.*, vol. 28, no. 1, pp. 36-45, 2013.

[71] T. Pan, H. Chiu, S. Cheng, and S. Chyng, "An improved single-stage flyback PFC converter for high-luminance lighting LED lamps," in *2007 8th International Conference on Electronic Measurement and Instruments, ICEMI*, 2007, pp. 4212-4215.

[72] S. Cha, D. Park, Y. Lee, C. Lee, J. Choi, J. Lee, and H. Lee, "AC/DC converter free LED driver for lightings," in *Digest of Technical Papers — IEEE International Conference on Consumer Electronics*, 2012, pp. 706-708.

[73] N. Ning, Z. Tong, D. Yu, S. Wu, W. Chen, and C. Feng, "Highly AC voltage fluctuation — resistant LED driver with sinusoid — like reference," *J. Power Electron.*, vol. 14, no. 2, 2014.

[74] D. G. Lamar, A. Fernández, M. Arias, M. Rodríguez, J. Sebastián, and M. M. Hernando, "Limitations of the flyback power factor corrector as a one-stage power supply," in *PESC Record — IEEE Annual Power Electronics Specialists Conference*, 2007, pp. 1343-1348.

[75] W. Chen, S. N. Li, and S. Y. R. Hui, “A comparative study on the circuit topologies for offline passive light-Emitting diode (LED) drivers with long lifetime & high efficiency,” in *2010 IEEE Energy Conversion Congress and Exposition, ECCE 2010 — Proceedings*, 2010, pp. 724-730.

[76] Infineon, “TDA4862 Power-Factor Controller (PFC) IC for High Power Factor and Active Harmonic Filter,” *Technical data sheet TDA 4862, rev 2005-02-17*, 2005. [Online]. Available: http://www.infineon.com. [Accessed: 19-Aug-2013].

[77] W. Frank and M. Herfurth, “TDA4862 — Technical Description,” *Application note AN-PFC-TDA4862-1, rev. 1.2*, 2003. [Online]. Available: http://www.infineon.com. [Accessed: 19-Aug-2013].

[78] ON Semiconductor, “NCP1653 Compact, Fixed-Frequency, Continuous Conduction Mode PFC Controller,” *Technical data sheet NCP1653/D, rev. 9*, 2013. [Online]. Available: http://www.onsemi.com/pub_link/Collateral/NCP1653-D.PDF. [Accessed: 19-Aug-2013].

[79] O. Tetervenoks, “Sensorless converter for low-power LED lamp with improved power factor,” in *Electric Power Quality and Supply Reliability Conference (PQ 2014)*, 2014, pp. 285-290.

[80] Cree Inc., “Cree® XLamp® XM-L2 LEDs,” *Product family data sheet: CLD-DS61 Rev. 2C*. [Online]. Available: http://www.cree.com/LED — Components-and-Modules/Products/XLamp/Discrete-Directional/XLamp-XML2. [Accessed: 19-Apr-2014].

[81] I. Galkin, O. Tetervenoks, and I. Milashevski, “Comparative Estimation of Efficiency of LED Dimmers at Different Modulation Techniques,” in *Proceedings of the 14th European Conference on Power Electronics and Applications (EPE2011)*, 2011, pp. 1-9.

[82] H. Van Der Broeck, G. Sauerländer, and M. Wendt, “Power driver topologies and control schemes for LEDs,” in *Conference Proceedings — IEEE Applied Power Electronics Conference and Exposition — APEC*, 2007, pp. 1319-1325.

[83] T. Szepesi, “Stabilizing the Frequency of Hysteretic Current-Mode DC/DC Converters,” *IEEE Trans. Power Electron.*, vol. 2, no. 4, 1987.

[84] I. H. Oh, “An analysis of current accuracies in peak and hysteretic current controlled power LED drivers,” in *Conference Proceedings — IEEE Applied Power Electronics Conference and Exposition — APEC*, 2008, pp. 572-577.

[85] Fairchild Semiconductor, “LED Application Design Guide Using Half-Bridge LLC Resonant Converter for 100W Street Lighting,” *Application note AN-9729, rev. 1.0.1*, 2011. [Online]. Available: https://www.fairchildsemi.com/application-notes/AN/AN-9729.pdf. [Accessed: 12-Nov-2014].

[86] D. Caicedo and A. Pandharipande, “Distributed illumination control with local sensing and actuation in networked lighting systems,” *IEEE Sens. J.*, vol. 13, no. 3, pp. 1092-1104, 2013.

[87] L. H. Koh, Y. K. Tan, Z. Z. Wang, and K. J. Tseng, “An energy-efficient low voltage DC grid powered smart LED lighting system,” in *IECON Proceedings (Industrial Electronics Conference)*, 2011, pp. 2883-2888.

[88] A. Molderink, V. Bakker, M. G. C. Bosman, J. L. Hurink, and G. J. M. Smit, “Management and Control of Domestic Smart Grid Technology,” *Smart Grid, IEEE Trans.*, vol. 1, no. 2, pp. 109-119, 2010.

[89] A. Andreičiks, I. Steiks, and O. Krievs, “Design of efficient current fed DC/DC converter for fuel cell applications,” in *Proceedings — ISIE 2011: 2011 IEEE International Symposium on Industrial Electronics*, 2011, pp. 206-210.

[90] I. Galkin, L. Bisenieks, and A. Suzdalenko, “Impact of pulse modulation method of LED dimmer for street lighting on its efficiency,” *4th Eur. Educ. Res. Conf. (EDERC 2010)*, pp. 160-164, 2010.

[91] W. A. Rodrigues, L. M. F. Morais, P. F. Donoso-Garcia, P. C. Cortizo, and S. I. Seleme, “Comparative analysis of power LEDs dimming methods,” in *IECON Proceedings (Industrial Electronics Conference)*, 2011, pp. 2907-2912.

[92] W. Chen and S. Y. R. Hui, “A dimmable light-emitting diode (LED) driver with mag-amp postregulators for multistring applications,” *IEEE Trans. Power Electron.*, vol. 26, no. 6, pp. 1714-1722, 2011.

[93] C. L. Chiu and K. H. Chen, “A high accuracy current-balanced control technique for LED backlight,” in *PESC Record — IEEE Annual Power Electronics Specialists Conference*, 2008, pp. 4202-4206.

[94] M. Rico-secades, J. Uceda, J. Sebastian, and F. Aldana, “Static and Dynamic Modelling of Tapped-Inductor DC-to-DC Converters,” in *Proceedings of the IEEE Power Electronics Specialists Conference (IEEE — PESC 1987)*, 1987, pp. 281-288.

[95] M. Rico-Secades, J. Garcia, J. Cardesin, and A. J. Calleja, “Using tapped-inductor converters as LED drivers,” in *Conference Record - IAS Annual Meeting (IEEE Industry Applications Society)*, 2006, vol. 4, pp. 1794-1800.

[96] F. Cathell, “Offline Buck Converter with Tapped Inductor Offers Improved Performance.,” *ON Semiconductor, Application note AND8318/D, rev. 0*, 2008. [Online]. Available: http://www.onsemi.com/pub_link/Collateral/AND8318-D.PDF. [Accessed: 12-Apr-2014].

[97] D. G. Lamar, M. Fernandez, M. Arias, M. M. Hernando, and J. Sebastian, “Tapped-inductor buck HB-LED AC-DC driver operating in boundary conduction mode for replacing incandescent bulb lamps,” *IEEE Trans. Power Electron.*, vol. 27, no. 10, pp. 4329-4337, 2012.

[98] ON Semiconductor, “Self-Supplied Monolithic Switcher for Low Standby-Power Offline SMPS,” *Technical Datasheet NCP1010/D, rev. 22*, 2010. [Online]. Available: http://www.onsemi.com/pub_link/Collateral/NCP1010-D.PDF. [Accessed: 12-Apr-2014].

[99] I. Milashevski, I. Galkin, and O. Tetervenok, “Assessment of buck converter powered by current or voltage sources for LEDs luminary,” in *Proceedings of the Biennial Baltic Electronics Conference, BEC*, 2012, pp. 239-242.

[100] I. Milashevski, O. Tetervenok, and I. Galkin, “Assessment of Energy Efficient LED Ballasts Based on their Weight and Size,” *Scientific Journal of Riga Technical University. Power and Electrical Engineering*, vol. 29, no. -1. pp. 105-112, 2011.

[101] D. Graovac, “MOSFET Power Losses Calculation Using the Data Sheet Parameters,” *Infineon Technical Documentation, Application Note 2006-07-31 (V1.1)*, 2006. [Online]. Available: http://www.btipnow.com/library/referenceMaterials.php. [Accessed: 12-Apr-2014].

[102] NPX Semiconductors, “Understanding power MOSFET data sheet parameters,” *Application Note AN11158 (Rev. 4)*, 2014. [Online]. Available: http://www.nxp.com/documents/application_note/AN11158.pdf. [Accessed: 12-Apr-2014].

[103] L. H. Dixon, “Inductor and Flyback,” *Magnetics Desigh Handbook from Texas Instruments*, 2001. [Online]. Available: http://www.ti.com/lit/ml/slup127/slup127.pdf. [Accessed: 08-Jun-2014].

[104] H. Schmidt-Walter, “Design of Inductors and High Frequency Transformers,” *Switch Mode Power Supplies*. [Online]. Available: http://schmidt-walter.eit.h-da.de/snt/snt_eng/snte_pdf.html. [Accessed: 08-Jun-2014].

[105] Seoul Semiconductor, “W724C0 Technical Data Sheet,” *Document No. : SSC-QP-7-07-24 (Rev.00)*, 2008. [Online]. Available: http://www.seoulsemicon.com/_upload/Goods_Spec/W724C0.pdf. [Accessed: 05-Apr-2014].

[106] O. Tetervenoks and I. Milashevski, “Dimmable LED Drivers Operating in Discontinuous Conduction Mode,” *Electr. Control Commun. Eng.*, vol. 2, no. 1, pp. 27-33, 2013.

[107] N. Mohan, T. M. Undeland, and W. P. Robbins, *Power Electronics: Converters, Applications, and Design*. Willey, 2003.

[108] R. W. Erickson and D. Maksimovic, *Fundamentals of Power Electronics, 2nd edition*. Springer, 2001.

[109] I. Galkin, O. Tetervjonok, and I. Milashevski, “Comparative study of steady-state performance of voltage and current fed dimmable LED drivers,” in *International Conference-Workshop Compatibility in Power Electronics , CPE*, 2013, pp. 292-297.

[110] I. Galkin, O. Tetervenoks, and I. Milashevski, “Static Losses and Controllability of Current Fed Dimmable LED Drivers,” in *Proceedings of the 15th European Conference on Power Electronics and Applications (EPE 2013)*, 2013, p. P.1-P.10.

[111] I. Galkin and O. Tetervenoks, “Validation of direct current control in LED lamp with non-inverting buck-boost converter,” in *39th Annual Conference of the IEEE Industrial Electronics Society (IECON 2013)*, 2013, pp. 6021-6026.

[112] Linear Technology, “LTC3454 1A Synchronous Buck-Boost High Current LED Driver,” *Data Sheet No. LT 0309 (Rev. A)*, 2005. [Online]. Available: http://cds.linear.com/docs/en/datasheet/3454fa.pdf. [Accessed: 15-May-2014].

[113] S. Rao, Q. Khan, S. Bang, D. Swank, A. Rao, W. McIntyre, and P. K. Hanumolu, “A 1.2-A buck-boost LED driver with on-chip error averaged senseFET-based current sensing technique,” in *IEEE Journal of Solid-State Circuits*, 2011, vol. 46, no. 12, pp. 2772-2783.

[114] H. Jianming, X. Kun, and W. Chunhua, “Modulating method for noninverting Buck-Boost power inverter,” Patent Nr. CN102136797A, 2011.

[115] International Rectifier, “IRS254(0,1)(S)PbF LED buck regulator control IC,” *Data Sheet No. PD97524*, 2010. [Online]. Available: http://www.irf.com/product-info/datasheets/data/irs25401pbf.pdf. [Accessed: 24-May-2014].

[116] OECD/IEA, “Light’s Labor’s Lost. Policies for Energy-efficient Lighting.,” 2006. [Online]. Available: https://www.iea.org/publications/freepublications/publication/light2006.pdf.

[117] I. Galkin, I. Milashevski, and O. Teteryonok, "Comparative study of steady-state performance of LED drivers at different modulation techniques," in *2011 7th International Conference — Workshop Compatibility and Power Electronics, CPE 2011 — Conference Proceedings*, 2011, pp. 382-387.

[118] IXYS Integrated Circuits Division, "CPC9909 High Efficiency, Off-Line, High Brightness LED Driver," *Data Sheet No. DS-CPC9909-R04*, 2013. [Online]. Available: http://www.ixysic.com/home/pdfs.nsf/www/CPC9909.pdf. [Accessed: 24-May-2014].

[119] AEC ILLUMINAZIONE, "LED Products Dimming Systems," *Description of standard dimming options*. [Online]. Available: http://www.aecilluminazione.com/the-company/led-products-dimming-systems. [Accessed: 11-Jun-2014].

[120] The United States Naval Observatory (USNO) Astronomical Applications Department, "Sun or Moon Rise/Set Table for One Year," *a table for any location worldwide*. [Online]. Available: http://aa.usno.navy.mil/data/docs/RS_OneYear.php. [Accessed: 11-Jun-2014].

[121] Power Sources Manufacturers Association Inc., *Handbook of Standardized Terminology for the Power Sources Industry*, 2nd ed. 1995.

[122] W. R. Frensley and N. G. Einspruch, Eds., "Heterostructures and Quantum Devices," *A volume of VLSI Electronics: Microstructure Science*. [Online]. Available: https://www.utdallas.edu/~frensley/technical/hetphys/hetphys.html.

[123] R. Dingle, W. Wiegmann, and C. H. Henry, "Quantum states of confined carriers in very thin AlxGa1-xAs-GaAs-AlxGa1-xAs heterostructures," *Phys. Rev. Lett.*, vol. 33, no. 14, pp. 827-830, 1974.

[124] Truesense Imaging Inc, "Fundamental Radiometry and Photometry," *Reference document PS-0060, revision 1.0*, 2012. [Online]. Available: http://www.truesenseimaging.com/support/reference-documents/doc_download/21-fundamental-radiometry-and-photometry. [Accessed: 15-Sep-2014].

[125] Osram Sylvania Corporation, "Lumens and Mesopic Vision," *Application Note FAQ0016-0297*, 2000. [Online]. Available: http://www.pioneerlighting.com/new/pdfs/Lumens and Mesopic Vision.pdf. [Accessed: 15-Sep-2014].

[126] C. DeCusatis Eit, *Handbook of Applied Photometry*. New York: American Institute of Physics, 1997.

[127] International Commission on Illumination (CIE), "Selected Colorimetric Tables," *Downloads*. [Online]. Available: http://files.cie.co.at/204.xls. [Accessed: 15-Sep-2014].

[128] M. Tkalcic and J. F. Tasic, "Colour spaces: perceptual, historical and applicational background," *IEEE Reg. 8 EUROCON 2003. Comput. as a Tool.*, vol. 1, 2003.

[129] M. D. Fairchild, *Color Appearance Models*. Willey, 2005.

[130] W. K. Lun, K. H. Loo, S. C. Tan, Y. M. Lai, and C. K. Tse, "Bilevel current driving technique for LEDs," *IEEE Trans. Power Electron.*, vol. 24, no. 12, pp. 2920-2932, 2009.

[131] K. H. Loo, W. K. Lun, S. C. Tan, Y. M. Lai, and C. K. Tse, "On driving techniques for LEDs: Toward a generalized methodology," *IEEE Trans. Power Electron.*, vol. 24, no. 12, pp. 2967-2976, 2009.

[132] M. Doshi and R. Zane, “Control of solid-state lamps using a multiphase pulsewidth modulation technique,” *IEEE Trans. Power Electron.*, vol. 25, no. 7, pp. 1894-1904, 2010.

[133] E. Romero — Cadaval, M. I. Milanes — Montero, E. Gonzalez — Romera, and F. Barrero — Gonzalez, “Power Injection System for Grid — Connected Photovoltaic Generation Systems Based on Two Collaborative Voltage Source Inverters,” *IEEE Trans. Ind. Electron.*, vol. 56, no. 11, 2009.

[134] L. Bisenieks, D. Vinnikov, and I. Galkin, “New isolated interface converter for grid-connected PMSG based wind turbines,” in *2011 10th International Conference on Environment and Electrical Engineering, EEEIC.EU 2011 — Conference Proceedings*, 2011.

[135] International Rectifier, “IRF540N HEXFET Power MOSFET,” *Datasheet PD — 91341B*, 2001. [Online]. Available: http://www.irf.com/product-info/datasheets/data/irf540n.pdf . [Accessed: 14-Apr-2014].

[136] Fairchild Semiconductor, “MUR840, MUR860, RURP840, RURP860 - 8A, 400V-600V ultrafast diodes,” *Datasheet (Rev. C1)*, 2013. [Online]. Available: http://www.fairchildsemi.com/ds/RU/RURP860.pdf. [Accessed: 14-Apr-2014].

[137] M. Brown, *Power supply cookbook [electronic book]/ Marty Brown*. 2001.

[138] Micrometals, “Power Conversion and Line Filter Applications,” *Application note, issue L*, 2007. [Online]. Available: http://www.micrometals.com. [Accessed: 03-May-2014].

[139] T. Einchhorn, “Estimate Inductor Losses Easily in Power Supply Designs,” *Power Electronics Technology magazine*, Apr-2005. [Online]. Available: http://powerelectronics.com/content/estimate-inductor-losses-easily-power-supply-designs. [Accessed: 03-May-2014].